ABSTRACT

NANOPARTICLE FORMATION AND COATING USING SUPERCRITICAL FLUIDS

by
Abhijit Aniruddha Gokhale

Jet breakup phenomenon and nanoparticle formation

The focus of this dissertation is to study the SAS process to manufacture nanoparticles with minimum agglomeration, controlled size and size distribution. Solution jet breakup and solvent evaporation into supercritical fluid (SC CO_2) is studied using high speed charged coupled device (CCD) camera facilitated with double shot particle image veloimetry (PIV) laser and a high pressure view cell. Particles formation using SAS is studied. Polyvinylpyrrolidone (PVP) particles are formed using micron size capillary nozzles and combination of thermodynamically good and poor solvents in order to achieve nano-sized particles with reduced agglomeration and narrow size distribution. Effects of operational parameters on physiochemical properties of particles are investigated. Since the proposed method is based on general thermodynamic properties of polymer-solvent systems, it should be applicable to a wide variety of polymers for applications ranging from the improvement of the flow and packing properties of powders to the control of particle interaction with their external surroundings for drug delivery systems.

Fine particle coating and encapsulations using supercritical fluids

In certain applications, particle surfaces need to be modified or functionalized by coating them with another material to serve a specific purpose. As nanoparticles are extremely cohesive, it is very difficult to coat an individual particle by traditional

methods. In this research, nanoparticles coating is investigated through supercritical fluid-based methods. Agglomeration of particles is reduced by combining poor solvent and ultrasonic techniques. The first technique uses a proprietary co-axial ultrasonic nozzle to spray the solution suspension into the SC CO_2. Ultrasound is very effective in breaking agglomerates, and the introduction of the co-axial flow enables CO_2 to not only serve as an antisolvent, but also as a mixing enhancer. The second technique uses a combination of thermodynamically good and poor solvents to tune the supersaturation of the polymer which serves as the coating material. Other methods like raid expansion of supercritical solution (RESS) and particles from gas saturated solution (PGSS) are also investigated and compared with SAS.

Syneresis of silica gel

Effects of gravity, silica concentration in gel and time on syneresis are studied by exposing the simulants of gel propellants to higher gravities. Scanning electron microscopy (SEM) and nuclear magnetic resonance (NMR) are used to characterize the gel. Based on results of experimental studies, a multi-scale computational strategy for modeling gel formation and syneresis is proposed. Based on the analysis of the existing literature, directions for experimental and theoretical approaches for particles formation and coating are proposed, and form the main parts of this thesis. This summary section outlines the major components of proposed research; first, important features of the nanoparticles formation using SAS techniques are discussed followed by the nanocoatings and finally syneresis of silica gels.

NANOPARTICLE FORMATION AND COATING USING SUPERCRITICAL FLUIDS

by
Abhijit Aniruddha Gokhale

A Dissertation
Submitted to the Faculty of
New Jersey Institute of Technology
in Partial Fulfillment of the Requirements for the Degree of
Doctor of Philosophy in Mechanical Engineering

Department of Mechanical Engineering

January 2007

APPROVAL PAGE

NANOPARTICLE FORMATION AND COATING USING SUPERCRITICAL FLUIDS

Abhijit Aniruddha Gokhale

12/11/06

Dr. Boris Khusid, Dissertation Co-advisor — Date
Professor of Mechanical Engineering, NJIT

12/11/06

Dr. Rajesh Dave, Dissertation Co-advisor — Date
Distinguished Professor of Chemical Engineering, NJIT

12/11/06

Dr. Robert Pfeffer, Committee Member — Date
Distinguished Professor of Chemical Engineering (Emeritus), NJIT

12/11/06

Dr. Edward Dreizin, Committee Member — Date
Professor of Mechanical Engineering, NJIT

12/11/06

Dr. Mirko Shoenitz, Committee Member — Date
Research Assistant Professor of Mechanical Engineering, NJIT

BIOGRAPHICAL SKETCH

Author: Abhijit Aniruddha Gokhale

Degree: Doctor of Philosophy

Date: January 2007

Undergraduate and Graduate Education:

- Doctor of Philosophy in Mechanical Engineering,
  New Jersey Institute of Technology, Newark, NJ, 2007
- Master of Science in Mechanical Engineering,
  New Jersey Institute of Technology, Newark, NJ, 2003
- Bachelor of Engineering in Mechanical Engineering,
  Maharashtra Institute of Technology, Pune, India, 2000

Major: Mechanical Engineering

Presentations and Publications:

Gokhale A., Khusid B., Dave R., Pfeffer R.,
Formation of particles by injecting a polymer dissolved in a mixture of good and poor solvents into supercritical carbon dioxide through micronozzles, Manuscript in preparation.

Khusid B., Gokhale A., Dave R., Pfeffer R.,
US patent filed - "Method of manufacturing polymer or drug nanoparticles with rapid drying and reduced agglomerations" at New Jersey Institute of Technology.

Gokhale A., Shen Y., Khusid B., Dave R., Pfeffer R.,
Formation and coatings of fine particles in jets of supercritical fluids, NSTI Nanotechnology Conference and Trade Show - NSTI Nanotech 2006, Technical Proceedings, Boston, MA, May 7-11, pp.827-829.

Gokhale A., Khusid B., Dave R., Pfeffer R.,
Formation of polymer nano-particles in supercritical fluid jets, NSTI Nanotechnology Conference and Trade Show - NSTI Nanotech 2005, Technical Proceedings, Anaheim, CA, May 8-12, pp. 215-217.

Shen Y., Gokhale A., Wei D., Dave R., Pfeffer R.,
Coating of ultra-fine particles using ultrasonically enhanced supercritical anti-solvent fluids, Fifth World Congress on Particle Technology, Orlando, Fl, April 23-27, pp.1-6, 2006.

Gokhale A., Khusid B., Dave R., Pfeffer R.,
Formation of polymer nanoparticles in supercritical fluid micro jets, International Symposium on Supercritical Fluids, Orlando, Fl, May 1-4, 2005.

Shen Y., Gokhale A., Dave R., Pfeffer R.,
Particle formation using ultrasonic nozzle in SAS, International Symposium on Supercritical Fluids, Orlando, Fl, May 1-4, 2005.

Gokhale A., Khusid B., Dave R., Pfeffer R.,
Supercritical antisolvent precipitation of a polymer in a mixture of good and poor solvents, AIChE annual meeting, Austin, Tx, Nov 8-11, 2004.

Luo J., Gokhale A., Wang Y., Dave R., Pfeffer R., Michniak B.,
Production, characterization and dissolution of Drug-Loaded Matrix from Supercritical Antisolvent Precipitation, AIChE annual meeting, San Francisco, CA, Nov 16-21, 2003.

Luo J., Gokhale A., Wang Y., Michniak B., Dave R., Pfeffer R.,
Designing of Drug Loaded Matrix by Supercritical Fluid Technology and Testing of Sustained Drug Release, American Asso of Pharma Sc conference, Salt Lake City, Utah, 2003.

Luo J., Gokhale A., Dukhin S., Zhu C., , Dave R., Khusid B., Pfeffer R., Chavez F., Debenedetti P., Jet phenomena below and above the critical points of fluid mixture with application to supercritical anti-solvent based particle formation, AIChE annual meeting, Minnesota, November 3-8, 2002.

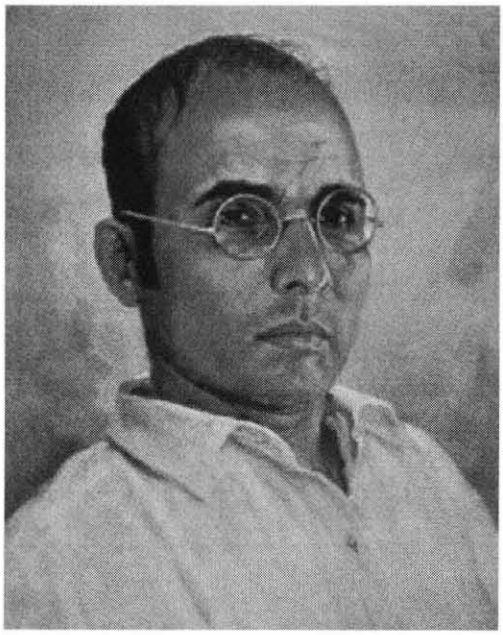

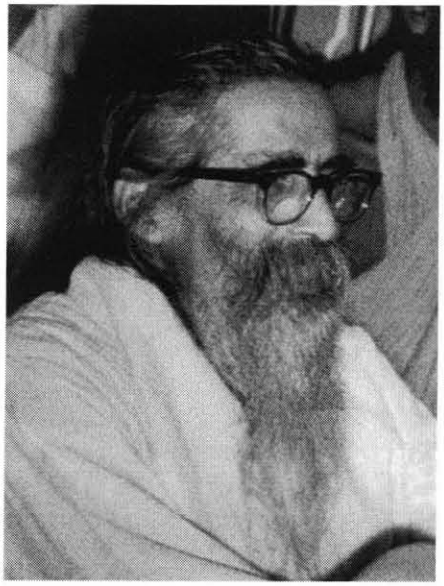

The Legends of Maharashtra

ACKNOWLEDGMENT

I take this opportunity to express my deep gratitude towards my adviser, Dr. Boris Khusid, for giving the prospects to work in the most advanced and exciting field with his excellent guidance throughout the research.

I feel very fortunate to have Dr. Rajesh Dave as my co-advisor. Without his morale and financial support it was merely impossible to do the research. I always got very constructive comments and resourceful suggestions from him because of which I could elevate the standard of my research.

I am very thankful to Dr. Edward Dreizin for taking invaluable time out of his busy schedule to give suggestions and corrections in the dissertation document. I would also like to thank Dr. Robert Pfeffer and Dr. Mirko Shoenitz for participating in my committee and giving many helpful suggestions and corrections.

During my graduate research I was fortunate to receive help from number of people Dr. Yueyang Shen, Dr. Amit Banerjee, Dr. Anil Kumar, Mike Yeksel and Jose Quevedo. I truly appreciate their assistance.

TABLE OF CONTENTS

TABLE OF CONTENTS
(Continued)

TABLE OF CONTENTS
(Continued)

LIST OF FIGURES

LIST OF FIGURES
(Continued)

LIST OF FIGURES
(Continued)

LIST OF FIGURES
(Continued)

LIST OF TABLES

CHAPTER 1

INTRODUCTION

1.1 Motivation and Objective of the Research

Jet breakup phenomenon and nanoparticles formation

Polymer nanoparticles have applications in different areas of human activities like biology, neurology such as targeted drug delivery into the brain for cancer treatment [1, 2]. Rapid developments in nanoparticles synthesis methods and the control on their properties show an optimistic picture in the development of future medicines and related products. There is a wide range of applications of polymer nanoparticles in pharmaceutical and related fields like biological labels, drug delivery systems, tissue engineering to name a few [3]. In case of drug delivery systems, biodegradable polymers have captured special attention. Biopolymers encapsulations in both targeted as well as controlled release systems are being researched. It is been observed that nano size biopolymers has better encapsulation efficiency and controlled release than micron size ones [4]. The smallest capillary in the body is around 5 μm so the particle size should be significantly smaller to avoid embolism [1, 5]. Drugs in nano size are often unstable and encapsulation of nano drug in biopolymers particles of size less than 200 nm can provide required stability and better control of drug release [6-11]. For more sophisticated targeted delivery applications, required particle size is even less than 80 nm [12]. Because of the smaller size, nanoparticles can penetrate through smaller capillaries, sustaining intracellular dexamethasone levels and deliver drugs into the tissues with stable release kinetics [13]. Particle surface becomes an important issue especially in

drug delivery when drug is attached / absorbed onto the surface [10-15]. Surface smoothness minimizes drug – carrier particle interactions resulting in more efficient drug detachment from the carrier particle surface which shows tremendous improvement in drug release efficiency [15-17].

Conventional technologies for manufacturing micrometer- and nanometer-sized polymer particles, such as dry and wet grinding and solution precipitation, do not provide the required flexibility to tailor the particle properties, as well as control the particle size distribution, morphology, and purity. Methods utilizing Supercritical Fluids for the formation of particles have the potential to overcome these drawbacks. The supercritical antisolvent (SAS) process is an emerging technology for the production of polymer particles for a wide variety of biomedical and pharmaceutical applications.

The objectives of this work are to quantify the relation between the particle formation and the jet breakup regime, and to determine the effect of solvent composition, nozzle size, and operating pressure on nanoparticle formation.

Fine particles coating and encapsulation using supercritical fluids

Another application of supercritical fluids is nanoparticles coating. Nanoparticle coatings are required in many applications to achieve desired surface properties. Conventional techniques like fluidized bed coating or dry powder coating do not provide efficient coating to an individual nano or sub-micron sized particles because of strong cohesive forces [5]. Hence, the supercritical fluid technology is investigated for nanoparticles coating. The objective of this study to compare various supercritical fluid based coating

techniques to achieve nanoparticle coating and investigate the effects of process parameters on coating and particles agglomeration.

Syneresis of silica gel

Solid or liquid propellants are widely used in conventional rockets and missiles [18, 19]. Gelled propellants are researched as an alternative to solid or liquid propellants which overcome the drawbacks associated with solid or liquid propellants. The objective of this work is to investigate the gel dynamics and to propose a strategy for modeling gel formation and syneresis. Silica gels were used as simulants for gelled propellants. Characterization of silica structure in gels was an important step to obtain the qualitative data. Supercritical fluid technique was used to extract the water from gels to get the dry silica structure.

1.2 Thermodynamic Properties of Supercritical Fluids

Nanoparticles formation and coating is investigated by supercritical fluids methods. Following are the concept and properties of the supercritical fluids.

Concepts of Supercritical Fluids:

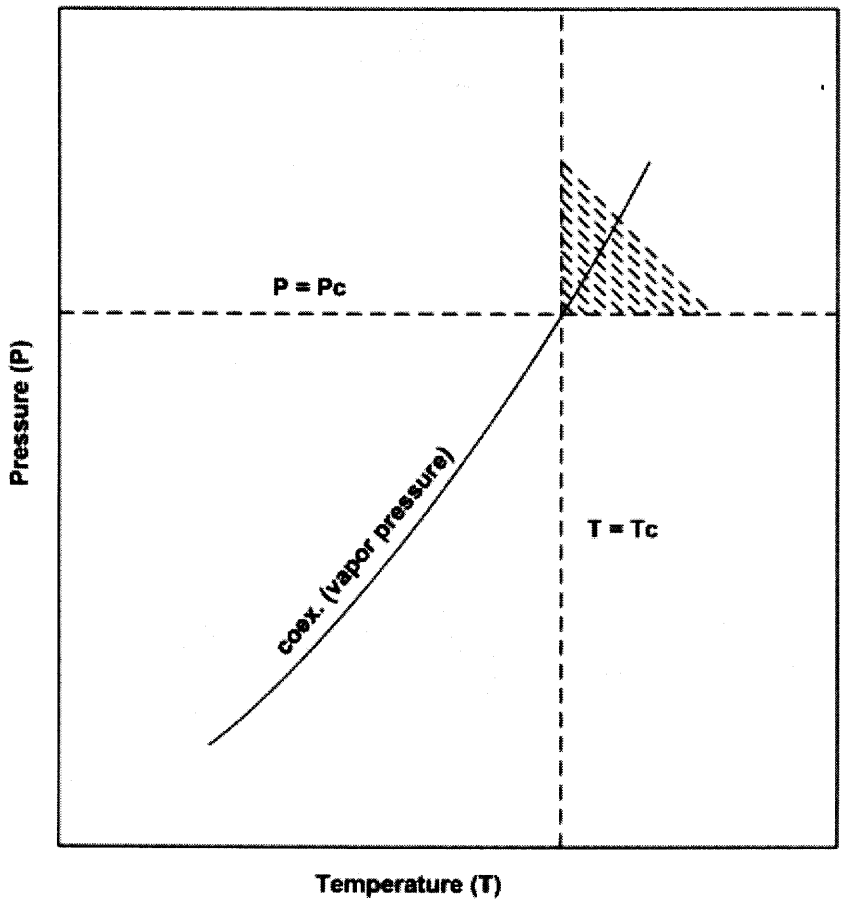

Figure 1.1 Graph of pressure - temperature. Hatch lines show supercritical region [18].

Supercritical fluids (SCF) are substances at temperatures and pressures above their critical points. SCFs have density values that enable appreciable solvation power, while the viscosity of solutes in SCF is lower than in liquids and the diffusivity of solutes is higher, which facilitates mass transfer [20]. SCFs are highly compressible, particularly

near the critical point, and their density and thus the solvation power can be carefully controlled by small changes in temperature and/or pressure. In Figure 1.1, the region in pressure (P) – temperature (T) phase space is defined where the fluid is supercritical according to the above definition, the first quadrant. In $P-T$ diagram, the vapor pressure curve indicates the conditions under which the vapor and liquid coexist and the critical point corresponds to the point where the distinction between vapor and liquid disappears [20, 21]. In Figure 1.1 the critical isotherm is indicated $T = T_c$ and critical isobar is indicated $P = P_c$. If the liquid is heated at a constant pressure exceeding the critical pressure, it expands and reaches a vapor-like state without undergoing a phase transition. This phenomenon is called as "the continuity of state" [21].

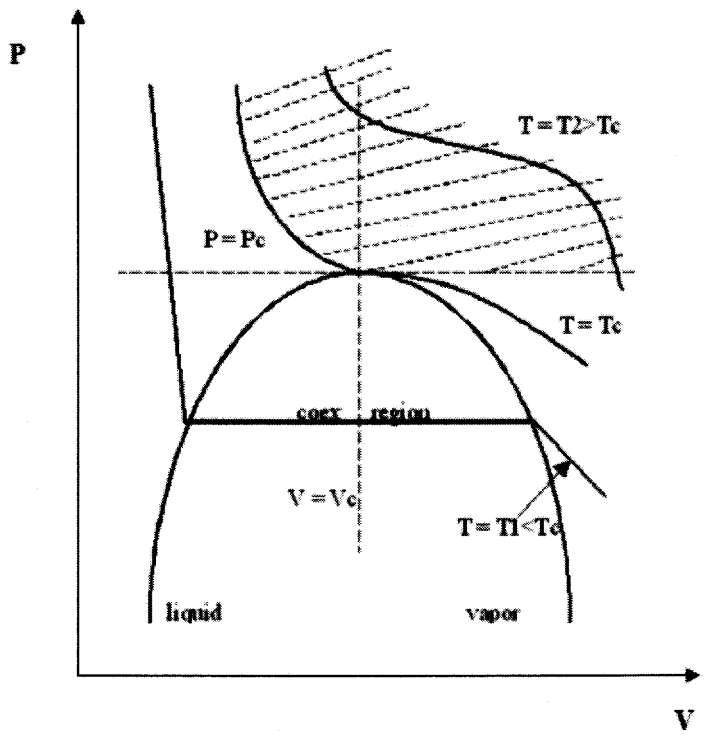

Figure 1.2 Represents pressure - volume diagram of fluid. The hatched lines show supercritical region.

Figure 1.2 represents the pressure - volume diagram of the same fluid. The region corresponds to the supercritical states in Figure 1.1. The single vapor pressure curve corresponds to a coexistence curve with two branches, one for the vapor and another for the liquid; the branches meet in the critical point where the difference between the two phases disappears. The critical isochore $V = V_c$ is indicated. Coexisting vapor and liquid states have the same pressure but different molar volume, so that the isothermal compressibility is infinite throughout the two-phase region. The critical point is the last point in two-phase region, and the only point in the one-phase region, where the compressibility is infinite. All supercritical isotherms have finite slope everywhere, but the slope may be very small (the compressibility very high) in the vicinity of the critical isochore. The critical isotherm is the first isotherm to reach zero slope which is the indication of infinite isothermal compressibility and incipient instability.

Thus, a fluid is critical when the difference between coexisting liquid and vapor phases disappears. At this point the isothermal compressibility of the one phase fluid becomes infinite. In the supercritical region, a state of liquid-like density can transform into one of vapor like-density by tuning the pressure or the temperature, without the appearance of an interface. The further from the critical point, the easier it is to manipulate the density by tuning pressure or temperature. In the Supercritical Fluids, a range of intermediate-density states can be reached which are not available at sub critical temperatures and pressures [21].

1.3 Particles Formation and Coating using Supercritical Fluids

1.3.1 Review of Particles Formation and Coating Technologies:

Various techniques for the formation of micro/nano particles and coatings are described in the literature. These techniques are divided into two categories namely dry and wet synthesis methods. Dry synthesis methods consists of jet milling, ball milling, micronizer whereas wet milling consists of solvent evaporation, emulsion/double emulsion method, spray drying, fluidized bed coating and others.

Jet Milling: In jet milling, the powder is exposed to a high speed jet of air to apply extreme pressure and friction. This method is useful for formation of micron sized particles. Wear and friction causes distortions in the particles. As there is very little control on the process, wide particles size distribution is observed in this method [22].

Ball Milling: Ball milling can be used with or without a liquid. In this method, a rotating cylinder is filled with the material to grind and balls which collide with each other and the grinding material to be ground and exert shear forces on the grinding material. This method causes lot of friction and wear in the material so is not ideal for the soft matter like biodegradable polymer. This method is useful for formation of micron sized particles or composites where the distortions in the particles due to friction is not crucial [23].

Micronizer: Micronizer, similar to the jet milling uses flow of high pressure air (or gas like nitrogen) which causes a friction in the grinding material. This method is useful to form micron sized particles where the distortions in the particles due to the friction and heat generation is not crucial [24].

All of the above methods suffer with disadvantages like heat generation due to friction, lack of control on particles size distribution [22-24]. Wet methods of particles formation or coating as described below:

Solvent Evaporation: In case of solvent evaporation, the compound of interest is dissolved in an organic phase and then the single phase solution is heated under vacuum or atmospheric pressure until the solvent evaporates. The compound precipitates from the solution in the form of particles and form aggregates. The disadvantage of this method is lack of control of particles size distribution and aggregation of particles [25].

Emulsion/Double Emulsion Method: The emulsion method is used for particles formation as well as coatings. For the compounds which are not soluble in water, in the emulsion method, a compound of interest is dissolved in an organic solvent. The solution is then dispersed in an aqueous media containing surfactant. The precipitated particles are then vacuum dried. If the compound is soluble in water, the aqueous media is replaced by a solvent in which the compound of interest is not soluble [26]. A double emulsion is similar to emulsion method. In double emulsion method, multiple emulsions are employed. The primary emulsion is added into the aqueous solution containing surfactant and subjected to mixing. The particles are then collected by filtration and then vacuum dried. These methods are commonly used for formation of drug particles as well as coating of particles. Compared with emulsion method, double emulsion has higher coating efficiency. This method is useful for micron as well as sub-micron sized particles formations. Individual coating is submicron sized particles is not possible to achieve in this method. Also, solvent removal and excessive use of solvents are disadvantages associated with this method [26].

Spray Drying: The spray drying is widely used for micron sized particles formation for active pharmaceutical ingredients (API). The compound of interest is dissolved in an organic solvent. The solution is then sprayed through a nozzle into a chamber having higher temperature (typically above boiling point of the organic solvent). The particles are collected at the bottom of the chamber. Spray drying is used for particles formation as well as coating. It is widely used in the pharmaceutical and neutraceutical industry for preparation of micron or sub-micron sized drug particles [27].

Fluidized Bed Coating: The fluidized bed coating is used to coat micron sized particles. The host particles are suspended in the gas flow and then the solution containing coating material is introduced. The solvent evaporated in the gas and coating material precipitated on the host particles coating them. This method is very useful to achieve uniform coating. However, individual coating of the host particle 5 micron size is not possible with this method [28].

1.3.2 Review of Particles Formation and Coating Using Supercritical Fluids: Two main principles based on supercritical carbon dioxide for microsphere production can be distinguished, namely its use as solvent or as anti-solvent. In the RESS (rapid expansion of supercritical solutions) and SFN (supercritical fluid nucleation) a polymer solution in a supercritical fluid is expanded across a nozzle at supersonic velocities, leading to instantaneous particle formation by precipitation. Again, SFN can be subdivided into various techniques like gas as antisolvent (GAS), supercritical as antisolvent (SAS), aerosol solvent extraction system (ASES), particles from gas saturated solution (PGSS), and solution enhanced dispersion by supercritical fluids (SEDS) [29, 30].

Rapid Expansion of Supercritical Fluid Solution (RESS):

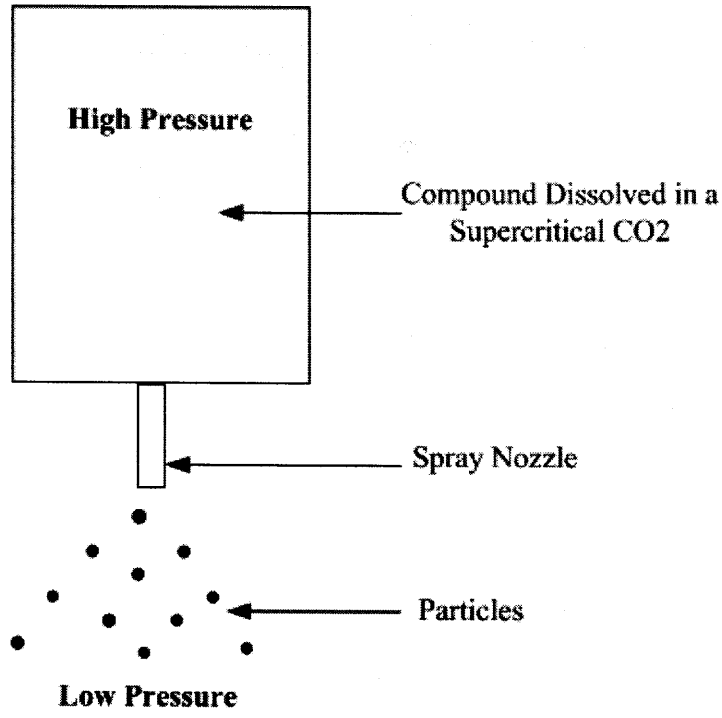

Figure 1.3 Particles formation using RESS.

RESS process is favorable for the compounds which are soluble in supercritical CO_2. The compound of interest is first dissolved in SC CO_2 and then the supercritical fluid solution expands rapidly through a capillary or orifice nozzle, to a low pressure and low temperature state, which leads to a very high supersaturation at an ultra-short time interval of about 10^{-7} s. The steep increase of supersaturation and rapid density drop leads to the outburst of homogeneous nuclei, and ultra-fine particles with a narrow size distribution are expected to form [30].

J. Tom and P.G. Debenedetti [31] reviewed the developments in RESS process. He reviewed the fundamentals, experimental methods, and applications of the process and summarized the available results of research conducted till 1990. The focus of RESS

processing was on formation of ceramics, organics, pharmaceuticals, and polymers particles. In the review, the theoretical developments to understand the phenomena of particle formation were also studied. The effects of operating parameters on particles properties were summarized. Two main conclusions were drawn from the review. First, the potential of the RESS process to reduce particles size and feasibility of production of drug loaded biopolymers were clearly shown. Secondly, the limited productivity with RESS process because of limited solubility of the materials in supercritical fluids was underlined in the conclusions.

P.G. Debenedetti et al. [31] studied the formation of polylactide acids using RESS process. The focus of this investigation was to form drug loaded polymer particles which could be used for sustained release. Effects of operating parameters on the particles formation was investigated in the research. Formation of polysaccharide (HYAFF-11) was investigated by L. Benedetti et al. [32]. The emphasis was on production of micron sized polysaccharide particles. Increased process pressures and temperatures e.g. 250 bar and 60C-80C respectively were used. Micronized and spherical shaped particles with 10μm size were formed. At lower temperature e.g. 40C, no particle formation was observed. Similarly, synthesis of polyethylene glycol and polyoxyalkylenealkylphenyl ether microspheres using supercritical carbon dioxide was investigated by K. Mishima et al. [33]. A.K. Lele et al. [34] investigated the formation of polycaprolactone, poly(methylmethacrylate) and a styrene / methyl methacrylate. Such operating conditions as temperature, nozzle inner diameter and pressure were found to affect the morphology of precipitated polymers. High temperature, high polymer concentration, low pressure or low capillary L/D ratio enhance the formation of high aspect ratio fibers, while opposite

conditions were found to favor the formation of spherical particles of micron size. Based on one-dimensional compressible flow calculations using an equation of state for pure solvent, it was proposed that the fiber formation occurs when a polymer rich phase is rejected from solution in the entry region to the capillary. The location of precipitation was found to be crucial in determining the characteristic time scale for the density reduction process. The solubilities of polymer compounds in carbon dioxide were often enhanced by adding organic co-solvents like acetone and ethanol.

Recently, several papers on use of RESS process for particle coating were published. Because only small amount of coating material is in proportion to the host material, the low productivity of the RESS process arising from the low solubility of polymers in supercritical fluids is not a significant drawback. For coating applications, the traditional volatile organic solvents are not completely replaced, but their amounts are reduced with carbon dioxide, thereby reducing the negative impact on the environment [35]. G. Tepper et al. [36] investigated the deposition of poly(dimethylsiloxane) films onto a sensing surface of a micro fabricated transducer using supercritical carbon dioxide as a solvent. These transducers were aimed at developing chemical sensors such as surface acoustic wave (SAW) devices, for which uniform thin deposition of the polymer layer is crucial. J.L. Fulton et al. [37] researched the coating of complex geometries such as cardiovascular stents with fluoroacrylate polymers using an electrostatic RESS technique. Polymer nanoparticles were formed by RESS process and these gas-phase particles were charged using a high voltage to the expansion nozzle. By this method, the charged nanoparticles were deposited on a solid surface forming uniform coatings with thicknesses from tens of nanometers to several micrometers. A unique aspect of this

process is that the small charged nanoparticles can be deposited on to electrically conducting microscopic regions with a spatial resolution better than 50 nm. Y. Chernyak et al., [38] reported the formation of droplets of perfluoropolyether diamide from carbon dioxide solutions for coating of porous materials encountered in historic and civil infrastructures. The effects of polymer concentration, pre-expansion temperature and pressure, and the nozzle geometry (length and diameter of capillary) on the spray characteristics and droplet size distributions were examined. Glebov et al. [39] investigated the coating of fused silica substrates and aluminum and magnesium powders by poly(vinylidene fluoride) and poly(4-vinylbiphenyl) using SC CO_2. The polymers were initially dissolved in carbon dioxide at high temperature and precipitated onto metal particles upon cooling and subsequent depressurization. The thickness of polymer films was evaluated using UV absorption spectroscopy revealing an average thickness in the range 1-30 nm.

The RESS process was modified to increase the solubility of polymers and other compounds in SC CO_2. The first method includes use of organic solvents to increase the solubility. K. Matsuyama [40] used ethanol as a cosolvent (up to 30% ethanol in carbon dioxide by weight) to dissolve polystyrene-b-(poly(methyl methacrylate)-co-poly(glycidyl methacrylate)), polyethylene glycol, bisphenol epoxy resin, PMMA, and poly(oxyalkylene) alkylphenyl ether in carbon dioxide. The mixtures were rapidly expanded to form micron sized particles. The co-solvency effect was utilized, that is the solubility of polymer is extremely low in either carbon dioxide or ethanol but becomes higher in a mixture of the two. Because ethanol is non-solvent for the polymers, dry powders of polymer could be obtained upon precipitation from the supercritical mixtures.

Y. Wang et al. [41] used a modified RESS process for coating of glass beads with poly(vinyl chlorideco-vinyl acetate) and hydroxypropyl cellulose using carbon dioxide with acetone as a cosolvent. In that study, the pressure and temperature of post-expansion stream (instead of pre-expansion stream) were regulated to control the resulting morphology. The coating of glass beads with polyvinyl chloride-co-vinyl acetate (PVCVA) and hydroxypropyl cellulose (HPC) was successfully achieved using this technique. It was found that the use of a cosolvent can improve the solubility of polymers and also affects the degree of crystallinity of the polymer coating. J. Shim et al., [42] synthesized poly(2-ethylhexyl acrylate) suspension in carbon dioxide using a siloxane-based surfactant as a stabilizer. The high-pressure mixture was rapidly expanded into water containing a hydrophilic surfactant to form stable aqueous latexes, which can be used for coatings and adhesives. S. Han et al. [43] used propane as a supercritical fluid to dissolve both isotactic polypropylene and ethylene-butane copolymers. The RESS process of the binary mixtures produced the blend of the two polymers with the resulting morphology of microfibers and a trace of microparticles. It was concluded that the phase domain size of ethylene-butene copolymer in the blends decreased as the content of ethyl branches in the copolymer increased.

RESS process is relatively easy to implement and simple at a small scale when a single nozzle can be used. But to form larger number of particles, it needs to have a multi nozzle device instead of single nozzle, which makes it costly and difficult to maintain. Instead of using multi nozzle, one can use a porous sintered disk through which pulverization occurs. However in both the cases, particle size distribution is not easy to control, and it may be much wider than in the case of a single nozzle. Moreover, particle

harvesting is complex, as it is in any process leading to very small particles. The biggest limitation of RESS development lies in the too low solubility of compounds in supercritical fluids, Its application is restricted to products that present a reasonable solubility in supercritical carbon dioxide (low polarity compounds) [44, 45].

Particles from Gas Saturated Solution (PGSS):

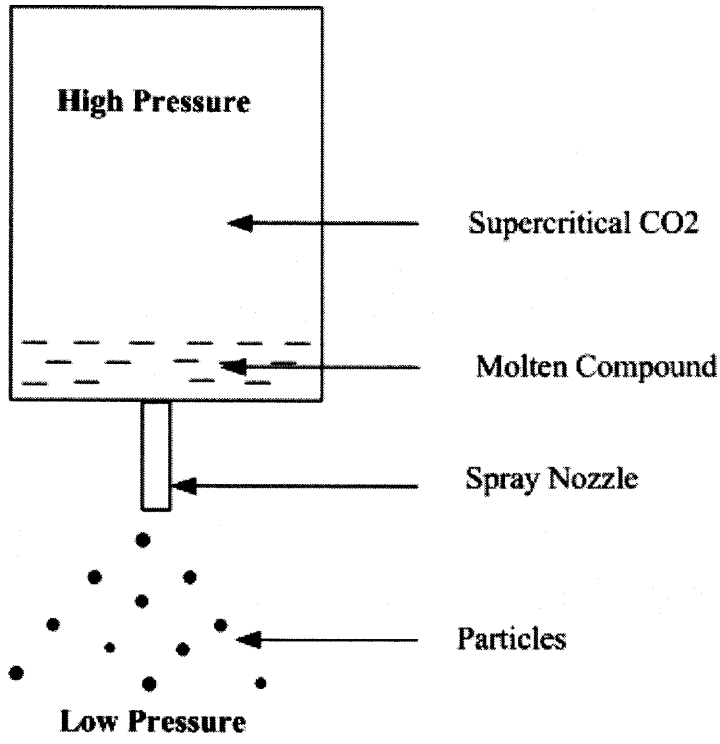

Figure 1.4 Particles formation using PGSS.

This process consists of dissolving the supercritical CO_2 into a molten polymer or compound and then the mixture is rapidly expanded through a capillary nozzle causing formation of solid particles [46, 47]. As the solubility of compressed gases (such as CO_2) in liquids and solids like polymers are usually high, and much higher than the solubilities of such liquids and solids in the compressed gas phase, the process consists of solubilizing supercritical carbon dioxide in melted or liquid-suspended substance(s),

leading to a gas-saturated solution / suspension that is further expanded through a nozzle with formation of solid particles. This process allows one to form particles from a great variety of substances that need not be soluble in supercritical carbon dioxide, especially with some polymers that absorb a large concentration (10–40 wt. %) of CO_2 that either swells the polymer or melts it at a temperature much below (~10–50°C) its melting/glass transition temperature [46, 47]. This process can also be used with suspensions of active substrate(s) in a polymer or other carrier substance leading to composite microspheres.

J. Kerc et al. [48] researched formation of poorly water-soluble nifedipine, felodipine and fenofibrate particles using the PGSS technique. Nifedipine was micronized at temperatures and pressures in the range of 165-185^{0}C and 100-200 bar, respectively. The average particle size of nifedipine was decreased to 15μm. In order to avoid agglomeration and thermal degradation of micronized nifedipine at high temperature (~185^{0}C), a hydrophilic polymer was added to lower the melting point as well as to enhance the dissolution rate. By increasing the pre-expansion pressure, the average particle size was reduced and dissolution rate of nifedipine was improved. The unprocessed and processed felodipine had the average particle size of 45 and 60 μm, respectively. Due to the very low wettability of the compound, both the unprocessed and micronized felodipine exhibited low dissolution rates of 0.26 and 0.29 mg/L after 1 h in pure water [49].

In this study, J. Morley et al. [50] investigated the feasibility of the PGSS process for the micronization of cyclosporine. Prior to the PGSS experiments, the phase behavior of cyclosporine in CO_2 was determined to find the feasible conditions for each process. The solubility of the SCF in the solute phase increases as the pressure increases. This

results in lowering the phase transition temperature such as melting or glass transition temperature. If the solubility of SCF into the solute phase is high, the melting point depression is significant. Melting point depression has been observed in several binary systems such as CO_2 - naphthalene and CO_2 - ibuprofen [51].

Micron-sized cyclosporine particles were successfully produced by PGSS technique by A. Tandya [52]. After micronization, the average particle size of cyclosporine precipitated was found to be less than 1 μm, which represented a 97% reduction compared with the processed cyclosporine. No significant change in the morphology and particle size was observed with respect to the extraction temperature and pre-expansion pressure, whilst an increase in nozzle diameter resulted in a slight increase in particle size and decrease in degree of aggregation. However, changes in the nozzle diameter resulted in the production of porous precipitates with larger particle size. The degree of crystallinity of cyclosporine was significantly reduced by the PGSS process.

PGSS is very easy to install, operate and maintain. It has low processing costs, and the very wide range of products that can be treated, opening wide avenues for development of PGSS applications, in spite of limitations related to the difficulty to monitor particle size [45].

Supercritical Fluid as Antisolvent (SAS):

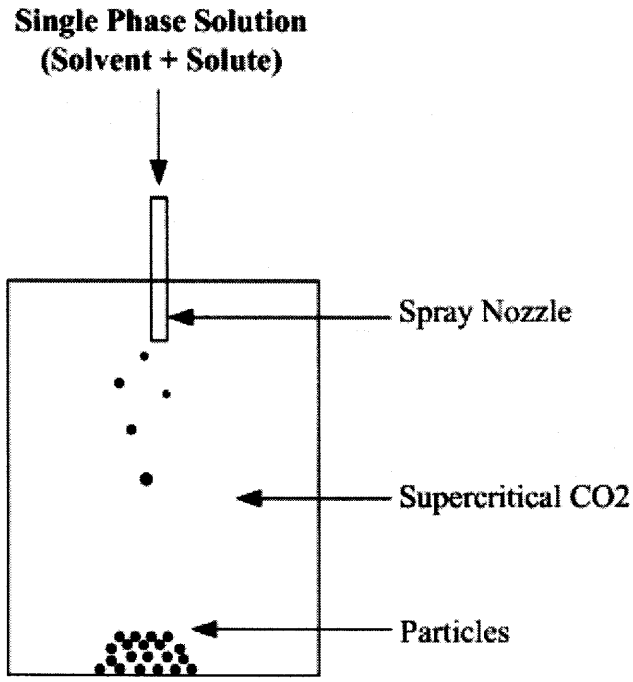

Figure 1.5 Particles formation using SAS.

In this method, the solvent power of a liquid solvent in which the compound of interest is dissolved is decreased by saturating it with carbon dioxide in supercritical conditions, causing the substrate precipitation or recrystallization. A batch of solution is expanded by mixing it with a dense gas in a vessel. Due to the dissolution of the compressed gas, the expanded solvent has a lower solvent strength than the pure solvent. The mixture becomes supersaturated and solute precipitates in micro or nano particles. CO_2 is kept flowing through vessel to ensure that obtained particles will become dry [45, 53, 54]. This process has a good control on the properties and composition of the particles with a great flexibility and for almost any kind of compounds.

E. Reverchon et al. [55] studied the effects of operating parameters on biodegradable polymer particles, like dextran and insulin together with

poly(hydroxypropylmethacrylamide) (HPMA) and poly lactic acid (l-PLA). Dimethyl sulfoxide (DMSO) and methylene chloride (DCM) were used as organic solvents for these polymers. Spherical microparticles of the biopolymers were formed. The paper concluded that even though there is an effect of the experimental variables, such as concentration, pressure and temperature, on particle size and morphology, the primary factors influencing the outcome are the properties of the specific polymers being processed. M. Sarkari et al. [56] studied the formation of linear polylactic acid (l-PLA) particles using not only carbon dioxide but also carbon dioxide-philic fluorinated liquids (HFE-7100), vertrel (decafluoropentane), and traditional organic liquids (ethanol and hexane) as antisolvents in SAS process. The liquid antisolvents were selected by considering the solvent polarity. The solutions of l-PLA in methylene chloride were sprayed through a nozzle into carbon dioxide at high pressure as well as into the liquid antisolvents at atmospheric pressure.

A. Breitenbach et al. [57] investigated the relationship between the morphology of SAS processed biopolymers and their physical properties. Unlike earlier studies that were focused on either modifying the flowing modes of the polymer solution and the antisolvent, or on changing the experimental conditions in order to achieve a target morphology (mostly microspheres) of existing biopolymers, that study was focused on modifying the chemical and physical properties of biopolymers in order to obtain the spherically shaped microparticles precipitated in a given antisolvent process. The linear polyesters (l-PLA and dl-PLA) and branched polyesters prepared with a polyvinyl alcohol (PVA) were synthesized and subjected to the SAS process. It was found that the high degree of polymer crystallinity was the key factor for successful microsphere

formation. Similarly, B. Shekunov et al. [58] investigated the structural changes and plasticization effect of l-PLA particles to understand the mechanism of precipitation and particle agglomeration. The tendency of the biopolymer particles to form agglomerates was explained by a combination of a kinetic mechanism during nucleation and a slower process of structural changes occurred after the nucleation. It was concluded that with optimization of the process conditions such as nucleation rate, solution viscosity and quality of the solvent for polymer it was possible to control the agglomeration.

In recent years, several papers are published with the focus on hydrodynamic and thermodynamic effects of the process on the particles formation. J. Werling [59, 60] presented a model for mass transfer between the solvent and surrounding supercritical fluids. Two different sets of operating conditions were investigated. The first condition for the model was considered as a supercritical with respect to the pure antisolvent, but subcritical with respect to the solvent - antisolvent mixture. Hence, the two phases were present during the particles formation process. The second condition was considered above critical point of mixture. It was concluded that for the low molecular weight solutes, solute concentration in the solvent does not play crucial role in particles morphology as the crystallization kinetics for low molecular weight solutes are much faster than the mass transfer process. However, for the high molecular weight solutes like polymers, the nucleation kinetics might be slower and hence the solute concentration in the solvent dictates the region of phase diagram in which precipitation occurs, affecting the morphology of the particles. The difference in droplet behavior at subcritical and supercritical conditions has implications for particle production using SAS. Supercritical conditions result in faster mass transfer resulting in higher degree of droplet

supersaturation in the presence of a solute, resulting in higher nucleation rates and smaller particles. It was also concluded that solvent–antisolvent mass transfer alone does not determine particle size and morphology. Jet hydrodynamics, which determine the spray characteristics, and the nature of the solute, which determines the phase behavior and the nucleation and growth processes, also influence the final product characteristics.

E. Carretier et al. [61] investigated the hydrodynamics effects on particles morphology. The precipitation vessel was considered as a well-mixed reactor auto agitated by the sprayed liquid phase, and the residence time distribution of the polymer solution in the vessel was experimentally measured. It was found that the particle morphology changed from fibrous to spherical as the liquid flow rate increased. The direct visualization of the spraying process, correlated with the particle morphology, allowed for an estimation of the l-PLA precipitation time, which turned out to be in the order of few milliseconds. J. Badens et al. [62] investigated the jet breakup regimes of solvent jets and derived a new correlation between the jet Reynolds number and the Ohnesorge number. The co-relation would be used to identify the transition to atomization regime.

Majority of the research is focused on biopolymers for pharmaceutical applications. There is an acceleration of investigations for deeper understanding of the particle formation mechanism, and the influence of factors such as the hydrodynamics of mixing, particle precipitation kinetics, phase separation path, and clearly the influence of polymer properties on the end-morphology.

1.4 Applications of Supercritical Fluids

As supercritical fluids exist in a single phase with several advantageous properties of both liquids and gases, SCFs have numerous applications in various fields; few of them are discussed here briefly.

1.4.1 Pharmaceutical Industry

Supercritical fluid technology is very attractive for manufacturing therapeutic particles, either of pure active compounds or mixtures of excipients and active compounds. Drug formulation and particle design using supercritical fluids can be operated by several different processes, the choice between them depending on the aimed particle structure, morphology and size distribution, opening new ways for solving drug delivery problems [45]. Active Pharmaceutical Ingredients (API) generally possess low melting temperature and lower stability in amorphous form. To avoid the thermal degradation, it is important to keep the process temperature lower than the melting temperature of API. SCF processing facilitates the lower processing temperature and single step production including encapsulation with expedients [46].

Supercritical processes can produce micro or nano sized particles with narrow size distribution and can also be used to achieve micro encapsulation, surface coating of an active substance particle with a polymer or co-crystallization with excipients. The bioavailability of pharmaceutical molecules depends on their absorption by the gastrointestinal tract, which is governed by their dissolution and membrane permeation rates. Micronization techniques, and especially those using SC CO_2, can lead to an increase in the specific surface area can significantly contribute to this improvement in

bioavailability [63]. The development of dry powder inhalers (DPI) in which the drug is directly delivered to the lungs requires also fine powders with a mean particle size in the range of 2 to 5 μm. Microencapsulation, coating and formation of composite particles are also extremely desirable for controlled delivery systems [63].

1.4.2 Food Industry

In recent years, there has been a growing interest in functional foods because they can provide physiological benefits additional to nutritional and energetic, as, for instance, antihypertensive, antioxidant or anti-inflammatory [64]. A functional food can be defined as a food that produces a beneficial effect in one or more physiological functions, increases the welfare and/or decreases the risk of suffering a particular disease. Furthermore, new types of products, derived from food have recently been developed. These products, usually employed as food supplements, are marketed as tablets and pills, and can provide important health benefits [64].

Functional foods are obtained from traditional foods enriched with an ingredient able to provide or promote a beneficial action for human health. These ingredients are called functional ingredients. These ingredients are preferred by consumers to have a natural origin (i.e. non-synthetic origin) being commonly extracted from natural sources, such as plants, food by-products. These types of marine sources are receiving much attention, mainly because of their contents of functional ingredients, such as polyunsaturated fatty acids [65, 66], b-carotene and other pigments (antioxidants) [67, 68] sulphated polysaccharides (antiviral), and sterols (antimicrobials). Among different compounds with functional properties, antioxidants are the most widely studied [67, 69].

These compounds can play an important role in food technology because of their usefulness against lipid peroxidation. Usually, food production, process and storage can generate important losses of endogenous antioxidants that limit their own protection against lipid oxidation. Moreover, the important role of antioxidants in human health has been demonstrated, thus increasing the interest in such products and their demand by consumers [70].

The traditional extraction methods used to obtain these types of products have several drawbacks: they are time consuming, have lower selectivity and low extraction yields. Moreover, these traditional techniques employ large amounts of toxic solvents. At present, extraction methods able to overcome the above-mentioned drawbacks are being studied; among them, supercritical fluid extraction (SFE) and subcritical water extraction (SWE) are among the more promising processes [71]. These extraction techniques provide higher selectivities, shorter extraction times and do not use toxic organic solvents. Numerous vegetable matrices have been used as natural sources for compressed fluid extraction. Legumes, spices, aromatic plants, and even fruit beverages, such as natural orange juice [72] have been processed to obtain natural antioxidant compounds.

1.4.3 Chromatography (SCFC)

The benefits of using SCFs are their liquid-like densities offering higher solubility and increased column loading. They have low viscosity and are highly diffuse enabling faster separation and extraction. The reduction in the use of organic solvents has cost, health, and safety benefits as well as faster (cleaner) sample recovery during experimental procedures.

This would be the method of choice for compounds that are not easily amenable to gas chromatography (GC) or liquid chromatography (LC) separation. W. Shen et al. [73] obtained the separation of tetrabutyltin and tetraphenyltin using carbon dioxide and a SB Octyl 50 capillary column (50 mm i.d., 195 mm o.d., 0.25 mm film thickness and 2.5 m length). The chromatographic conditions for the separation were optimized in the univariant mode by evaluating the effect of isobaric pressure, pressure ramp and hold time in the pressure program. Base-line resolution for the mixture of tetraorganotins was obtained when the initial pressure of 100 atm was held for a minute followed by a pressure ramp of 80 atm/min to a final pressure of 200 atm. That paper also showed the capability of SCFC to obtain multi-element chromatograms by monitoring the same element at different isotopes.

N. Vela and J. Caruso [74] used SCFC for the speciation of tetra and triorganotin compounds utilizing a SB biphenyl capillary column and carbon dioxide mobile phase. Parameters in SFC such as hold time, carbon dioxide pressure program, mobile phase composition and column length are optimized for a mixture containing tetrabutyl tin (TBT), tributyltin chloride (TrBT-Cl), triphenyltin chloride (TrPT-Cl), and tetraphenyltin (TPT). Detection limits for these organotin are 0.26, 0.80, 0.57 and 0.20 pg, respectively, with linear dynamic ranges of three orders of magnitude.

1.5 Organization of Chapters

Jet breakup phenomenon and nanoparticle formation

Analysis presented above of the current state of supercritical antisolvent (SAS) technology reveals that the problems in the technology are related to formation of nanoparticles and nanocoatings with control on the physiochemical properties. Based on the analysis of the existing literature, directions for experimental and theoretical approaches for SAS development to address some of the above listed problems form the main parts of this dissertation.

To understand the SAS process completely, it is important to study the solution jets hydrodynamics, droplets formation and mass transfer which lead to particles formation. In second chapter the jet breakup and droplet disappearance phenomenon was studied using high speed CCD camera coupled with double shot Particle Image Velocimetry (PIV) laser. The experiments are conducted just above the critical point of mixture. Various solvents, combination of solvents and PVP solutions are used to record the jet breakup phenomenon. The nanoparticle formation is studied using solutions injected through various capillary nozzles sized between $10\mu m$ to $127\mu m$. Polyvinylpyrrolidone (PVP) is used as a model biopolymer. Effects of operating parameters like solution flow rate, pressure, capillary nozzle sizes and molecular weight of the polymer on particles are investigated. Various characterization techniques like scanning electron microscopy (SEM), photon correlation spectroscopy (N4 Plus), Fourier transform infrared spectroscopy (FTIR) and the image processing software - Sigmascan Pro (version 5) are used to investigate the particles properties. A poor solvent concept is used to achieve better particle properties.

Fine particles coating and encapsulations using supercritical fluids

In certain applications, particle surfaces need to be modified or functionalized by coating them with another material to serve a specific purpose. As nanoparticles are extremely cohesive, it is very difficult to coat an individual particle by traditional methods. In third chapter, coatings on nanoparticles are investigated using various Supercritical Fluids techniques like SAS, RESS and PGSS. In SAS techniques, ultrasonic nozzle is used to generate a spray of the solution to facilitate the faster mass transfer. RESS and PGSS are *solvent free* techniques and are very easy to scale up. Different sizes of silica ranging from $180nm$ to $2\mu m$ are used as host particles and polymethyl methacrylate (PMMA), polyethylene glycol (PEG) and polyvinyl fluoride (PVDF) are used as guest materials. The effects of operating parameters on coatings and degree of agglomeration are investigated using various characterization techniques.

Syneresis of silica gel

In fourth chapter centrifuging experiments are conducted on water-based silica gels provided by CFD Research Corp. (CFDRC). Centrifuging of gels over a broad range of accelerations is used for measuring the dynamics of syneresis. The supercritical water extraction in liquid carbon dioxide and the Oxygen-17 NMR relaxation are employed for the quantification of gel structures and the particle-water interactions. The proposed multiscale computational strategy for simulating gelled propellant systems combines Brownian dynamics modeling of the gel formation and a continuum approach for the syneresis dynamics. Parameters needed to model the gel formation will be measured using the supercritical solvent extraction and the Oxygen-17 NMR relaxation.

CHAPTER 2

JET BREAKUP PHENOMENON AND NANOPARTICLE FORMATION

Supercritical Antisolvent Precipitation (SAS) process has been developed for last two decades and applied to several new generation drug molecules and other pharmaceutical products [75]. Its strong potential for forming nanoparticles has been widely proved and the current challenge is to control characteristics such as the particle size, the particle size distribution, polymorphic nature etc [75]. In this process, the solution containing compound of interest dissolved in an organic solvent is injected into the supercritical fluid (e.g. SC CO_2). The organic solvent and SC CO_2 are miscible into each other but the compound is not soluble into SC CO_2. Hence, once the solution comes into the contact with SC CO_2, the organic phase evaporates into SC CO_2 and at the same time SC CO_2 diffuses into the solution. The simultaneous mass transfer between SC CO_2 and organic solvent supersaturates the solute, which then precipitates out of the solution. Capillary nozzles with inner diameter varying from 127 μm to 504 μm are most commonly used to inject the solution into SC CO_2 [76, 77]. As the solutions form jets in the SC CO_2 in this process, a good control of such processes requires the knowledge of the mechanisms of solution jet disintegration and the mass transfer kinetics between the jet and the antisolvent phase.

2.1 Experimental Procedure for Jet Visualization Study

Experimental setup used to investigate the jet breakup phenomenon is shown in Figure 2.1. This setup consists of a high-pressure view cell and a high speed CCD camera coupled with a double shot PIV laser. The view cell consists of a square (cross-sectional area of 12.7mm × 12.7mm) high-pressure view cell of 75 ml in capacity (Jerguson Gauge, T19-32) having front and back double-sided sapphire windows (320mm × 16mm). The view cell can withstand pressures up to 200 atm (3000 psi) and temperatures up to 200^{0}C.

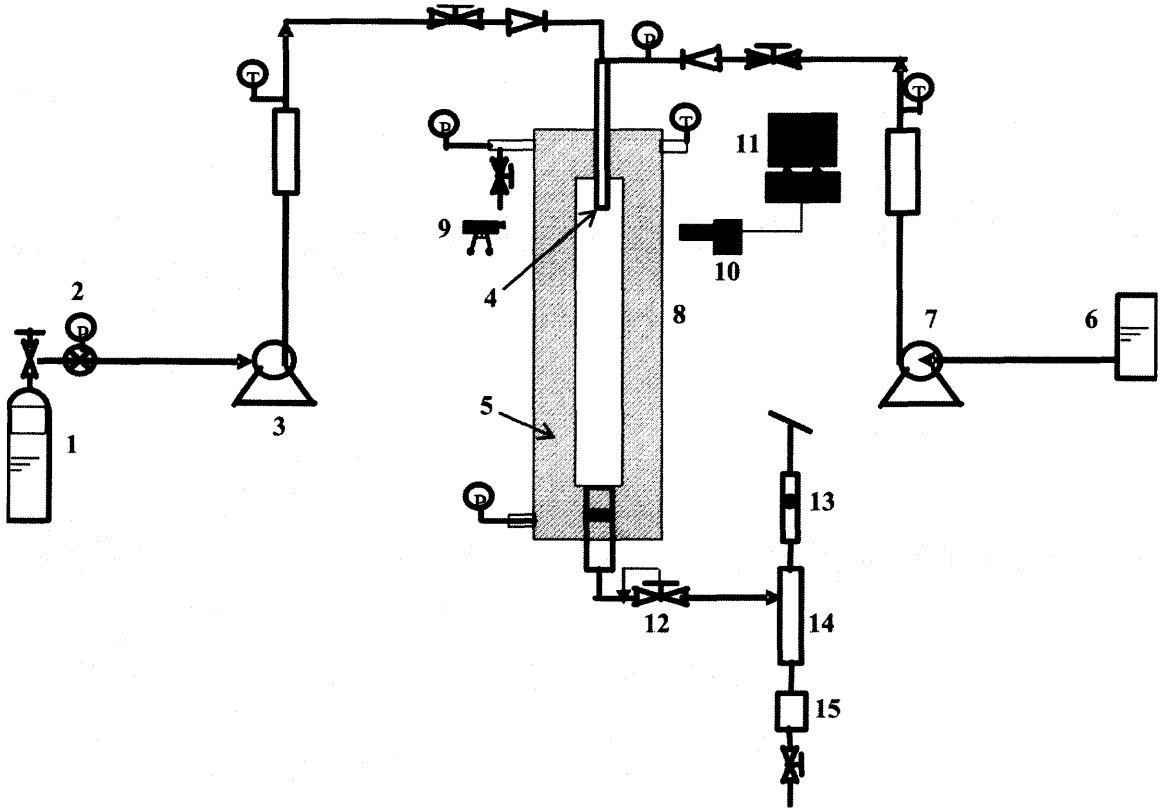

Figure 2.1 A setup for the visualization of the jet patterns.
1. CO cylinder, 2. high pressure regulator, 3. CO2 pump, 4. capillary nozzle, 5. high pressure view cell, 6. solution tank, 7. solution pump, 8. heating tapes, 9. double shot PIV laser, 10. high speed CCD camera, 11. computer

The visualization system comprises of microscope lens (Edmund Industries), a CCD camera (Flow Master, LaVision), a computer with image capture software (Davis 6.2, LaVision) and an Nd:YAG dual cavity pulsed laser (Solo III, New Wave Research)

that produces double shots with an exposure time. The images have a pixel resolution of 1280 × 1024 per frame.

A relatively large difference in refractive indices between the solution (about 1.36) and CO_2 (1.05 - 1.25, depending on the density) allows for visualization of the jet patterns with a resolution of several microns. A high pressure-metering pump (Prep 100, Scientific Systems) is used to inject a solvent or a polymer solution into supercritical CO_2 through a micronozzle (inner diameters of micronozzles varies from $10\mu m$ to $127\mu m$) following a 15-min injection of CO_2 into the view cell from a CO_2 cylinder. The view cell is equipped with heating pads (SRFG-512 and FGH051-060, Omega) and a thermocouple (SMPW-T-M, Omega) to maintain it at a given temperature. The CO_2 and solution buffers are wrapped in heating tapes (SS316L-50DF4-150, Swagelok), equipped with thermocouples (SMPW-T-M, Omega) and are maintained at a given temperature by proportional-integral-derivative controllers (D85011, Dwyer). The setup was wrapped with an insulating tape to reduce heat loss. The view cell was equipped with pressure gages (Matheson Gas Company) to monitor compressed CO_2 at a desired pressure. The flow rate of CO_2 through the view cell is measured with a rotameter (VA 22440, Dwyer) and a cyclone separator located after the backpressure regulator is used to recover solvent accumulated in a collector.

The total volume of the pressurized system is large enough to collect about 50 images of the well-developed jet pattern (in about 20 sec) using the high-speed CCD camera while keeping the addition of a solvent to the chamber atmosphere negligibly small. About after 20 sec, the chamber saturates with the liquid so the jet images are taken only for first 20 sec. Typically 20 images were used to measure the jet length

utilizing the image analysis software Davis 6.2 (LaVision) provided with the camera. After each run, the pump is purged with a solvent to remove polymer residues left inside and the view cell is purged of CO_2 mixed with solvent vapor.

2.2 Jet Breakup Phenomenon for Solvents and Solutions

When the solvent or the solution is injected through a capillary nozzle, various models of jets are observed depending upon the liquid-liquid or liquid-gas system or other operating conditions [78]. These regimes are categorized as (i) the dripping regime, in which the droplets are formed at the outlet of the capillary nozzle; (ii) the laminar regime, in which the jet has a smooth and continuous aspect before a break-up zone where there is quasi-periodic emission of droplets identical in size; and (iii) the turbulent regime, in which the jet surface presents irregularities and the resulting droplets have different sizes [78].

The appearance of the unstable modes of laminar jets is under the control of the competing processes affecting on the jet. The capillary, inertial, aerodynamic and viscous forces are involved whereas gravity effects are neglected. For the lower Reynolds numbers, the first mode observed for a laminar jet is characterized by axially symmetrical disturbances, named varicoses, producing the jet break-up. The first theory on the mechanism of drop formation resulting from an axisymmetrical jet has been proposed by Rayleigh [79]. The Rayleigh analysis assumes that surface tension is the chief force controlling the break-up of an axisymmetrical jet. Weber extended Rayleigh's theory to the break-up of a viscous jet, when both viscous and inertial forces offer significant resistance [80]. For higher Reynolds numbers, the inertial forces compete with the capillary forces. The jet breakup zone follows a lateral motion with increasing amplitude, which leads to the formation of an asymmetrical jet, which can be either sinuous or helicoidal. When the flow rate goes beyond a certain value, the aerodynamic effects become quite strong and the jet is atomized.

Regardless of the type of flow, disintegration or atomization are favored by air friction and the break-up distance decreases as the pressure increases [81]. A laminar jet can be characterized by: (i) the jetting velocity (velocity at the transition from the dripping to the laminar jet regime), (ii) the jet length (length of coherent portion of liquid jet) or break-up length, (iii) the critical jet velocity (velocity at the atomization transition). When a liquid jet is dispersed in a low density fluid, the breakup mechanism depends on the jet diameter, jet velocity, liquid density, interfacial tension and viscosity. The break-up mechanism can be predicted using dimensionless numbers: the Reynolds number and the Ohnesorge number ($Oh = We^{0.5} / \mathrm{Re}$). At atmospheric pressure, empirical correlations can be used to classify the jet disintegrations. The Ohnesorge chart describes the dispersion modes as a function of the Reynolds number and the liquid properties [82]. Three different zones are distinguished: the Rayleigh break-up zone, a second zone where the jet has a sinuous or a twisted shape and finally the atomization zone. Qualitatively, when the density of the continuous phase increases, this chart is no longer valid and the boundaries between the different zones shift to lower Reynolds numbers. As a matter of fact, an increase in the continuous phase density leads to an increase in the aerodynamic influence on the jet. Liquid jet dispersion into pressurized carbon dioxide has already been investigated for many years [83-87] and more recently various works have focused on the jet dispersion occurring in SAS processes [84, 85, 87].

All the modes of dispersion cited above and initially described for liquid–gas and liquid–liquid systems have been observed for liquid-supercritical systems as reported below. Experimental observations have been made and discussed about organic solvent dispersion into a dense gas by Dukhin et al. [83], Carretier et al. [84], Kerst et al. [85] and

Czerwonatis and Eggers [86]. Chavez et al. [81] investigated the characteristic times of jet break-up, mass transfer and nucleation using the system ethyl alcohol/carbon dioxide under immiscible conditions. It is worth no

]ting that Chavez's work showed that the characteristic time for the mass transfer is at least two orders of magnitude larger than the one for the jet instability development.

S. Dukhin [83] observed that the traditional flowing regimes in experimental conditions above the critical point of mixture prove the existence of an interface and the interfacial tension between the dispersed and the continuous phase. Since the solvents commonly used in SAS processes are miscible with SC CO_2 for the pressure and temperature conditions used, this case is often encountered. The pure solvent and the continuous phase come into contact on the boundary of the jet surface. A decrease in the concentration gradient, due to the antisolvent - solvent mutual diffusion, leads to the decrease in the interfacial tension, which tends to become zero when the equilibrium is approached. Between the initial state (when a new surface is created) and the final equilibrium state, a series of intermediate dynamic interfacial tensions are involved. The concept of dynamic interfacial tension is explained below.

According to the equilibrium thermodynamics, the interface does not exist above the critical point. However, the existence of a metastable interface under supercritical conditions is experimentally verified [88, 89]. Although the interfacial tension is zero at the critical point under the thermal equilibrium conditions, it does exist at the critical point when a temperature gradient and a density gradient exist in the fluid and it exerts a noticeable influence on the fluid motion. A molecular dynamics simulation [88] showed that there is no substantial difference in the interfaces between the supercritical and

subcritical states.

Let us consider the jet of a DCM in CO_2 just above the critical point of mixture (Figure 2.2). Under this condition, both solvent (DCM) and antisolvent (CO_2) are fully miscible into each other. The solvent and the antisolvent meet each other on the boundary of the capillary tip or the jet surface. At the time of contact the initial boundary, which corresponds to a metastable interface with a large deviation from the equilibrium, is very sharp. This interfacial tension is known as Zero Time Dynamic Interfacial Tension (ZTDIT) and can be calculated by the model [90]. The mutual diffusion results in a decrease in concentration gradient and an increasing boundary thickness along the jet. The decrease in the concentration gradient leads to the decrease in interfacial tension [91] and leads to a gradual approach to the equilibrium at the critical point of mixture. After the moment of solvent and antisolvent contact, dynamic interfacial tension exists during a time τ till the onset of surface equilibrium. This characterizes the duration of surface relaxation to the equilibrium state and is called the relaxation time. Hence, dynamic interfacial tension contributes towards preserving an initial section of a jet and stabilizing it against the enhancement of waves or instability by the aerodynamic interaction.

If jet breakup time T is very short and $T<\tau$, the real interface exists before the jet breakup and the jet transforms into droplets. On the other hand, if $\tau<T$, dynamic interfacial tension manifests through a short jet near the capillary tip and then a gas-like jet forms in the absence of any interfaces [87]. The existence of stabilized jet and transient droplets near or above the critical point of mixture (in this case the critical point of mixture is 78 bar at 35°C) indicates that two phases are present. It means that locally an interface exists corresponding to a dynamic interfacial tension.

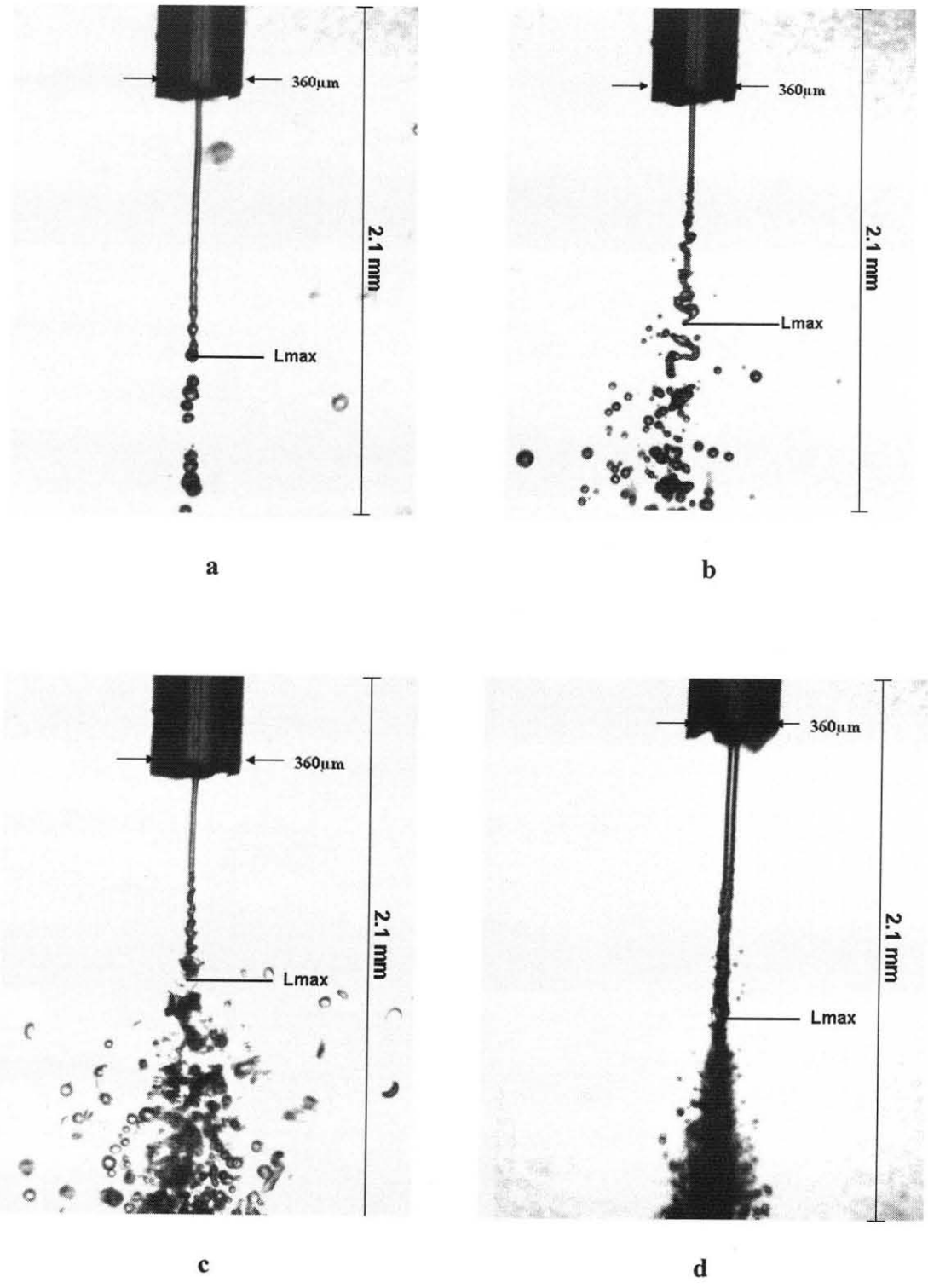

Figure 2.2 The jet breakup of solvents into supercritical carbon dioxide.

The operating conditions for Figure 2.2 are (a) acetone, $20\mu m$ nozzle, flow rate 0.8 ml/min; (b) dichloromethane (DCM), $20\mu m$ nozzle, flow rate 0.12 ml/min; (c) DCM 40 vol% in acetone, $20\mu m$ nozzle, flow rate 0.15 ml/min; (d) PVP (Mw 1,300,000) 2 wt/vol% in mixture of DCM 40 vol% in acetone, $40\mu m$ nozzle, flow rate 0.8 ml/min. The chamber pressure was 82 bar and the temperature 35°C.

Solvent jets of DCM and acetone were studied using capillary nozzles $20\mu m$ and $40\mu m$. The operating temperature and pressure were chosen just above critical point of mixture (35 C and 82 bar). Despite of the fact that the solvents are fully miscible into supercritical carbon dioxide (SC CO_2) under these operating conditions, the behavior of the jets appeared to be similar to that observed for the injection of a liquid into an immiscible liquid [83]. Typical jet break ups of solvents are shown in Figure 2.2. The breakup length L_{max}, of a liquid jet was determined as the distance from the nozzle orifice to the tip of the pinched jet where the disruption of the jet occurs. The variation of the breakup lengths measured using different images of the same jet lie within $\pm 2.5\%$.

As observed for immiscible liquids, bending (asymmetric) disturbances arise in the jets for the wind-induced breakup regimes. For the Rayleigh and wind-induced breakup regimes, the drops are formed far downstream of the nozzle. Within the Rayleigh breakup regime, the sizes of the drops pinched off from the jet are on the order of the jet diameter since they are formed through the growth of long-wave disturbances. With increasing jet velocity, the drop size slowly decreases, but remains comparable to the nozzle diameter for the wind-induced breakup regions. A further increase in the jet velocity leads to spraying.

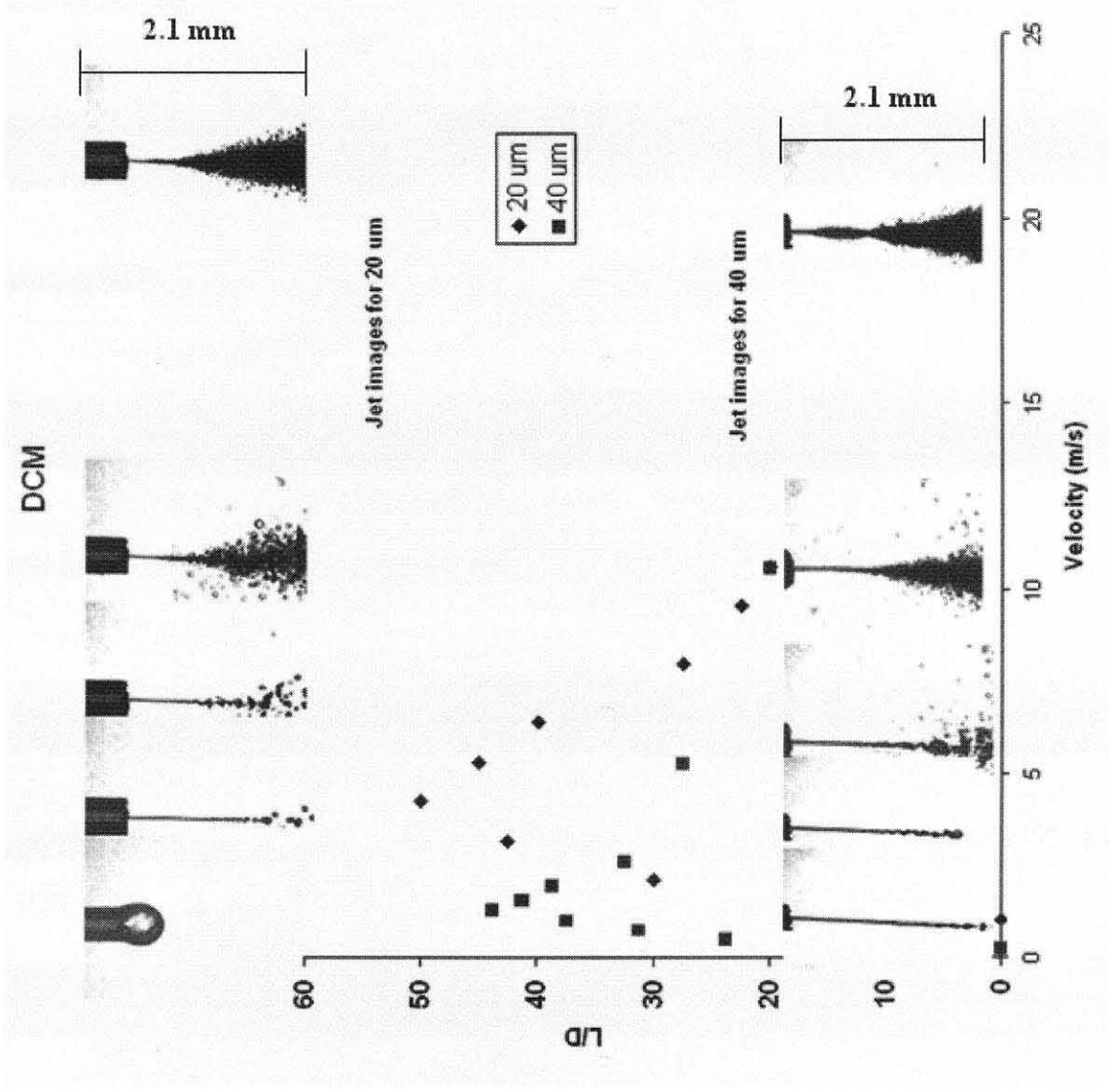

Figure 2.3 The breakup processes of DCM injected vertically into CO_2 at different jet velocities.

Figure 2.3 represents plots of the ratio of the jet breakup length L to the nozzle diameter d as a function of the injection velocity U . The chamber pressure 82 bar and temperature 35°C. Photos show the jet breakup patterns. At very low velocity of solvent injection, the dripping flow was observed. With increase in jet velocity (0.53 m/s for 40μm and 2.12 m/s for 20μm), a systematic column of jet was formed (Raleigh's regime of jet breakup). The jet length increased with increase in jet velocity until it reached to

maximum (1.75 mm at 1.32 m/s for 40 μm and 1mm at 4.24 m/s for 20μm nozzle). With further increase in the jet velocity, a sinusoidal wave (wind induced breakup region) of solvent jet was found. From this point, the maximum jet length reduced with increase in jet velocity. With further increase in jet velocity a spray was formed where the jet length reduces to minimum and the exact length can no more be measured (above 11 m/s for 20 μm and above 16m/s for 40 μm nozzle).

The significant variation of the density and viscosity of the liquids does not appear to substantially affect the ratio L/d at a given jet velocity (Appendix A). Using data given in Figure 2.3, the duration of the jet breakup processes, $t = L/U$ was estimated to range from several tenths of milliseconds to several milliseconds, depending on the jet velocity and the nozzle diameter. For low liquid velocities within the jetting regime, the ratio L/d increases linearly with the jet velocity (the Rayleigh regime) until it reaches a maximum (the first wind-induced breakup region) and then decreases with increasing jet velocity (the second wind-induced breakup region). The similarity between the behavior of the jets in these experiments and jets of immiscible liquids clearly indicates the presence of a transient interfacial tension at the jet surface during the breakup processes, even though the solvents and CO_2 were completely miscible under our experimental conditions [83]. Its appearance is caused by the presence of stress in the transition zone between the injected solvents and CO_2 due to large compositional and density gradients. This stress acts like an interfacial tension in immiscible fluids, causing the breakup of a jet into drops. Similar observations for jets of supercritical liquids were also reported in the References [92-95].

2.3 Mass Transfer Between Supercritical CO_2 and Solution Jets

Review of previous studies as well as jet breakup study of different solvents and solutions shown in section 2.2 underlines that the particles are not precipitated out of solution jets. Solution jet breaks up and then the droplets are saturated and particles are precipitated from the droplets. To verify the jet breakup study, the mass transfer between solution jets and surrounding SC CO_2 was calculated to determine the diffusion layer thickness of at the instance of jet breakup.

To approximate the diffusion coefficients at infinite dilution, following equation was used, which adapts the Stokes-Einstein equation to a binary mixture when the molecules of both constituents are of the same order of magnitude [96].

$$D_{12}^{L} = 8.93 \cdot 10^{-8} T \left(v_1 / v_2^2\right)^{1/6} \left(P_2 / P_1\right)^{0.6} / \mu_2$$

Where, the diffusion coefficient is in cm^2/s, T is the temperature in K, v_1 and v_2 are the molar volumes of the constituents at their normal boiling points in cm^3/mol, P_1 and P_2 are the Parachor parameters [97] and μ_2 is the viscosity of the pure constituent in cP. The viscosity of DCM / acetone solvents at 35°C as function of the acetone content can be described by the following expressions:

$$\mu(\text{Pa} \cdot \text{s}) = (0.08x + 0.28) \cdot 10^{-3}$$

where x is the volume fraction of DCM. The viscosity was measured using a standard Cannon Fenske tube viscometer (Fisher Scientific). These measurements correlate within $\pm 2.5\%$ with data reported for DCM [98, 99] and acetone [100]. The viscosity of CO_2 at 35°C was obtained from NIST webbook [101]. The molar volumes of solvents at their normal boiling points were computed as follows: $65.08 cm^3/mol$ for DCM (Mw: 84.93,

boiling point: 40.7^{0}C) by extrapolating data on its density for 15^{0}C and 20^{0}C [102] and the measurements done for 35^{0}C and 76.34cm^3/mol for acetone (Mw 58.08, boiling point 56.3^{0}C) by extrapolating data on its density from 14.5^{0}C to 50^{0}C [102] whereas the density of CO_2 was obtained from the NIST webbook [101]. The Parachor number for CO_2 and DCM was obtained from the reference [87] whereas for acetone it was obtained from [93]. The values of all of the parameters are listed in the Table 2.1.

Table 2.1 Parameters Used in Diffusion Coefficient Calculations.

Parameter	CO_2	Acetone	Dichloromethane
P	80.6	161.2	150.1
μ (at 35C)	0.0335	0.287	0.36
v cm^3/mol (at b.p.)	34	81.83	64.93

To evaluate the concentration dependence of the binary diffusion coefficient, equation 2 for a mixture of two miscible liquids was used [96].

$$D_m = \left(D_{12}^L\right)^{x_1}\left(D_{21}^L\right)^{1-x_1}$$

Where, x_1 is the mole composition of the mixture and D_{12}^L and D_{21}^L are the diffusion coefficients of the solvent in carbon dioxide and carbon dioxide in solvent, at infinite dilution, respectively. The binary diffusion coefficients for the contact concentration were calculated for $x_1 = 1/2$.

Table 2.2. The Diffusion Coefficients at 82 bar and 35C.

Diffusion Coefficient	Values in m^2/sec
CO_2 in DCM	$4.97.10^{-10} m^2$ / sec
DCM in CO_2	$3.01.10^{-8} m^2$ / sec
CO_2 in acetone	$6.02.10^{-10} m^2$ / sec
Acetone in CO_2	$2.99.10^{-8} m^2$ / sec
Binary diffusion coefficient for DCM – CO_2 system	$1.50.10^{-8} m^2$ / sec
Binary diffusion coefficient for Acetone – CO_2 system	$1.34.10^{-8} m^2$ / sec

The estimation of the diffusion coefficient of acetone in CO_2 correlated well with the interpolation $2.78 \cdot 10^{-8} m^2/s$ for 82 bar from the measurements reported in the literature [103].

The transient interfacial tension between the injected solvents and CO_2 relaxes through diffusion as the system approaches the spatially uniform, equilibrium state. Equation 3 gives the thickness of the diffusion layer formed during the jet breakup.

$$\Delta \sim \sqrt{D_m t}$$

Where, D_m is the binary diffusion coefficient and t is the duration of the jet breakup process. Similar to reference [95], the diffusion coefficients for DCM - CO_2 and acetone - CO_2 systems were approximated using available empirical equations.

Using the values of these coefficients and data on the jet length presented in Figure 2.2, it was found that the thickness of the diffusion layer Δ formed during the breakup period is about $1-3\mu m$ for jet velocities below 2 m/s and less than several tenths

of a micrometer for jet velocities above 5 m/s. Therefore, the total mass transfer into and out of the jet over the breakup process is very small. Correspondingly, the transient interfacial tension at the jet surface does not have sufficient time to relax, thereby causing the jet behavior similar to that of immiscible liquids (Figure 2.2).

The breakup of a jet into drops increases the mass transfer between the injected liquid and the surrounding CO_2. The behavior of falling drops was studied using jets of DCM issuing vertically into CO_2 through a $50\mu m$ nozzle at a flow rate of 0.2 ml/min and 0.4ml/min, for a chamber pressure of 82 bar. Photos presented in Figure 2.4 show typical images of drops at several distances below the tip of the pinched jet. Once the droplets are detached from the jet, they dissolve into SC CO_2 at around 50 mm to 75 mm below the tip of the nozzle. The evolution of a fluid drop falling in a lighter miscible fluid is governed by the competition between the hydrodynamic instability and diffusion mixing [104-107]. The main parameters associated with the falling drops were as follows: the drop volume is about $60 - 70\,\text{pL}$; the drop Reynolds number, $\text{Re} = \rho_{CO_2} Ud / \mu_{CO_2}$ where ρ_{CO_2} and μ_{CO_2} are the density and viscosity of CO_2 and $\text{d} = 50\mu\text{m}$, is of the order of several hundreds; the ratios of the viscosities and densities for DCM and CO_2 are about 9 and 2.4, respectively. The Schmidt number, $Sc = \dfrac{\mu_{CO_2}}{\rho_{CO_2} Dm}$ which relates the ratio of inertial to molecular diffusive transfer, is about 5.

Despite the fact that studies available in the literature [104-107] of a drop falling in a lighter miscible fluid are limited to liquid-liquid systems and μL and mL drops, with drop Reynolds numbers ranging from several tenths to several tens and $\text{Sc} \sim 10^4 - 10^5$ the initial steps in the drop evolution in our experiments resemble the

reported observations [104-107]. Specifically at the beginning, the presence of a transient interfacial tension tends to maintain the spherical shape of a falling drop (Figure 2.4). As the transient interfacial tension relaxes, eventually approaching zero at equilibrium, the shape of the drop tends toward to become oblate. In particular, the side view of the drops in Figure 2.4 resembles the shape of drops in photos presented in References [104-107]. Similar to Reference [105] for drops less than $1mL$ with a surfactant added to decrease the interfacial tension, the development of bulges on a falling drop causing its fragmentation into smaller drops was not observed in these experiments (Figure 2.4). The shape of the drops in Figure 2.4 indicate that they mix with the ambient fluid through intensive hydrodynamic and diffusion mixing that is consistent with the low values of the Schmidt number for supercritical CO_2. In contrast, the successive fragmentation of drops caused by the growth of hydrodynamic instabilities dominates in liquid-liquid systems [104-107] due to large values of the Schmidt number.

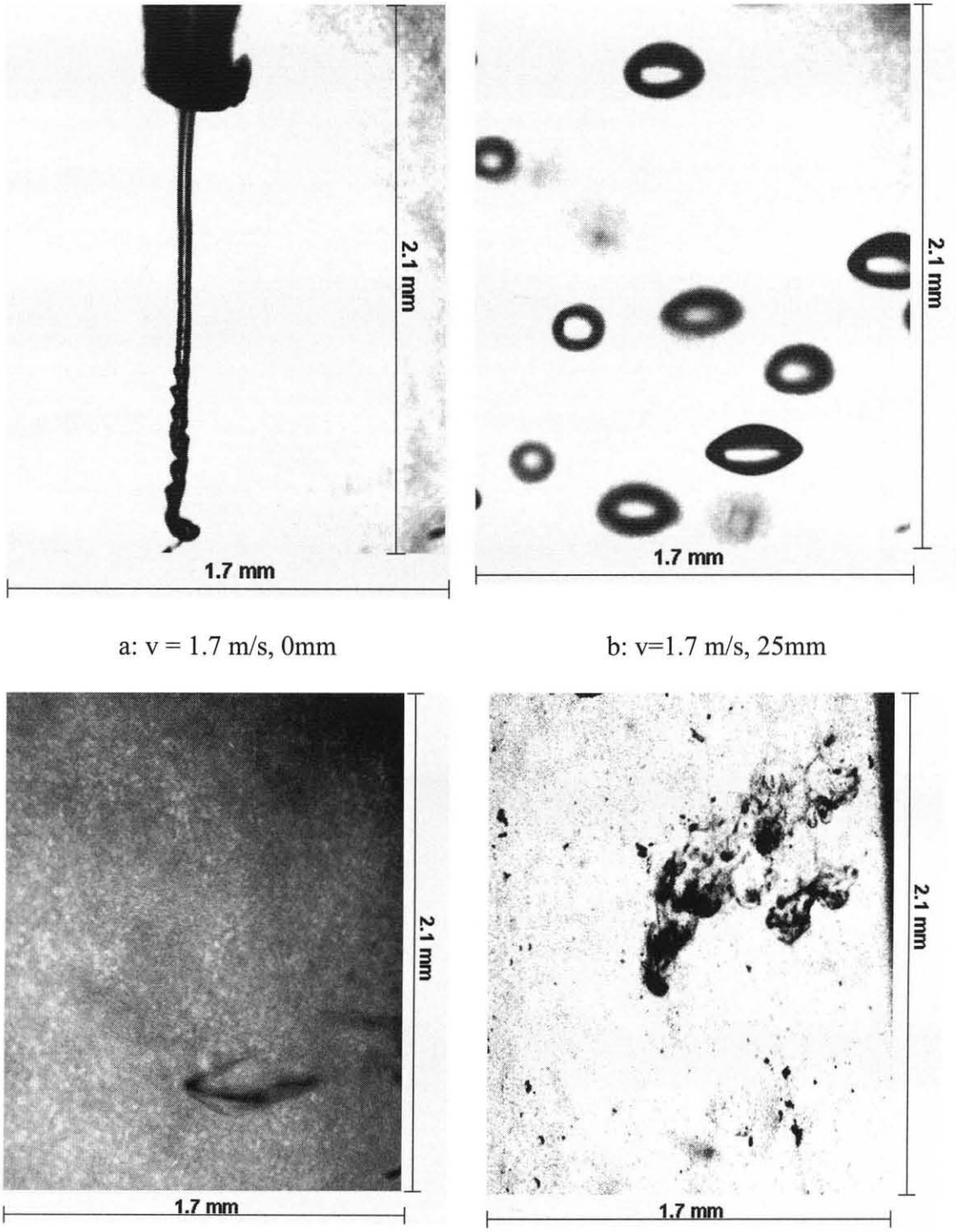

a: v = 1.7 m/s, 0mm

b: v=1.7 m/s, 25mm

c: v=1.7 m/s, 50mm

d: v=3.4 m/s, 50mm

Figure 2.4 DCM droplets falling from the nozzle at various different velocities. 50μm nozzle was used to inject DCM into SC CO_2 maintained at 82 bar and 35 C.

2.4 Poor Solvent Concept to Alter the Solubility of Solvents

A physical property which depends on the configuration of the polymer molecule ordinarily can be expressed as a function of an average dimension of one sort or another. The dimension of a polymer molecule most widely used to characterize its configuration, is the distance *r* from one end group to the other of the chain molecule. This is known as *displacement length* or *contour length* of the chain [108]. An average value for r for the polymers is the root mean square $\sqrt{\overline{r^2}}$. Another important measure of the effective size of a polymer molecule is the root-mean-square distance of the end elements of the chain from its center of gravity, $\sqrt{\overline{s^2}}$ known as the radius of gyration of the molecule [108].

For a polymer-solvent system, three types of solvent environments can be found. In a good solvent, the energy of interaction between a polymer element and a solvent molecule adjacent to it exceeds the mean of the energies of interaction between the polymer-polymer and solvent-solvent pairs, the molecule will tend to expand further so as to reduce the frequency of contact between pairs of polymer elements. In a poor solvent, the energy of interaction is unfavorable (endothermic) and hence the smaller configurations in which polymer-polymer contacts occur more frequently will be favored. The portion of the solution volume that is inaccessible to polymer chain segments due to prior occupancy by other chain segments is known as excluded volume. In short, excluded volume repulsive interactions swell the chain (good solvent). Monomer - monomer attractions shrink the chain (poor solvent). If the solvent medium is sufficiently poor, i.e., if the interaction energy with the polymer is sufficiently positive, the energy of interaction may compensate exactly the influence of volume exclusion. When this condition is achieved, the polymer chain will assume its random flight configuration, its

overall dimensions then being determined solely by bond lengths and angles. The mean square dimensions ($\sqrt{\overline{r^2}}$ and $\sqrt{\overline{s^2}}$) are controlled entirely by the short-range intramolecular interactions, and they are unaffected by the solvent. In this case, the solvent is known as Θ (theta) solvent for the particular polymer. In a Θ solvent, excluded volume repulsion balances exactly the monomer - monomer attractions [109]. For the good solvent the value of $\alpha^2 > 1$, for poor solvent $\alpha^2 < 1$ and for theta solvent $\alpha^2 = 1$.

For the polymeric solution system, the dilute polymer solution may be regarded as a dispersion of clouds, dilute clusters, or segments. Each such cloud will be approximately spherical with an average density. The density is maximum at the center and decreases with the distance from the center. Each molecule in a very dilute solution in a good solvent will tend to exclude all others from the volume which it occupies. The excluded volume can be evaluated by calculating the interaction between a pair of molecules and the centers of gravity. Once the interaction is known as a function of the intermolecular distance *a*, the excluded volume *u* can be obtained. For a given polymer-solvent system, if the solvent becomes progressively poorer as the temperature is lowered, eventually a temperature may be reached below which the polymer and solvent are no longer miscible into each other and the polymer precipitates out of the solution. This temperature is called as theta (Θ) temperature. It can be calculated by the equation: $\Theta = K_1 T / \Psi_1$ [108]. Where, K_1 is the parameter expressing the energy divided by KT of interaction between a solvent molecule and polymer, T is the absolute temperature and Ψ_1 is the entropy of dilution of polymer with solvent. The excess chemical potential can be written as $(\mu_1 - \mu_1^0)E = -RT\Psi_1(1-\Theta/T)v_2^2$ [108]. Where, μ_1 is

the chemical potential of the polymer, E is the internal energy, R is the gas constant, v_2^2 is volume fraction of a polymer in swollen network in equilibrium with pure solvent, μ_1^0 is the chemical potential of pure liquid. The chemical potential is defined as if to any homogeneous mass in a state of hydrostatic stress supposing an infinitesimal quantity of any substance to be added, the mass remaining homogeneous and its entropy and volume remaining unchanged, the increase of the energy of the mass divided by the quantity of the substance added is the potential for that substance in the mass considered. At the temperature $T = \Theta$, the chemical potential due to segment-solvent interactions is zero [108]. In general, chemical potential measures the tendency of polymer chain to diffuse.

The use of a mixture of good and poor solvents and the variation in their ratio provides an effective and simple method to control and manipulate the conformation of polymer molecules in the particles precipitating from the injected solution, while both solvents mix with CO_2. Hence, the solubility of the polymer in the solvent can be controlled by mixture of good and poor solvents. This phenomenon is used in the particle formation experiments as the supersaturation of the solution drops when injected into SC CO_2 is enhanced without increasing polymer concentration. Hence, as the process is operated at low polymer concentration, the agglomeration of the nanoparticles can be controlled.

Figure 2.5 represents the solubility of PVP polymer with two different molecular weights (Mw: 1,300,000 and 360,000) in the DCM and acetone mixtures. As can be seen from the Figure, the PVP solubility can be controlled by altering the ratio of DCM and acetone.

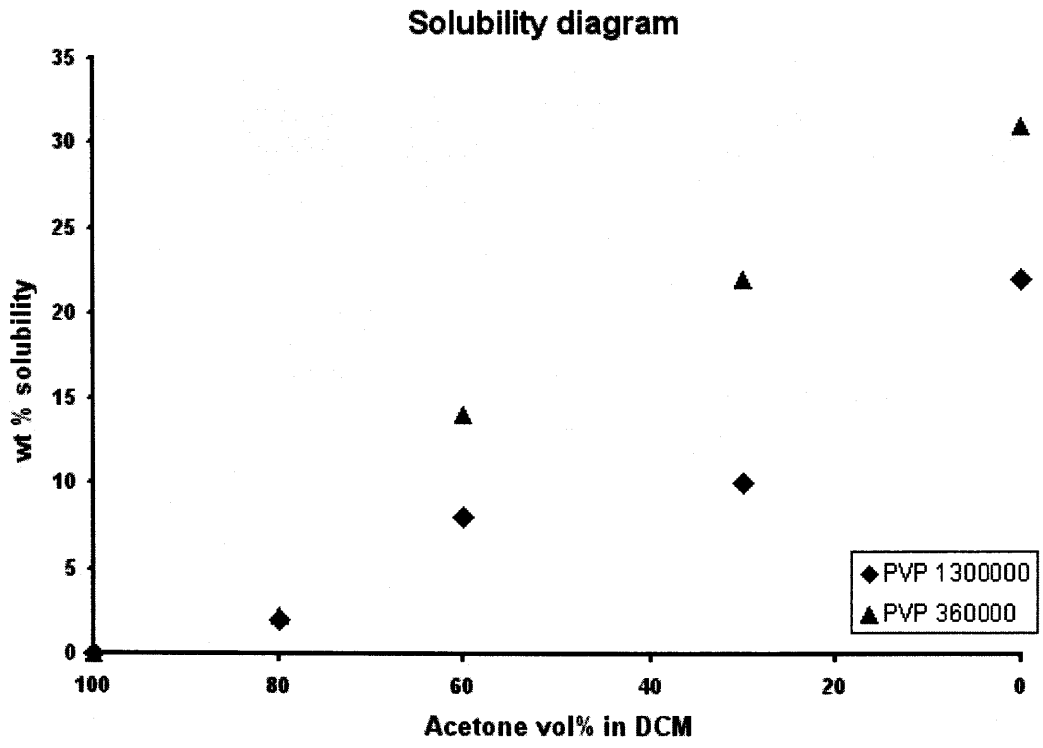

Figure 2.5 Solubility diagram of DCM - Acetone - PVP with two different molecular weights.

DCM and acetone are miscible with each other at room temperature and atmospheric pressure [110]. Photon correlation spectroscopy (Coulter N4 Plus) was used to determine the solubility of PVP in DCM-acetone mixtures at a room temperature (22^0C) and atmospheric pressure. Solutions were prepared for DCM 20 vol% in acetone for PVP 0.25 wt% to 4 wt% with increment of 0.25%. All solutions were kept for 24 hours for stabilization. Then, the solutions were analyzed for precipitation. N4 Plus measurements were done at room temperature (22^0C) for 3 hours of equilibration time for every measurement. Solutions with DCM 40 vol% in acetone with PVP 2 wt% to 10 wt% were prepared and kept for 24 hours for stabilization. They were analyzed for precipitation. Solutions with DCM 70 vol% in acetone with PVP 8 to 20 wt% with an

increment of 1 wt % were prepared and precipitations were measured in a similar fashion. At the precipitation concentration, more solutions were prepared with PVP 0.25 wt % in solvent mixtures and precipitations were analyzed for reproducibility. Solutions with DCM 100 vol% with PVP 10 to 25 wt% with increment of 1 wt% were prepared and precipitations were measured in a similar fashion. Solutions for all other operational parameters were prepared in similar fashion for both of the PVP molecular weights.

The particle size in the binary DCM-acetone solutions was found to lie in the range from 2 nm to 10 nm. The particle size in a ternary system fell within the same range as long as PVP was soluble in the binary solution. In contrast, the precipitation of PVP resulted in a larger particle size of about 1 μm.

2.5 Nanoparticle Formation using Supercritical Fluids

Polymer nanoparticles have wide range of applications in different areas of human activities like biology, neurology. Rapid developments in nanoparticles synthesis methods and the control on tailoring properties show a potential for development of future drugs and related products. There is a wide range of applications of polymer nanoparticles in pharmaceutical and related fields, biological labels, drug delivery systems, tissue engineering to name a few [111]. In case of drug delivery systems, biodegradable polymers have captured special attention. Biopolymers encapsulations in both targeted as well as controlled release systems are being researched. It has been observed that nano size biopolymers have better encapsulation efficiency and controlled release than micron size ones [112]. The smallest capillary in the body is around 5 μm so the particle size should be significantly smaller to avoid embolism [113, 114]. Drugs in nano size are often unstable and encapsulation of nano sized drug particles in biopolymers particles of size less than 200 nm can provide required stability, better control on drug release [115-120]. For more sophisticated targeted delivery applications, required particle size is even less than 80 nm [121]. Because of the smaller size, nanoparticles can penetrate through smaller capillaries, sustaining intracellular dexamethasone levels and deliver drugs into the tissues with stable release kinetics [122]. In particular, nanoparticles have been very useful in cancer therapy and anti HIV drugs delivery into the brain [123, 124]. Particle surface becomes an important issue especially in drug delivery when drug is attached / absorbed onto the surface [125]. Surface smoothness facilitates in minimizing drug - carrier particle interactions resulting in more

efficient drug detachment from the carrier particle surface which shows tremendous improvement in drug release efficiency [126, 127, 75].

In the Supercritical As Antisolvent (SAS) process, the compound of interest is first dissolved in an organic solvent. The single phase clear solution is then sprayed into a chamber containing supercritical fluid (e.g. CO_2). The supercritical fluid is miscible with the organic solvent but not miscible with the solute. Hence, the solute precipitated out upon saturation of solution. Carbon dioxide is a common choice for SAS applications since it is non-flammable, non-toxic, inexpensive, and environmentally benign. The important features of SAS include the wide range of materials that can be processed and the variety of particulate morphologies that can be formed.

E. Reverchon et al. [128-130] formed nanoparticles of superconductors like yttrium, samarium and neodymium acetates using dimethyl sulfoxide (DMSO) and *N*-methyl 2-pyrrolidone (NMP) as liquid solvents. Nanoparticles of a mean diameter of about 100 nm were obtained. All particles were smaller than 200 nm with a mean diameter of about 120 nm. Nanoparticles of zinc acetate, a catalyst precursor, were produced by SAS. The main process parameter that controlled particle size and particle size distribution was found to be the concentration of the liquid solution. Zinc acetate nanoparticles with sizes down to 30 nm and with a mean particle size of 50 nm have been produced. The nanoparticles showed different porosities depending on the concentration of the liquid solution.

Wu H. et al. [131, 132] produced nanoparticles of pigments by SAS method. The pigment red 177 and red 60 were used as a solute and DMSO was used as a solvent. He analyzed the influence of several process parameters on particle size. Spherical

nanoparticles down to 46 nm mean diameter were obtained. In that case, solubility of the pigment in the supercritical solution was not negligible; therefore, the yield of the precipitation process was low due to the partitioning of Red 60 in the fluid phase. P. Chattopadhyay [133] precipitated fullerene (C60) nanoparticles from a toluene solution. With SAS method, nanosized fullerene particles from 29 to 63 nm were obtained (with a standard deviation of 7–25 nm operating at various conditions).

E. Reverchon et al. [134] produced nanoparticles of antibiotic drugs. Griseofulvin, ampicillin, amoxicillin, and tetracycline were produced. Several solvents like *N*-methylpyrrolidone, dimethylsulfoxide, ethyl alcohol and methylene chloride were used to dissolve the solutes. Spherical nanoparticles were observed for tetracycline in *N*-methylpyrrolidone. These particles tend to coalesce in small aggregate-forming groups. The effect of the SAS process parameters on morphology, particle size and particle size distribution was studied for the system tetracycline - methylpyrrolidone. The coalescence of tetracycline particles decreases with the increase in operating pressure; whereas the diameter of the aggregates increases with tetracycline concentration in the liquid solvent. Operating at 180 bar, 408°C and at different concentrations, aggregates with mean diameters between 0.6 and 0.8 mm have been observed.

P. Chattopadhyay et al. [135, 136] proposed a SAS process with the addition of a vibrating surface in the precipitation vessel. The technique was named supercritical antisolvent with enhanced mass transfer (SAS-EM). He synthesized griseofulvin (antifungal, antibiotic) particles as low as 130 nm and lysozyme (enzyme) particles of about 190 nm.

Nanoparticles of some polymers have been produced by SAS method. E. Reverchon [137] processed dextran (a biopolymer) particles using DMSO. He performed the semi continuous antisolvent process injecting the solvent in a jet-swirl nozzle designed to enhance the mixing within a swirl chamber. Spherical particles with mean particle size ranging between 125 and 150 nm were found. The particle size showed a limited dependence on the process parameters. This was explained as follows: polymers are characterized by very large molecular weights and by a molecular weight distribution. These characteristics can be very relevant in conditioning the precipitation (nucleation and growth) processes thus hindering (masking) the dependency from the process parameters.

2.5.1 Experimental Procedure for Nanoparticles Formation

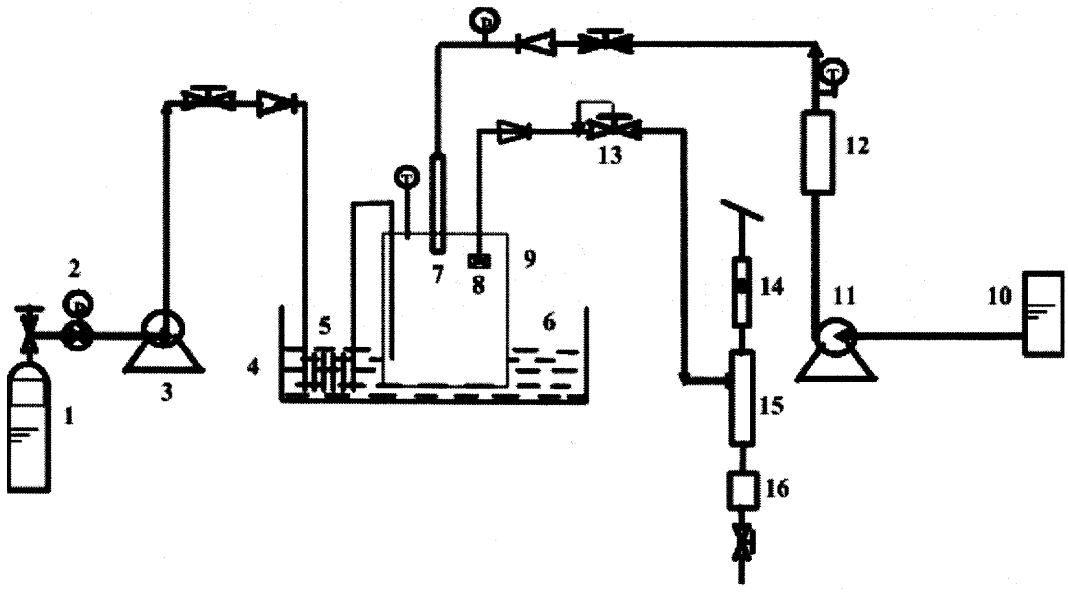

Figure 2.6 An Experimental Setup for the Particle Formation.

1 Liquid CO_2 cylinder, 2 pressure regulator, 3 CO_2 pump, 4 water tank, 5 submerged coil, 6 water, 7 capillary nozzle, 8 filter, 9 pressure vessel, 10 solution tank, 11 solution pump, 12 solution buffer with heating tapes, 13 back-pressure regulator, 14 rotameter, 15 separator, 16 collector

A schematic diagram of particle formation setup is shown in Figure 2.6. 1-L high-pressure chamber (PARR Instrument, 599 HC, R 283) was placed into a water bath. To maintain CO_2 and the chamber at the same temperature, CO_2 was delivered into the chamber through a 10-feet coil submerged into the water bath. Starting a minute before the injection of a polymer solution and finishing 90 min after, CO_2 continuously flowed through the chamber at a mass rate of $2.4 kg/m^3$ to avoid the saturation of the chamber atmosphere with a solvent. Rest of an experimental setup is the same as that for the jet breakup study. Polyvinylpyrrolidone (PVP) $[(C_6H_9NO)_n]$ was used as solute, dissolved in a binary solution of dichloromethane (DCM), and acetone. By operating in the

supercritical region, the pressure and temperature can be used to regulate the fluid density which, in turn regulates the solvent power of a supercritical fluid. The recovery and separation of the antisolvent from the solvent and solid products was then performed by a simple depressurization step.

PVP was chosen because it is widely used as a pharmaceutical excipient. PVP is used in more than a hundred drugs as a tablet binder, a dissolving agent for injection, a liquid dispersant, a stabilizer for enzyme and heat sensitive drugs, an antitoxic agent. It is hygroscopic in behavior and has exceptional adhesion to different materials. Its capacity for complex formation, good stabilizing and solubilizing capacity, insensitivity to pH, ready radiation-induced crosslinkability as well as good biological compatibility have made PVP one of the most frequently used specialty polymers. PVP can be easily attached to various monomers to alter the physiochemical properties. This makes PVP an excellent carrier for drugs in drug delivery systems. It has long enough circulation time and its tissue distribution is restricted. Moreover it is easy to introduce various monomers on radical polymerization to PVP. These results suggest that PVP is the most feasible polymeric modifier for localizing the conjugated drug in blood. PVP can be adopted not only to the bioconjugation of drugs but also to the steric stabilization of liposomes in vivo and the surface modification of particle carriers [138-141].

2.5.2 Materials

High pressure CO_2 cylinders (Bone Dry, 99.9% pure) are purchased from MG Industries. Acetone (HPLC Grade, 99.5+ %), DCM (HPLC Grade, 99.7+ %) and PVP (Mw:

1,300,000 and 360,000) are purchased from Alfa Aesar. All materials were used as received. Figure 2.6 shows the chemical structure of PVP [64].

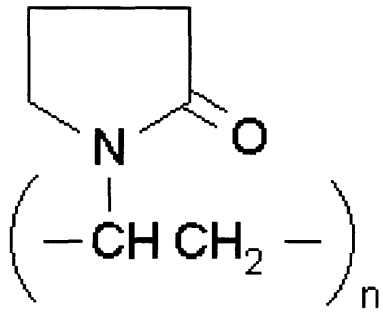

Figure 2.7 The Chemical Structure of PVP.

2.5.3 Characterization Techniques

2.5.3.1 Field Emission Scanning Electron Microscope (Leo 1530VP): A small amount of powder was placed on an adhesive tape and then sputter coated with carbon in a Baltec MED 020 unit. SEM images of particles obtained at high magnifications, 800 KX at 3 kV. These images were used to calculate the mean particle size and size distribution with the image analysis software Sigma Scan Pro, Version 5.0. At least 300 particles for each sample were used for image processing.

2.5.3.2 Particle Analyzer Coulter N4 Plus (Beckman Coulter, CA): Coulter N4 Plus employs dynamic light scattering to measure the mean diameter of nano-sized particles. A sample was prepared by sonicating a small amount of powder in acetone with a Fisher Scientific FS30 bath sonicator. Several samples were analyzed with Coulter N4 Plus at

different detection angles of the scattered light. Since data sets obtained for different angles were found to be consistent, the detection angle 63.5° was used for most of the samples. For comparison, several randomly chosen samples were also analyzed with Aerosizer (Model: LD, Amherst Instrument).

2.5.3.3 Fourier Transform Infrared Spectroscope (Nicolet Nexus 670, Thermo Electron, WI): A small sample was placed on ZnSe crystal and the FTIR spectrum was recorded in the wavenumbers range of 4000-650 cm^{-1} at a resolution of 4 cm^{-1}.

2.6 Effects of Operating Parameters on Particles

2.6.1 Effects of poor solvent

PVP (Mw: 1,300,000 and 360,000) was used as a solute and effects of various operating conditions were studied. The ratio of acetone was varied from 20 to 60 vol/vol % in DCM and the effects on particle shape and size for different nozzle diameters at different pressures were observed. The solution was sprayed in the supercritical carbon dioxide in a single phase.

As polymer is not soluble in acetone (Figure 2.5), acetone restricts the agglomeration of polymer particles due to re-dissolution in dichloromethane traces. This phenomenon is very important especially in drug delivery when drug is attached / absorbed onto the surface [142]. Surface smoothness facilitates in minimizing drug - carrier particle interactions resulting in more efficient drug detachment from the carrier particle surface which shows tremendous improvement in drug release efficiency [143-145].

Surface irregularities vanished with use of poor solvent. Aggregation was found to be reduced and closer particle size distribution was achieved with increase in poor solvent in the solution. Figure 2.8 shows the effects of poor solvent on the particles. 127 μm nozzle was used to inject the solution. PVP with Mw 1,300,000 was used as a solute. The solvents for these experiments were (a) DCM; (b) acetone 20 vol% in DCM and (c) acetone 60 vol% in DCM. Other experimental conditions such as pressure 82 bar and temperature 35C were kept constant for all three experiments.

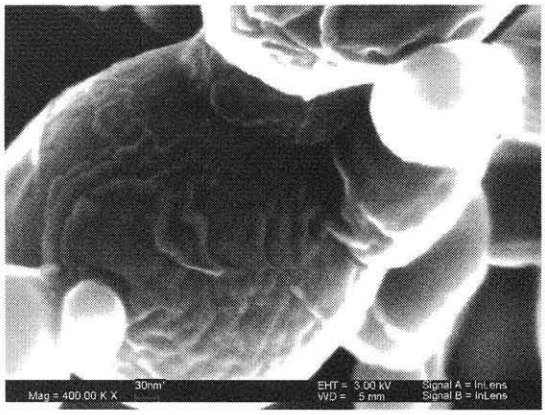

(a)

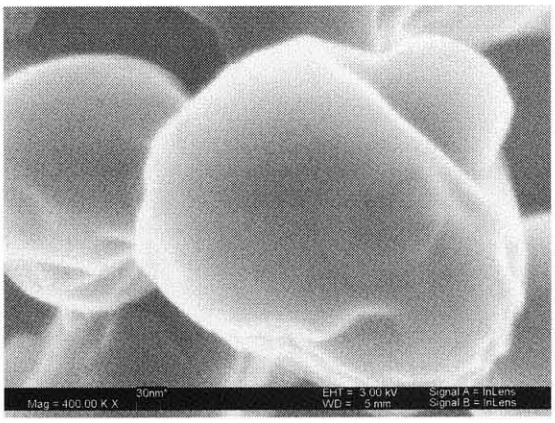

(b)

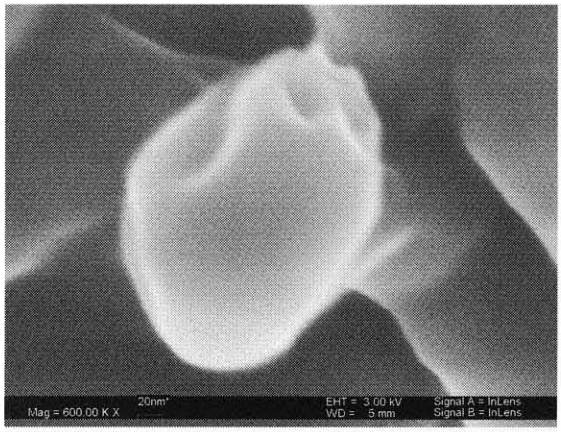

(c)

Figure 2.8 The effect of poor solvent on particle surface using 127μm nozzle.

Similar effects were seen when smaller capillary nozzles were used. Figure 2.9 represents the SEM images with (a) and (b) PVP particles (Mw: 360,000) formed at 82 bar, 35°C, solution concentration 2% at solution flow rate 0.2 ml/min at (a) solvent: DCM and (b) mixture of solvents DCM and acetone at 40:60 volume % and (c) and (d) represents PVP particles (Mw: 360,000) formed at 79 bar, 35°C, solution concentration 2% at solution flow rate 0.2 ml/min at (c) solvent: DCM and (d) mixture of solvents DCM and acetone at 40:60 volume %.

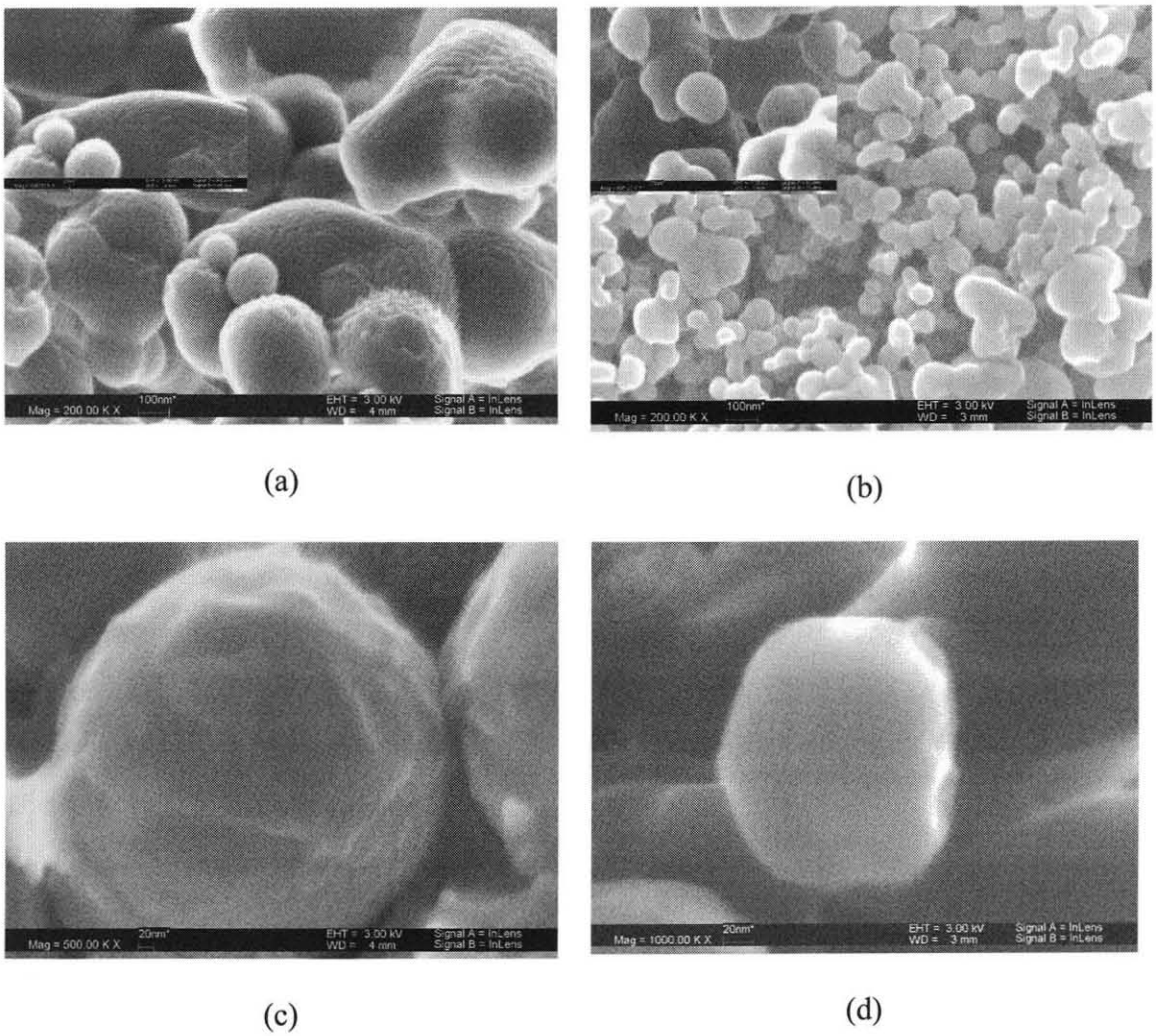

(a) (b)

(c) (d)

Figure 2.9 The effect of poor solvent on PVP particles surface using 40μm sized nozzle.

As can be seen from Figure 2.8 and 2.9, with use of poor solvent, surface irregularities vanished and smooth surfaced particles were collected. Particles were more spherical in shape and close particle size distributions were achieved as acetone percentage was increased. These are representative images. Several experiments in addition to above mentioned experiments were done to investigate the effects of poor solvents on physiochemical properties of particles and similar results were obtained.

Table 2.3 shows the mean particle size of the PVP polymer precipitated from the nozzles at various operating conditions.

Table 2.3 Mean Particle Size at Various Operating Conditions.

	Pressure	**DCM**	**Acetone 20 vol% in DCM**	**Acetone 60 vol% in DCM**
127 μm	82 Bar	680±250 nm	440±170 nm	430±130 nm
Nozzle ID	100 Bar	750±300 nm	500±250 nm	420±220 nm
40 μm	82 Bar	360±120 nm	200±100 nm	190±30 nm
Nozzle ID	100 bar	460±200 nm	250±150 nm	210±70 nm

Particle sizes are based on volume average calculations and for 127 μm and 40 μm nozzles at 100 and 82 bar, 35°C, 0.2 ml/min flow rate.

FTIR analyses of samples were done to analyze the chemical changes as well as solvent traces. No chemical changes in the processed polymer are observed in FTIR analysis (Figure 2.10). Also, no residual traces of DCM and acetone are observed in the processed sample. Figure 2.10 shows the representative FTIR analysis. Experiments were conducted at 82 bar, 127μm nozzle, 35^{0}C, 0.2 ml/min flow rate. (a) original PVP sample received from the vendor; (b) PVP processed with DCM; (c) acetone 20 vol% used in DCM; (d) acetone 40 vol% used in DCM; (e) acetone 60 vol% used in DCM. In addition to the FTIR analysis presented in Figure 2.10, several more samples with different operating conditions were analyzed using FTIR spectroscopy and similar results were obtained.

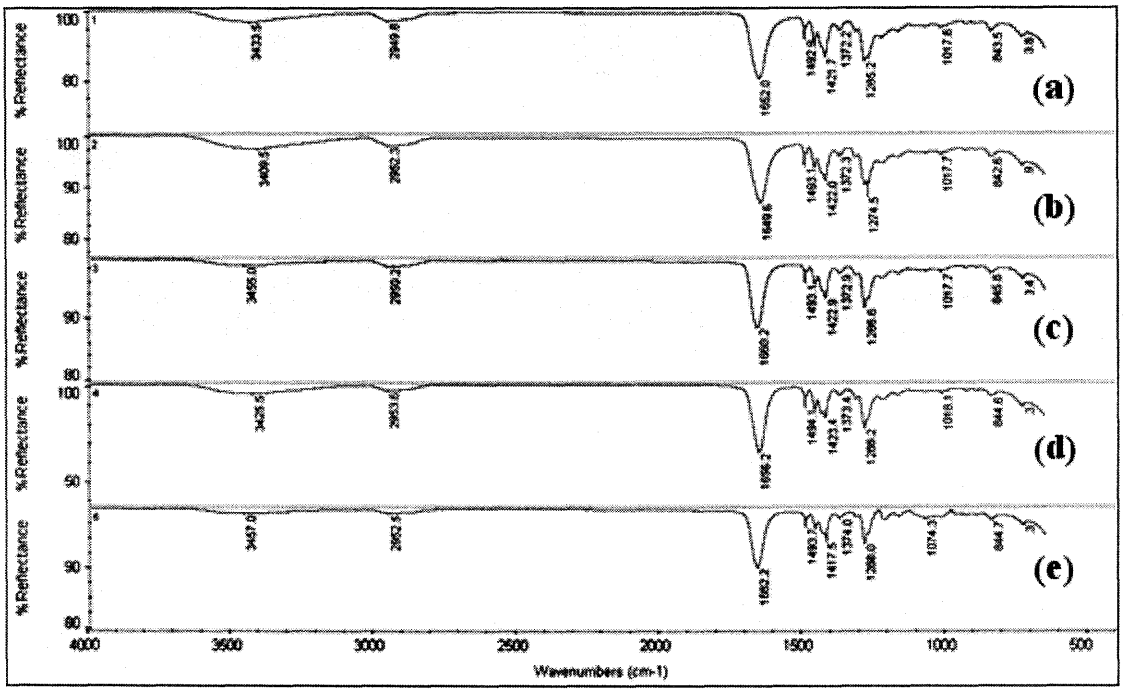

Figure 2.10 FTIR analyses for various percentage of acetone in dichloromethane.

2.6.2 Effects of Pressure

Effect of pressure on particle size for various compounds was being studied by varying pressure from 45 bar to as high as 400 bar by different researchers. Many researchers concluded that as working pressure increases, particle size decreases [146-150]. M Rantakyala [151] showed with increase in the pressure, the particle size increases. D. Dixon showed that there would not be any effect of pressure on particle size above 120 bar [148]. Hence, it can be seen that different compounds react to pressure differently. Particles size of few compounds becomes smaller with increase in operating pressure and for other compounds it becomes larger.

In this study, the pressure was varied from 79 bar to 120 bar. Particle size was found to be increasing with pressure. 82 bar was found to be ideal pressure to achieve

deagglomerated and spherical particles. Below 79 bar, the PVP particles did not precipitate. At higher pressures, particles size increased with increase in pressure. The experiments were done using 127μm, 40μm and 20μm sized nozzles for various combinations of DCM - acetone ratios. Experiments were conducted at various pressures for different nozzles diameters. The effects of pressure on particle size as well as shape were studied. Similar results were obtained in all of the cases. At pressure just above critical point of mixture (82bar), the narrow size distribution as compared to other pressures was found (Figure 2.11).

Figure 2.11 shows the particles size distribution of PVP particles formed using (a) DCM; (b) DCM 80 vol% in acetone; (c) DCM 40 vol% in acetone; temperature 35°C, solution flow rate 0.2 mL/min and 40μm nozzle. Similar experiments were done by using $20\mu m$ sized capillary nozzle to inject the solution. The particles size distributions are reported in Figure 2.12. The size distribution of polymer particles formed in jets of 2 wt% solutions of PVP (Mw: 1,300,000) in (a) DCM, and (b) DCM 40 vol% in acetone for chamber pressures 79 bar, 82 bar, 100 bar, and 120 bar. Other operating conditions like temperature 35°C, liquid flow rate 0.2 mL/min, nozzle 20μm were used to produce PVP particles.

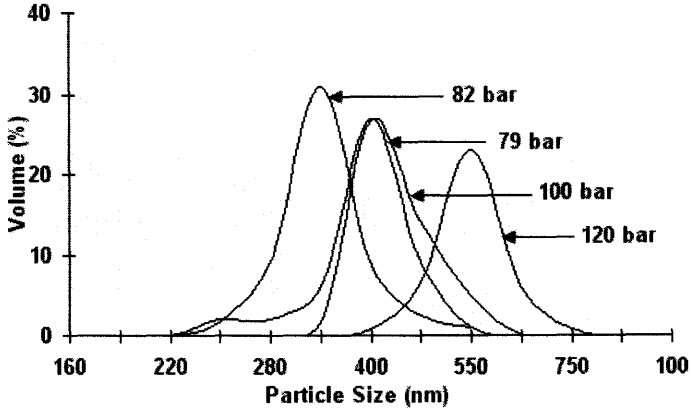

(a): DCM

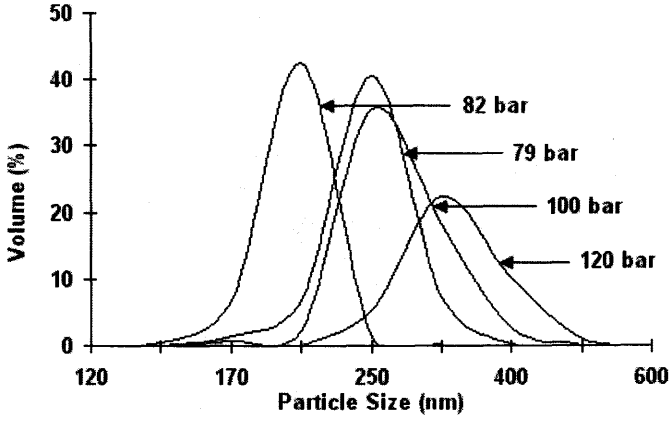

(b): DCM 80 vol% in acetone

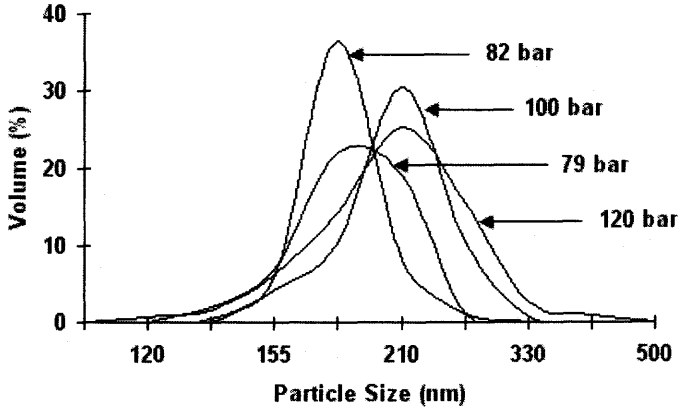

(c): DCM 40 vol% in acetone

Figure 2.11 Particle size distributions of PVP particles formed using 40μm nozzle.

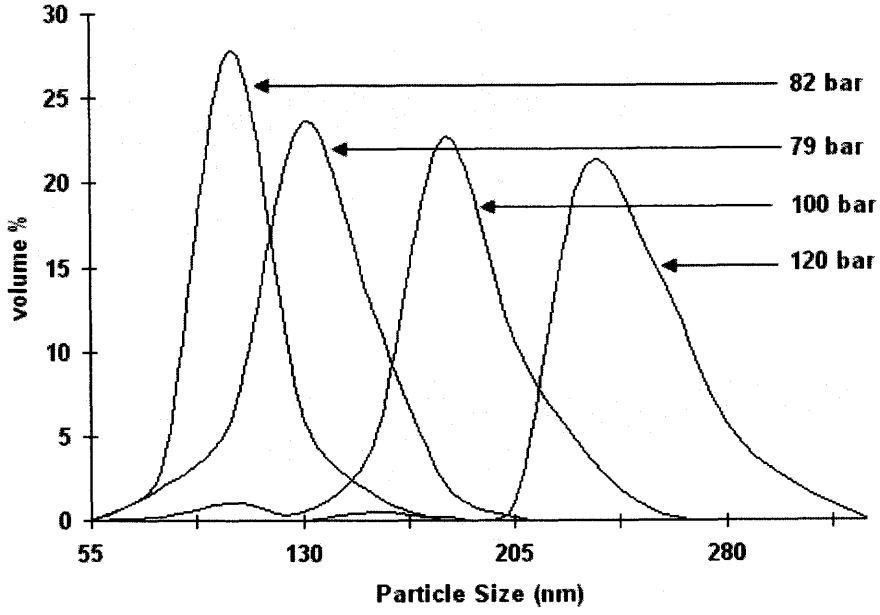

(a): DCM

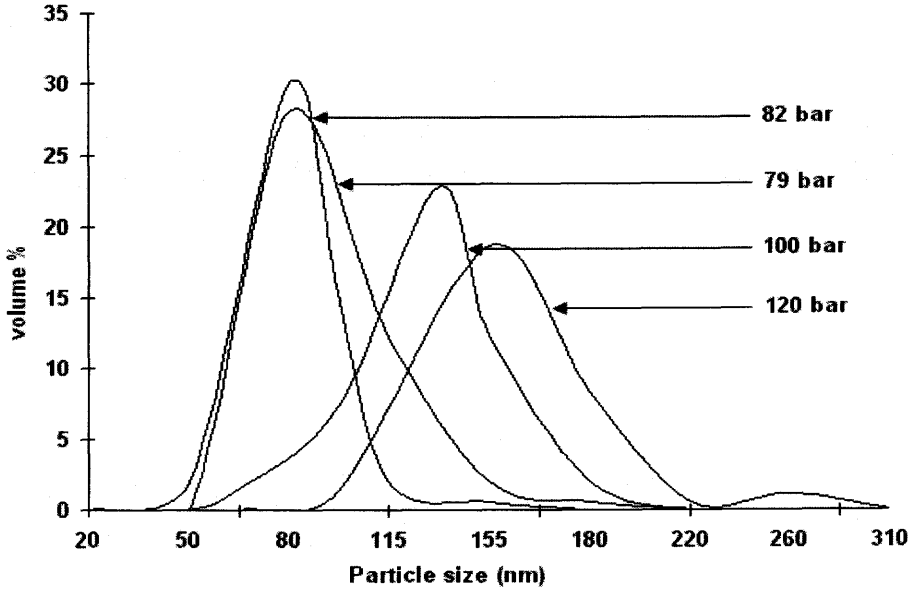

(b): DCM 40 vol% in acetone

Figure 2.12 Particle size distributions of PVP particles formed using 20μm nozzle.

2.6.3 Effects of Nozzle Diameter

H. Krober [152] investigated the effects of nozzle size on particles. He used tartaric acid as a model compound and ethanol/methanol mixture was used to dissolve the compound. Coaxial capillary nozzles of 50μm, 100μm, 150μm and a constant solution (10ml/min) and CO_2 flow rate (6Kg/Hr) were used to synthesis particles. He found that there was no substantial effect of nozzle on the particles size and morphology.

In this study, four nozzles having different inner diameter 127μm, 40μm, 20μm and 10μm were used to inject solution. Solution flow rate (0.2 ml/min) and CO_2 flow rate (2.4 Kg/hr) was kept constant. For different nozzles, different hydrodynamic jet patterns were observed. Variations in particle size and size distribution were observed for different operating conditions. Pure dichloromethane as well as mixture of DCM and acetone in different proportions were used to prepare the solutions.

Figure 2.13 presents the PVP (Mw: 1,300,000) particles precipitated from the solution containing PVP 2 wt/vol % to DCM. (a) shows PVP particles precipitated at 100 bar, 35°C with 127 μm nozzle at 0.2 ml/min flow rate. On the right hand side hydrodynamic regime of jet breakup is shown; (b) shows PVP particles precipitated at 100 bar, 35°C with 40 μm nozzle at 0.2 ml/min flow rate and (c) shows PVP particles precipitated at 100 bar, 35°C with 20 μm nozzle at 0.2 ml/min flow rate.

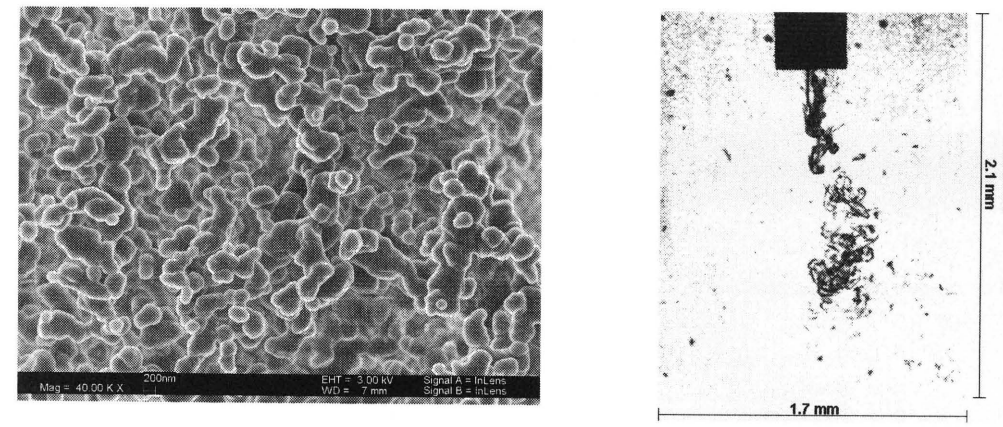

(a)

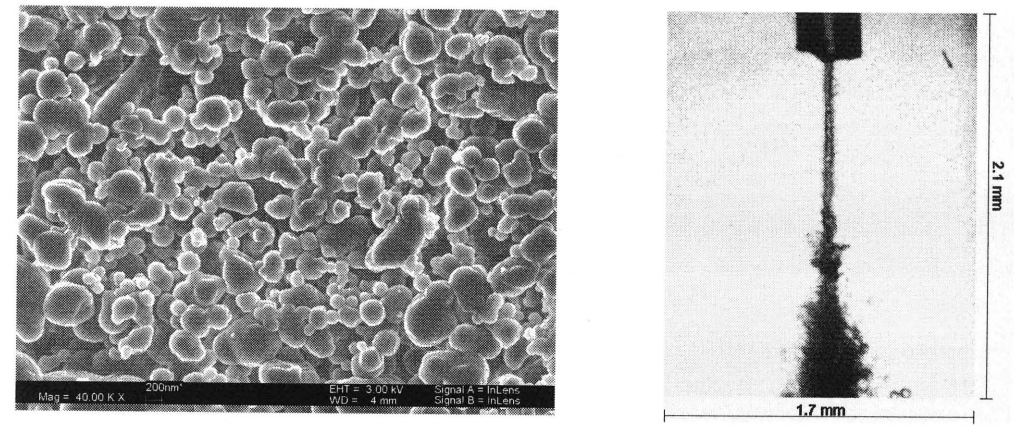

(b)

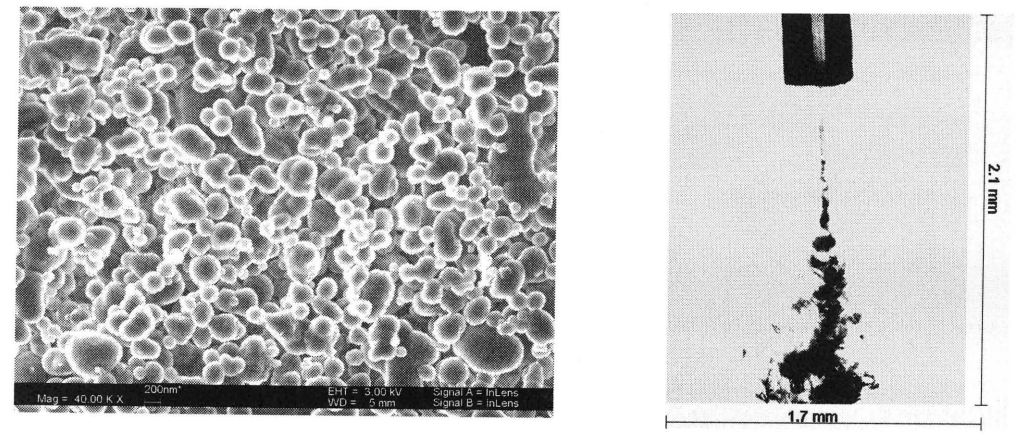

(c)

Figure 2.13 Particle size distribution of PVP particles precipitated from DCM at 100 bar, 35°C, 0.2 ml/min flow rate with 127, 40, 20 μm nozzles.

Table 2.4 show the mean size of PVP particles formed at various operating conditions.

Table 2.4 Mean Particle Sizes for Different Operating Conditions.

Solvent	Pressure	127 μm	40 μm	20 μm
DCM(100)	100 bar	750 ±250	460±200	170±50
DCM(40)/Acetone(60)	100 bar	420±55	200±70	130±70

Particle sizes are based on volume average calculation.

2.6.4 Effect of velocity on particle morphology

Though there is a literature available on effect of solution flow rate [151, 153] and velocity difference between solution and CO_2 on particles size and morphology [154, 155], there are no published studies to relate injection velocity and particles size.

In this research various nozzles from $10\mu m$ to $127\mu m$ were used to generate velocities from 0.2 m/s to 20 m/s. As velocity increases, particle size was found to be reduced. In Figure 2.14, the velocity of the injected solution is varied from 2.65 m/s (Re: 310) to 15.9 m/s (Re: 2215) with 40 μm nozzle at 82 bar and 35°C for solvent DCM and mixture of acetone and DCM. As can be seen from Figure 2.14, with Rayleigh's jet breakup, the larger size particles were formed. However, as the interaction between droplets is minimum in this regime, the aggregation was found to be minimum (Figure 2.14 a) as compared particles formed in other regimes. With increase in injection velocities, the particle sizes were found to be reducing (Figure 2.14 b-d) but the aggregation in particles was found to be increasing because of the jet breakup regimes.

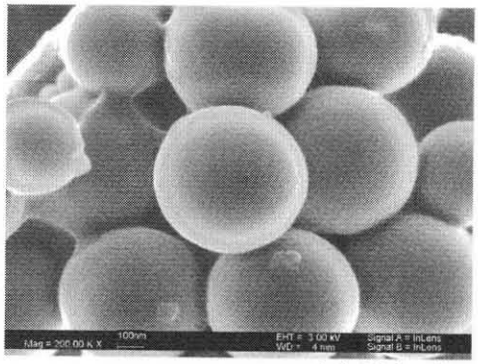
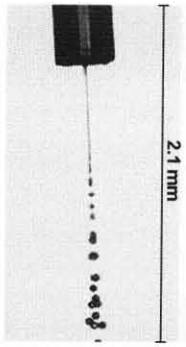

(a) Velocity: 2.65 m/s, Re: 370

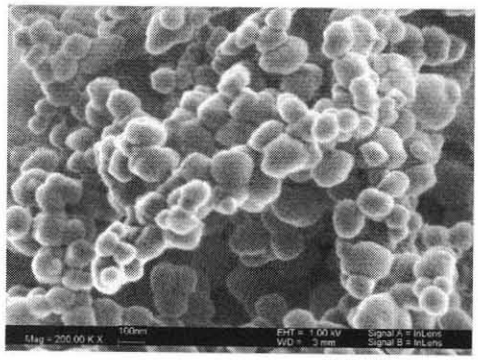
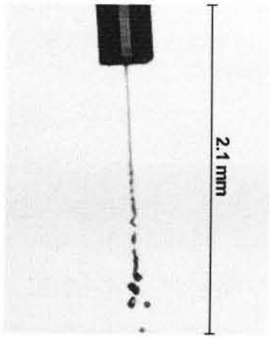

(b) Velocity: 5.3 m/s, Re: 740

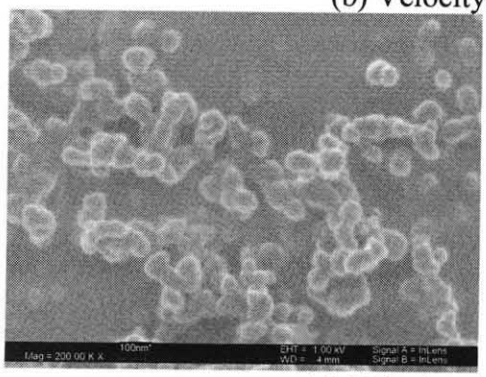
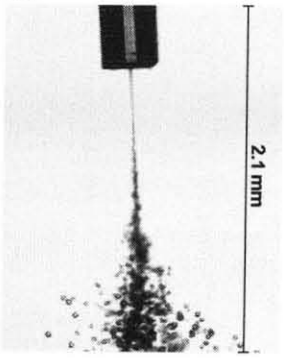

(c) Velocity: 10.61 m/s, Re: 1477

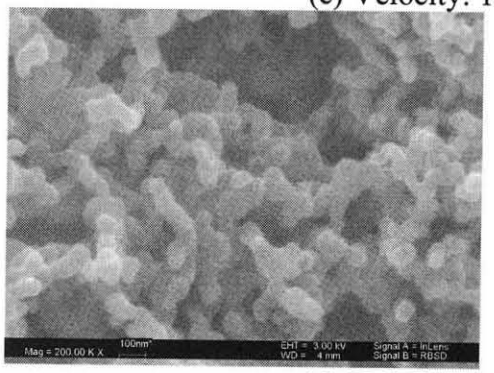
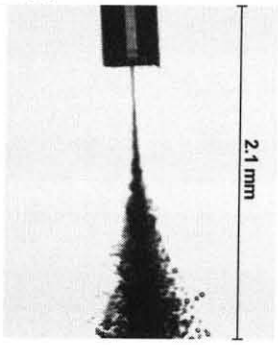

(d) Velocity: 15.91 m/s, Re: 2215

Figure 2.14 PVP particles precipitated with 40 μm nozzle, DCM (40%) and acetone (60%) solvent, at 82 bar, 35°C.

The mean particles size obtained through various experiments are listed in Figure 2.15. Experiments were done at 82 bar, 35 C. The effects of the DCM content of the solvent, the chamber pressure, and the nozzle diameter on the mean diameter of the particles formed in jets of 2wt % PVP Mw 1,300,000 and 360,000 solutions injected through nozzles of different diameters. Chamber pressure 82 bar, temperature 35°C, flow rate varies from 0.1 ml/min to 1.2 ml/min.

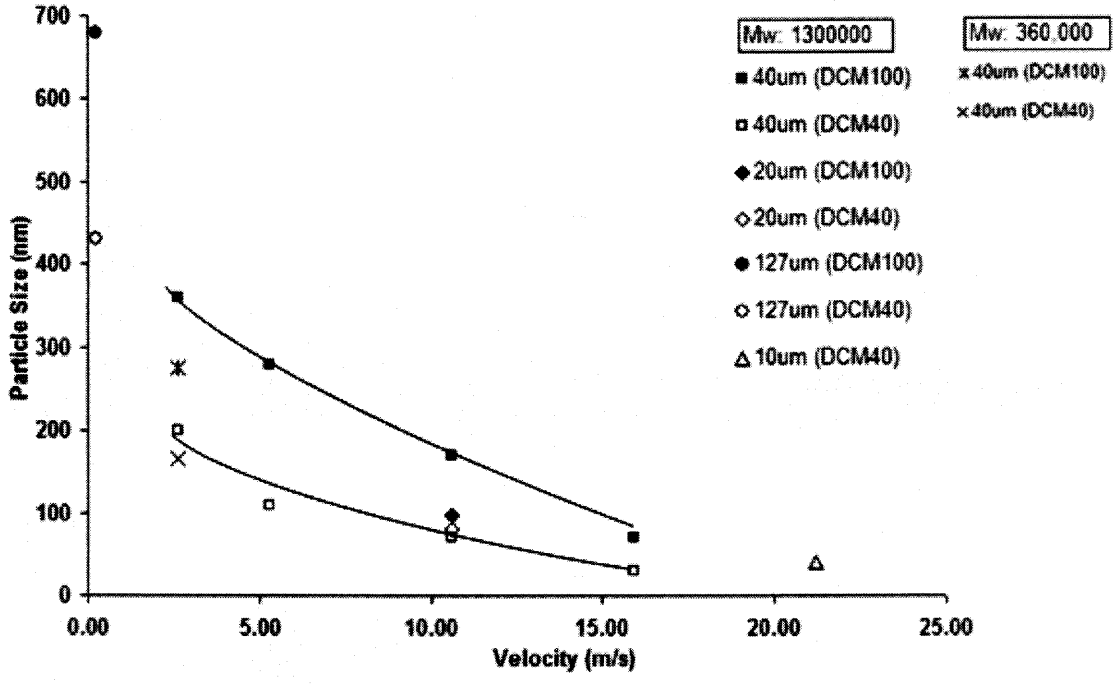

Figure 2.15 Graph of particle sizes obtained at different velocities for various nozzles.

2.6.5 Effects of Molecular Weight on Particles: PVP with two different molecular weights (1,300,000 and 360,000) were used to investigate the effects on particles size and morphology. No significant difference except slight size reduction with lowering the molecular weight was found in the particles size and morphology.

Table 2.5 represents the particles size at various operating conditions for two different molecular weights of PVP.

Table 2.5 Particle Size for Two Different Mw PVP.

	Pressure	**DCM(100) /Acetone(0)**	**DCM(40) /Acetone(60)**
Mw: 1,300,000	79 Bar	410±150	200±80
	82 Bar	350±120	190±80
Mw: 360,000	79 Bar	310±150	180±90
	82 Bar	270±100	170±50

2.7 Conclusion

By estimating the mass transport of CO_2 into the formed drops and the mass transport of solvents out of the drops, as compared to the mass transport during the jet breakup, it can be concluded that the droplets control the particle formation. The falling drops mix with CO_2 through intensive hydrodynamic and diffusion mixing. Since the proposed method of using the solvent mixtures is based on general thermodynamic properties of polymer-solvent systems, it should be applicable to a wide variety of polymers for applications ranging from the improvement of the flow and packing properties of powders to the control of particle interaction with their external surroundings for drug delivery systems. The analysis of the mass transfer presented above suggests that the mass transport of CO_2 into the falling drops and the mass transport of solvents out of the drops, rather than mass transport during the jet breakup, controls the particle formation. The hydrodynamic and diffusion spreading of the falling drops produce about $10^4 - 5 \cdot 10^5$ particles per drop.

A new approach for the synthesis of polymer nanoparticles in microjets based on the use of mixtures of thermodynamically good and poor solvents is developed. This novel approach allows for manipulation of supersaturation at low concentrations, thus facilitating nanoparticle formation. The effects of the solvent composition, nozzle diameter, operating pressure, and jet velocity on the particle size and morphology are investigated. Jet velocity is important to achieve smaller size particles whereas the jet breakup regime is important to control agglomeration of particles. With increase in jet velocity the particle size reduced. Raleigh regime of jet breakup minimizes the interactions between solution droplets minimizing the agglomeration. However, as the jet breakup regimes shifts to Weber instability and spray, the agglomeration of particles

increased because of more interactions between solution droplets. Nozzle diameter was found to affect the particle size, mainly because of increased jet velocity. With increase in pressure, the mean particle size increased but the effect is weak as compared with effects of poor solvent or jet velocity. Addition of poor solvent resulted in higher supersaturation at the same polymer concentration and thus provides smaller particle size. Surface smoothness was improved through combination of poor and good solvents. In case of PVP, molecular weight did not affect particle size and morphology. PVP did not precipitate below critical point of mixture.

CHAPTER 3

FINE PARTICLE COATINGS AND ENCAPSULATIONS USING SUPERCRITICAL FLUIDS

3.1 Particle Coatings using SAS Technique

Particle coatings involves the application of another material onto the surface of individual particles to modify their surface properties, such as flowability, wettability, controlled release, flavor, taste, etc [156]. It is difficult to coat individual submicron or nano sized particles with traditional techniques [157]. The coating or encapsulation of nanoparticles has been found to be of particular interest for the controlled release of drugs, genes, and other bioactive agents. Controlled release systems provide the benefits of protection from rapid degradation, targeting delivery, control of the release rate, and prolonged duration of bioactive agents [158].

Supercritical fluids show promise in the field of coating of nano and submicron sized particles. O. Boutin et al. [159] investigated the co-precipitation of herbicide and biodegradable polymers by the supercritical antisolvent technique. The purpose of the investigation was to coat the herbicide particles with biodegradable polymers to achieve controlled release of herbicide drug. Different coating substances were tested in order to study release kinetics. The positive effect of the polymer embedding upon the herbicide release was evidenced by a kinetic study. As the particle size was increased, its specific surface area was decreased and the kinetics of the release of the active molecule was found to be slowed down.

I. Santos et al. [160] investigated the coating of protein particles in order to achieve sustained-release. Lipids (Gelucire and Dynasan) were used as coating materials.

A controlled release with a limited burst effect was achieved at 37°C over a 24 hour period. With Gelucire, the initial burst was as small as 40% whereas with Dynasan, the initial burst was upto 70%. However, for coated protein, controlled releases for both of the lipids were obtained.

A novel technique was used by R. Schreiber et al. [161, 162] to coat the fine particles. Host particles (Silica or glass beads) were fluidized in a high pressure fluidized bed and then the homogeneous mixture of molten paraffin and SC CO_2 was injected from the bottom of the fluidized bed. Due to different conditions in the mixing-autoclave and the fluidized bed the paraffin precipitated in the vicinity of the nozzle and adhered to the solid particles. The coating experiments were carried out at fluid velocities up to 2.23 times the minimum fluidization velocity. The operating conditions for the coating process were determined by the investigation of the system paraffin-CO_2 by means of solubility and differential scanning calorimetry measurements. An even distribution of the coating material within the fluidized bed was observed at fluid velocities higher than 1.2 times the minimum fluidization velocity.

This technique could be used to coat the drugs for controlled release. Paraffin was uniformly distributed on the particles, but a complete coating could not be achieved with this method. Various particles with sizes between 100 and 200 μm were encapsulated with waxes commonly used in technical coating applications. A smaller pressure drop across the nozzle led to more uniform and even coatings. Glass beads, ceramic spheres, potassium chloride, and lactose showed similar coating results, whereas different morphologies were observed with a plastic material, characterized by a rougher surface and a lower surface energy. The high quality of the coating was confirmed by standard

dissolution tests with coated potassium chloride crystals and lactose agglomerates. A high-pressure fluidized bed was successfully used to create thin, uniform and solvent-free paraffin coatings. The use of paraffin having a low glass transition temperature near the operation temperature of the fluidized bed led to a high agglomeration tendency, whereas hardly any agglomeration was observed using paraffin with a higher glass transition temperature. Ceramic beads, potassium chloride crystals and lactose agglomerates were successfully coated as well. Interfacial tensions and surface energies seemed to have an influence on the spreading of the coating material on the surface. In the case of plastic granules the spreading was impeded also due to its rougher surface in comparison to the other materials.

H. Krober et al. [163] used supercritical fluidized bed to coat the fine and heat sensitive particles. Krober found that the fluidization of particles under sub or supercritical conditions is different from that under atmospheric pressure. With increasing pressure the minimum fluid velocity which is necessary to start the fluidization decreases. It was possible to fluidize glass beads with a mean particle size of 7.4 μm. Stearyl alcohol was used for the coating experiments with glass particles of a mean particle size of 70 μm. Complete coatings with a layer thickness between 1μm to 8μm was achieved depending on the coating time and process conditions.

Y. Wang et al. [157, 164] investigated the coating of nano and submicron sized silica particles using SAS process. He suspended the silica particles in the polymeric solution and then the suspension was sprayed into supercritical CO_2 using 254 μm sized capillary nozzle. Effects of various operating conditions like ratio of host particles to polymer, flow rate of solution injection, use of surfactant, temperature, and pressure were

investigated. Silica particles as small as 16 nm sized were successfully coated with this technique. The mechanism of the coating process was investigated by Y. Shen [165]. He used different biopolymers as coating materials. For different polymers, he found different types of coating with different coating thicknesses. Based on the experimental investigation he proposed a model explaining the mechanism of particles coating using supercritical fluids.

3.1.1 Experimental Setup

The SAS coating process is similar to the SAS particle formation process and can be performed near critical pressure and temperature. Polymethyl methacrylate (PMMA) polymer was dissolved in an organic solvent(s) and host particles (silica particles) were suspended in the solution. The solution was then sprayed into supercritical CO_2, precipitating polymer on the suspended host particles, coating them. An experimental setup used for coating work is same as described in Chapter 2 (Figure 2.1). A capillary tube is replaced by a coaxial ultrasonic nozzle to spray the suspension. Suspension is fed into high pressure chamber through the central capillary of the ultrasonic nozzle and CO_2 is fed through the outer capillary. Fresh CO_2 was circulated continuously before start of the suspension injection and continued to circulate for 2 hours after the injection was stopped to ensure the complete removal of solvents from the coated particles.

The ultrasonic nozzle is shown in the Figure 3.1. The smaller nozzle inside has an inner diameter of 300 μm with the wall thickness of 130 μm. The remaining part of bigger nozzle is a ring-shaped geometry with an inner diameter of 560 μm and outer diameter of 760 μm. between the tips of the two nozzles, there is a small mixing zone

with the length of 1.02 mm. The nozzle works at a fixed frequency of 60 kHz.

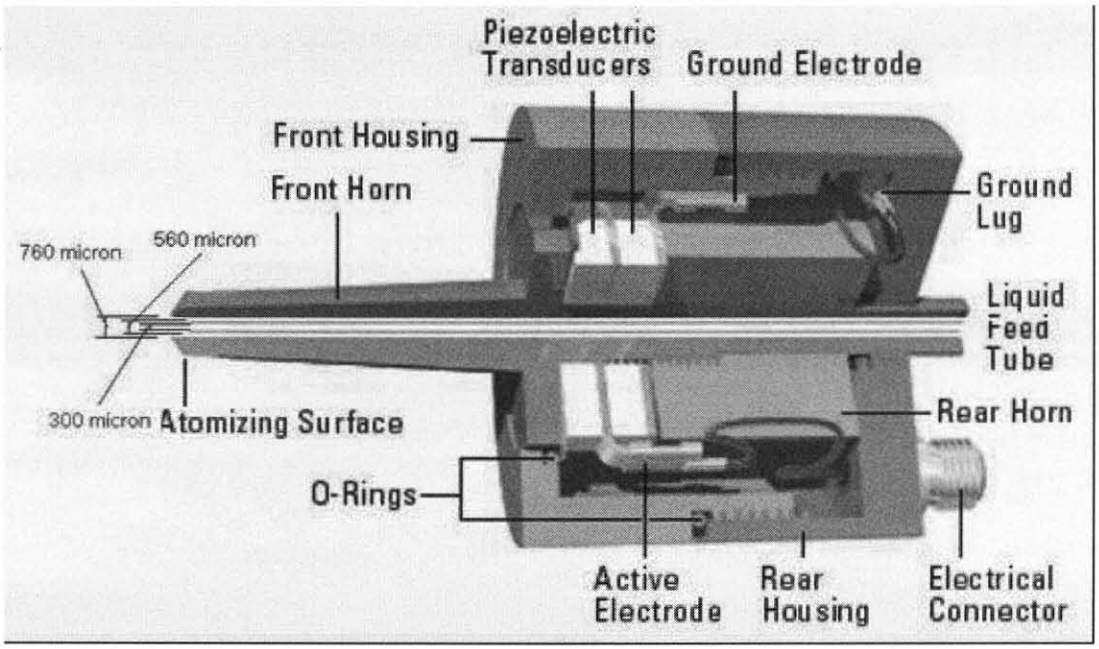

Figure 3.1 The schematic diagram of an ultrasonic nozzle.

High pressure CO_2 cylinders (Bone Dry, 99.9% pure) were purchased from MG Industries. Acetone (HPLC Grade, 99.5+ %), DCM (HPLC Grade, 99.7+ %) and PMMA were purchased from Sigma Aldrich. All materials are used as received. The critical point of pure CO_2 is 31.1^{0}C and 73.8 bar. At the operating temperature of 35°C, the critical pressures of the CO_2-DCM and CO_2-acetone mixtures are about 78 bar and 72 bar, respectively [166-168].

Characterization of the coated particles was done using the imaging technique like Field Emission Scanning Electron Microscope (Leo 1530VP) and particles size distribution was obtained using laser scattering instrument (Coulter LS 230). A small amount of powder was placed on an adhesive tape and then sputter coated with carbon in

a Baltec MED 020 unit. The coated particles were then analyzed under SEM instrument at various magnifications. Coulter LS 230 employs light scattering to measure the mean diameter of micron and submicron sized particles. A sample was prepared by sonicating a small amount of powder in deionized water with a Fisher Scientific FS30 bath sonicator. Several samples were analyzed with LS 230.

3.1.2 Results and Discussion

Silica particles (180nm and 2μm) were used as a host material. PMMA polymer was used as a coating material. Silica 2 wt/vol% to solvents was used in all of the coating experiments. The ratio of PMMA to silica was varied from 9.1 to 23 wt/wt%.

3.1.2.1 Effects of polymer ratio on the coatings

Silica particles 2μm and 180nm were used to coat with the PMMA polymer. The amount of polymer is important in controlling the coating thickness and agglomeration in coated particles. The host particles to polymers ratio was varied from 9.1 to 23 wt/wt %. Higher the polymer ratio higher the aggregation was found in the coated silica particles. Coated particles were analyzed in terms of mean particle size and particle size distribution to determine the degree of agglomeration. Figure 3.2 shows the SEM images of the 180 nm sized silica particles coated with PMMA. Acetone was used to dissolvent the polymer. The operating conditions were pressure: 80 bar, solution flow rate: 4 mL/min, CO_2 flow rate: 20 Lpm, temperature: 35C. Silica 180nm coated with PMMA 9.1 wt/wt % in (a); 16.7 wt/wt % in (b); and 23 wt/wt % in (c).

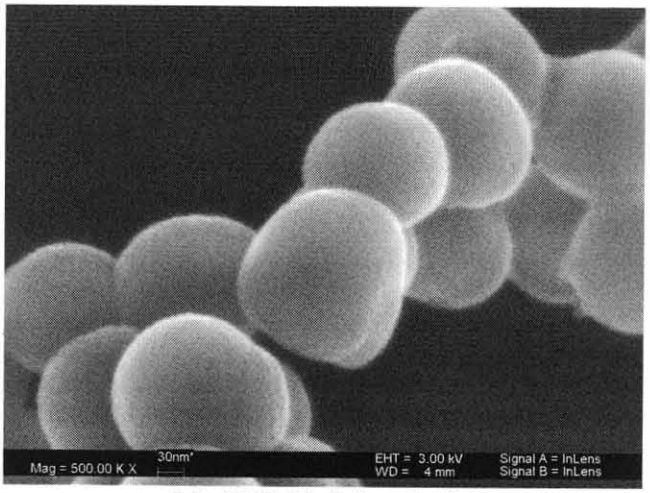

(a): PMMA 9.1 wt/wt%

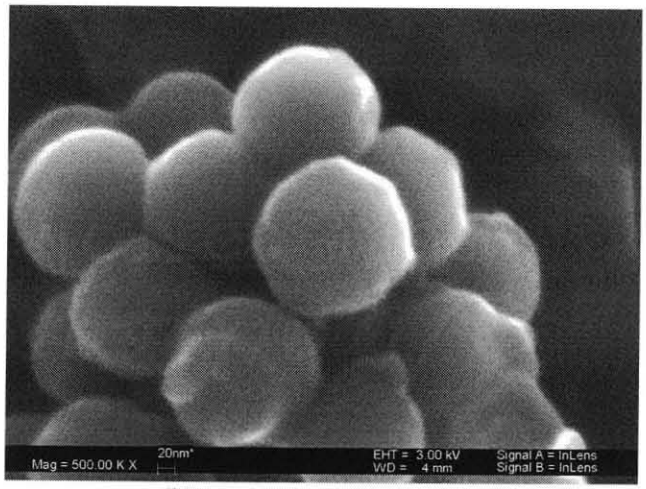

(b): PMMA 16.7 wt/wt%

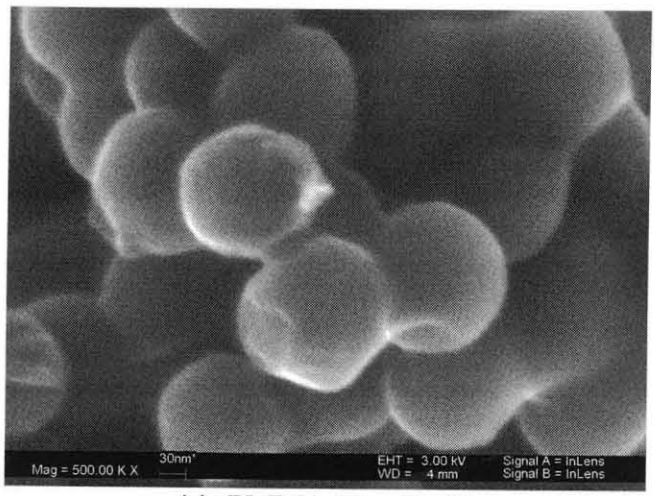

(c): PMMA 23 wt/wt%

Figure 3.2 PMMA coated Silica particles. Acetone is used as a solvent.

The particles size distributions for the PMMA coated silica particles are presented in Figure 3.3. Coated particles were dispersed in the deionized water. The suspension was sonicated for 15 min to ensure the homogeneous dispersion of the coated particles in deionized water. Laser scattering instrument was used to obtain the particle size distribution. The operating conditions were pressure: 80 bar, solution flow rate: 4 mL/min, CO_2 flow rate: 35°C and acetone was used as a solvent. The host particles size is 180nm in (a) and 2μm in (b).

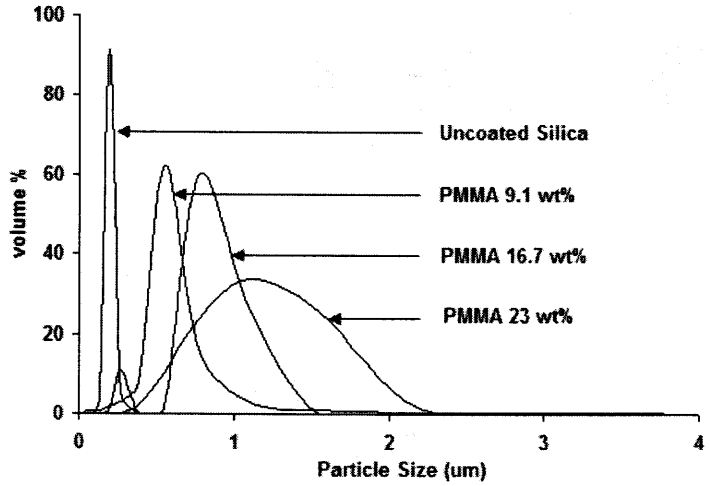

(a)

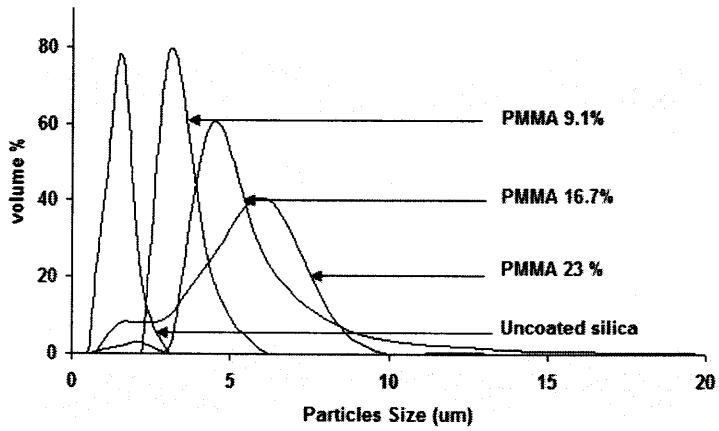

(b)

Figure 3.3 Particle size distribution for silica (a) 180nm and (b) 2μm coated with the PMMA. Acetone was used as a solvent.

3.1.2.2 Effects of solvent on the coatings

Choice of solvent is very crucial for the coating experiments. Better dispersion of host particles (e.g. silica) in the solvent helps in reduction in agglomeration in coated particles. Two different solvents (DCM and acetone) were used in the coating experiments and the results were compared for the degree of agglomeration in coated particles. Silica particles are dispersed better in acetone than in DCM. It can be seen from the particle size distribution that when acetone was used as a solvent, the degree of agglomeration was lower than when DCM was used. Figure 3.4 shows the particles size distribution of PMMA coated silica particles (180nm). The operating conditions used for the coating experiments were 80 bar, 4 Watts, 35°C, 4 mL/min. The PMMA to silica ratio is 9.1 wt/wt% in (a); 16.7 wt/wt% in (b) and 23 wt/wt% in (c).

Silica dispersion into the solvents was investigated by visual observation of the dispersions. Silica particles in 2 wt/vol% were dispersed in acetone and DCM. These two suspensions were sonicated for 5 minutes. Then, the dispersions were kept for stabilization. Silica in DCM dispersion segregated in two to three hours. However, the silica in acetone dispersion did not segregate even after 48 hours. Figure 3.4d shows the silica particles suspended in the DCM, acetone and in the mixture of DCM and acetone. As can be seen from the Figure 3.4d, silica particles disperse better in acetone more than in DCM.

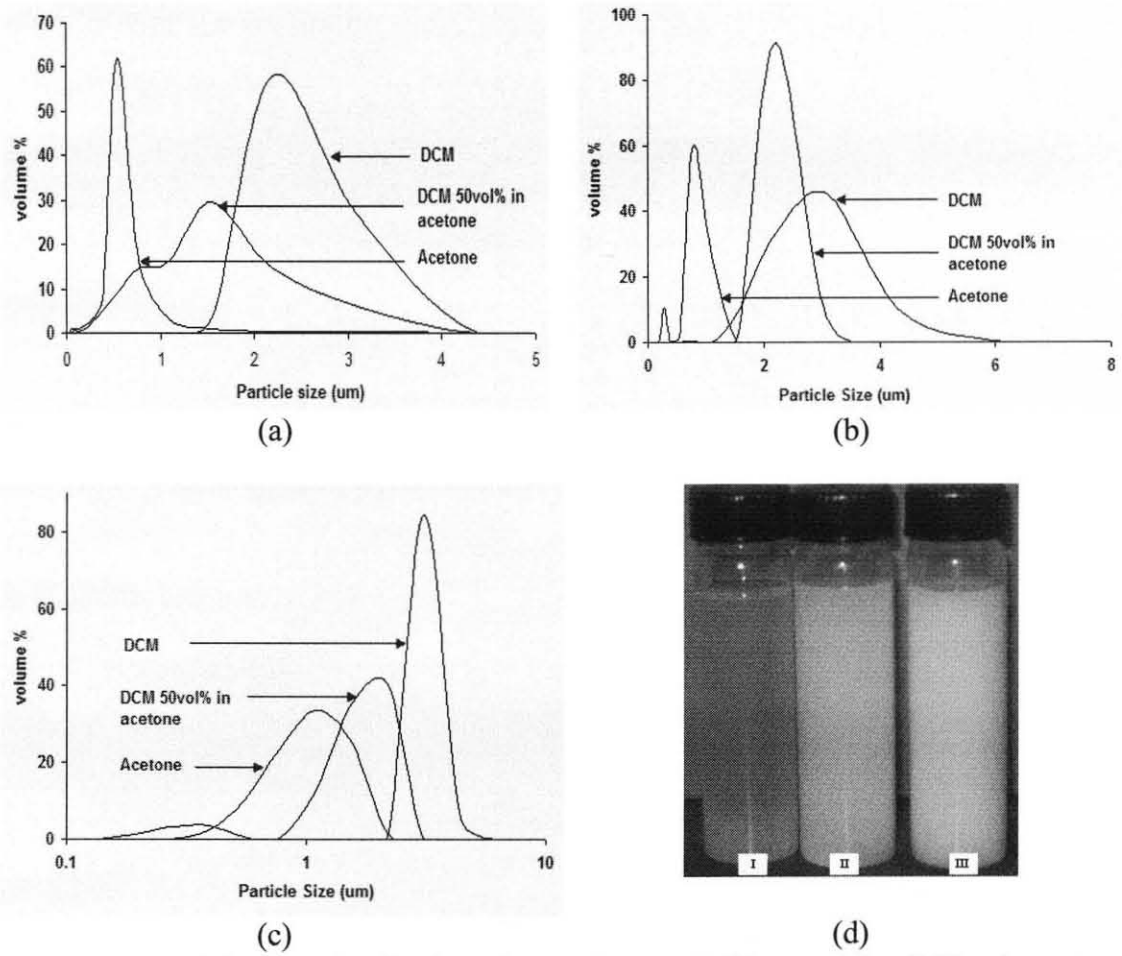

Figure 3.4 Particles size distribution of PMMA coated silica particles (180nm).

3.1.2.3 Effects of poor solvent on the coatings

The solubility of PMMA in hexane was investigated by photon correlation spectroscopy. PMMA does not dissolve in hexane. Hence, hexane was used as a poor solvent for PMMA. Silica 180nm sized particles were coated using PMMA dissolved in a mixture of DCM and hexane as well as acetone and hexane. Figure 3.5 shows the SEM images of the silica 180nm sized particles coated with the PMMA. (a) DCM only; (b) Hexane 30 vol/vol % in DCM; (c) acetone only; (d) Hexane 30 vol/vol % in acetone and (e) Water 30 vol/vol % in acetone.

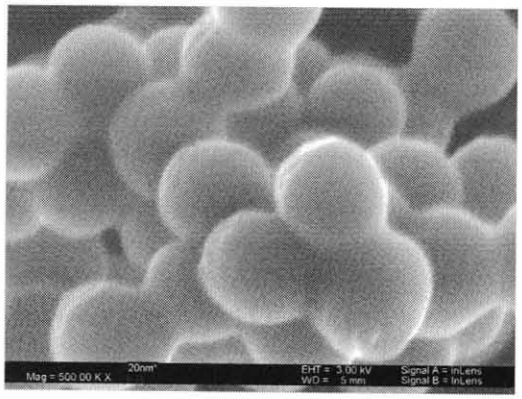

(a)

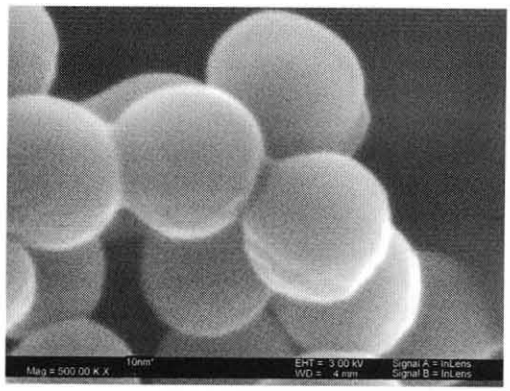

(b)

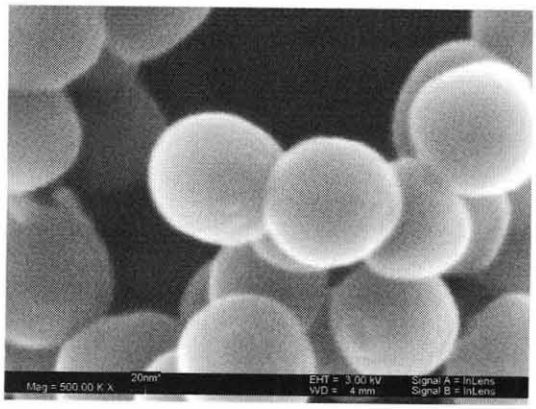

(c)

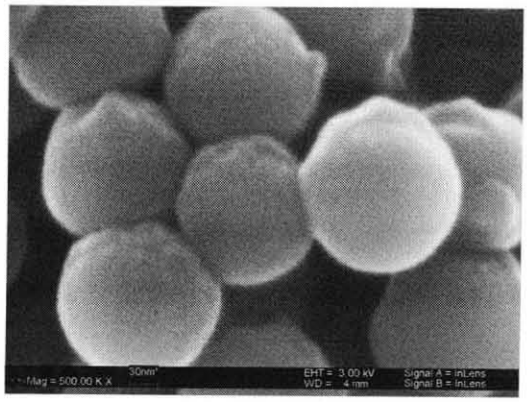

(d)

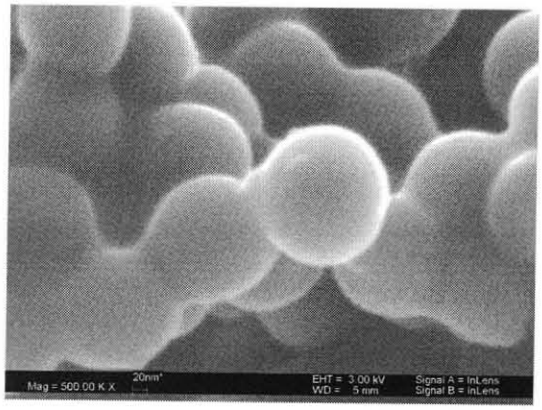

(e)

Figure 3.5 Effect of poor solvent on PMMA coated silica particles. PMMA 9.1 wt/wt % of silica was used for following experiments.

PMMA does not dissolve in deionized water. Hence, water also works as a poor solvent for PMMA. However, water is insoluble in SC CO_2 at 80 bar and 35C. Hence, when water was used as poor solvent, PMMA coated silica particles with moisture were obtained. The moisture was then removed with vacuum drying. As can be seen from Figure 3.5 and 3.6, when hexane was added into DCM for the coating experiments, the degree of agglomeration reduced. However, hexane-acetone mixture did not produce much reduction in the degree of agglomeration as compared to acetone alone. Use of water as a poor solvent did not produce good results and the removal of water from the coated particles became an additional process in the SCF coating process.

Figure 3.6 shows the particles size distribution for the silica 180 nm sized particles coated with PMMA. Solvents used are acetone, DCM, acetone-hexane, DCM-hexane and acetone-water to dissolve the PMMA polymer.

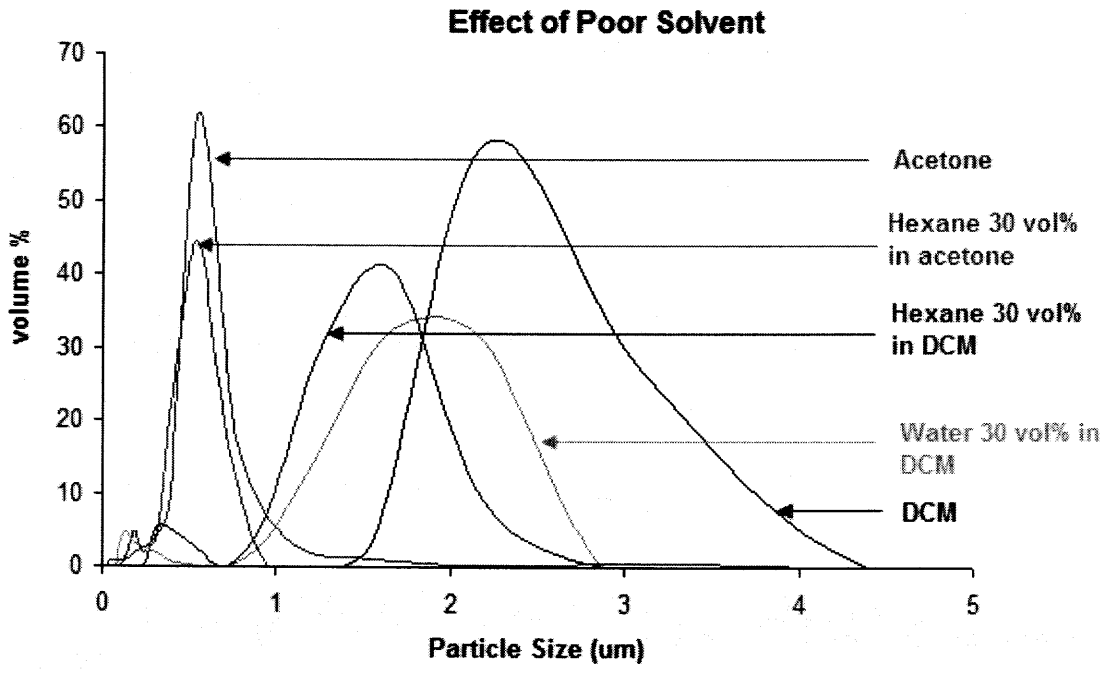

Figure 3.6 Particle size distribution of 180nm sized silica particles coated with PMMA.

Effect of poor solvent on aggregate size was studied by using 2μm sized silica as well. Figure 3.7 shows the particles size distribution of PMMA coated silica particles with and without use of poor solvent. (a) PMMA is 9.1 wt/wt % with silica; (b) PMMA is 16.7 wt/wt % with silica and (c) PMMA is 23 wt/wt% with silica.

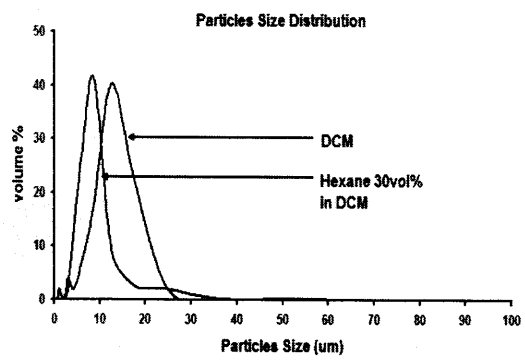

(a)

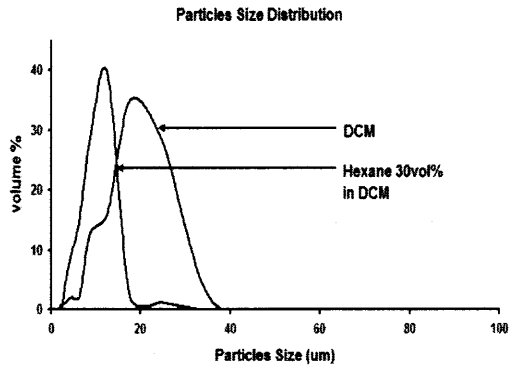

(b)

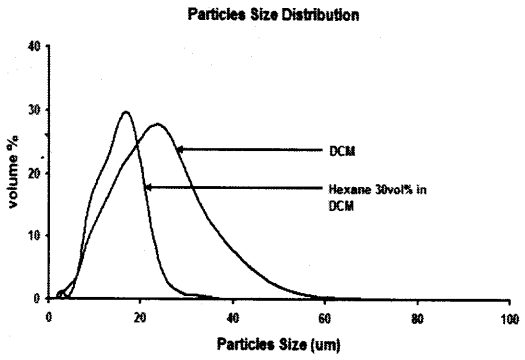

(c)

Figure 3.7 Particle size distribution of 2 μm silica particles coated with PMMA.

Y. Wang et al. [169] investigated the 500nm sized silica particles coating with eudragit polymer. Wang used 254 μm sized capillary nozzle to inject the suspension. Wang found the degree of agglomeration to be varying from 4.5 to 15 when the coating polymer (eudragit) was varied from 12 to 25 wt% of silica [169].

The degree of agglomeration increased with increase in polymer to silica ratio. However, it reduced with the increase in silica particles size. Aggregation found to be reducing with addition of poor solvent (hexane) in DCM but it did not have significant effect when added into acetone. When water was used as a poor solvent, the aggregation was increased. Figure 3.8 shows the degree of agglomeration at various operating conditions. The operating pressure, ultrasonic nozzle power, temperature and solution flow rate were kept at 80 bar, 4 watts, 4 mL/min and 35°C respectively.

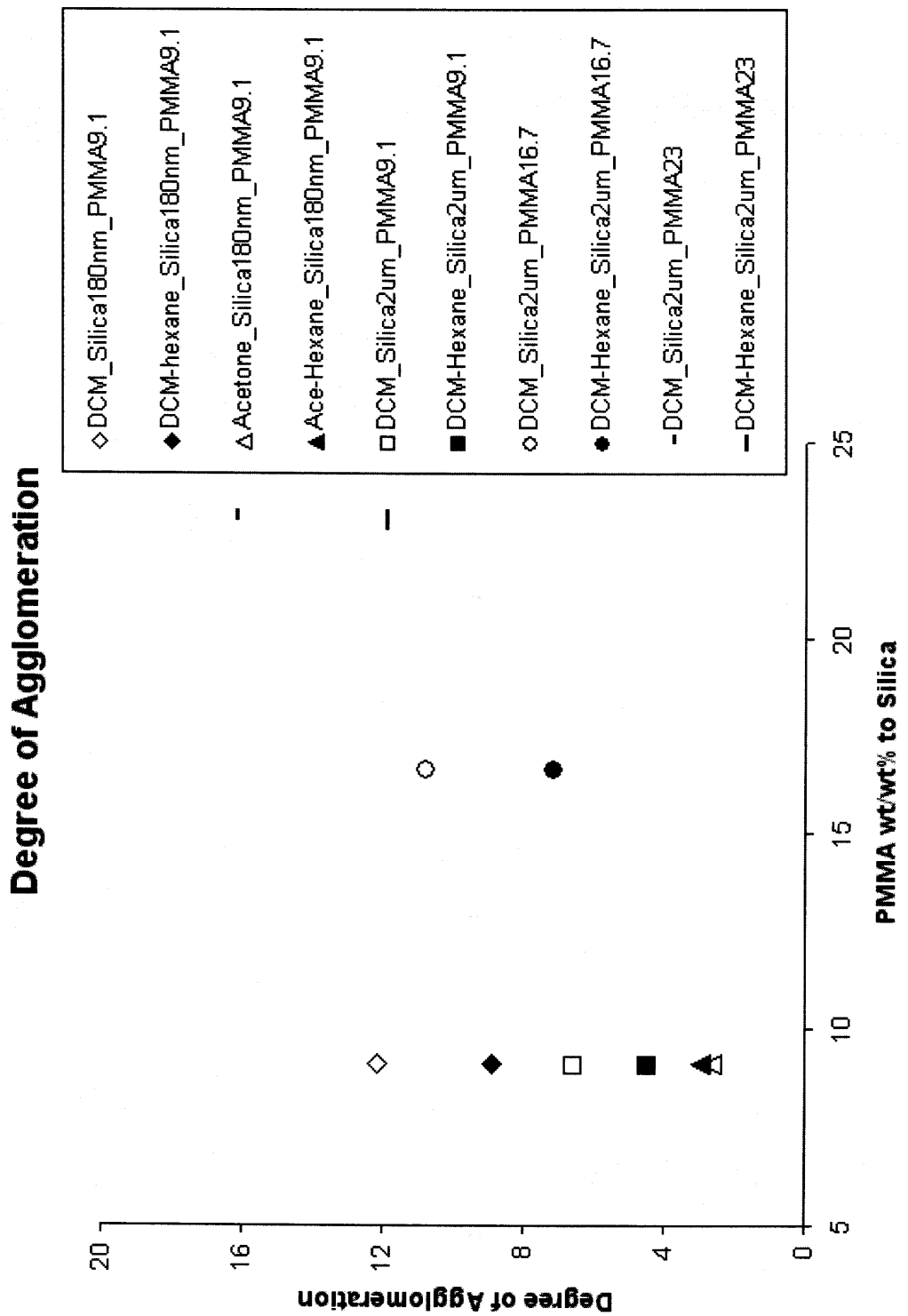

Figure 3.8 Degree of agglomeration at various operating conditions.

3.2 Particle Coatings using RESS Technique

In the Rapid Expansion of Supercritical Solution (RESS) process, the SCF is used to dissolve a nonvolatile solute. The resulting solution at high pressure and temperature; then expanded to the lower pressure and sharp decrease in the solvent density is achieved. This results in sharp decrease in solubility of SCF and the solute precipitates out. The expansion is a mechanical perturbation traveling at a very high speed and hence, the uniform conditions are ensured within the solution. Once the nucleation starts due to the sudden expansion, the supersaturation reaches uniformly within the solution. This results in narrow particles size distribution.

When the solute nucleates due to sudden pressure drop, the supersaturation uniformly reaches throughout the media resulting narrow particles size distribution [170]. RESS provides a useful tool to affect and control the size and morphology of the precipitated powders. When RESS is carried out in the usual mode a solvent free product is obtained.

Particles formation and coating using RESS method is gaining more and more attention as it is a solvent free process and sudden expansion gives smaller and deagglomerated particles. Kim et al. [171] studied micro encapsulation of naproxen through RESS process and Mishima et al. [172] did a similar study on RESS coating. They shared same disadvantage of the limited solubility of polymer inside CO_2 and besides that, the RESS process generally requires a very high operating pressure (above 200 bar) and temperature (80°C), which are undesirable for most of the drugs.

No surfactants or nucleating media are required to trigger the nucleation and the solvent is removed by a simple mechanical separation. The possibility of obtaining a full

solvent-free product, at the same time controlling the dimension of particles, is probably the most important feature when pharmaceutical substances are used. Potential applications of RESS in the pharmaceutical industry have been studied by several investigators [171, 172]. On the other hand, SCF solvent capacity is the essential requirement and also the main constraint for the development of RESS. For example, carbon dioxide (CO_2), which is useful for many applications, is not able to dissolve polar substances due to its low polarizability. Different SCFs could be chosen in this case: a second solvent (cosolvent) can be added to enhance the CO_2 solvent capacity, but it remains within the precipitated product. In general, polymers possess low solubility in SCFs, including CO_2 (with or without co-solvents).

3.2.1 Experimental Setup

The RESS coating process works on the same basic principle as the RESS particle formation process. In case of RESS method, coating material (polymer) is dissolved into SC CO_2 at high pressure and temperature. It is then expanded through small capillary nozzle. Sudden pressure drop results in reduction in solvation power of SC CO_2. Hence, the polymer precipitates out of CO_2. These polymer nuclei grow on host particles coating them partially or fully.

Polyvinyl fluoride (PVDF) was purchased from Sigma Aldrich. 2μm sized silica powder was purchased from Shin Etsu, Japan. 5 grams of silica particles was placed in a high pressure chamber. PVDF powder was then placed at pr-calculated quantity (9.1 to 23 wt/wt % to silica). The temperature and pressure of the chamber was then increased to 65C and 1500 psi or 2300 psi (depending on the experiment). The stirring of the

supercritical solution continued for two hours. The solution was then sprayed in another vessel maintained at the atmospheric pressure through a capillary nozzle (254 μm or 508 μm). The pressure and temperature of the vessel containing supercritical solution was maintained throughout the experiment. Stirring helps to prepare a uniform supercritical solution. As the supercritical solution was sprayed through a capillary nozzle to achieve the coating, fresh CO_2 was continuous fed to the supercritical vessel to maintain the pressure. An experimental setup for particles coating using RESS is shown in Figure 3.9.

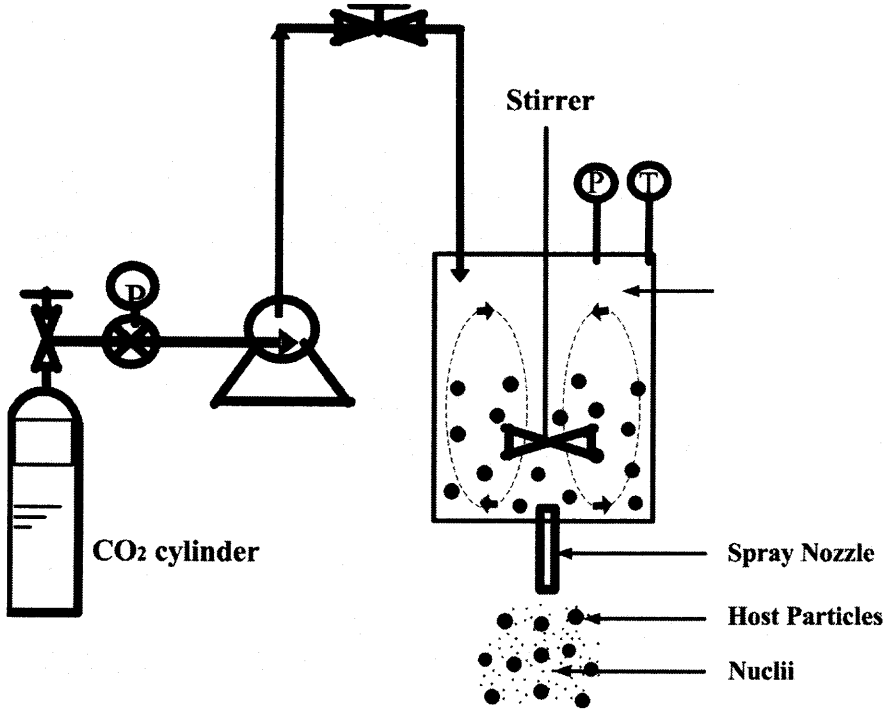

Figure 3.9 Schematic diagram of an experimental setup for particle coating using RESS method.

Characterization of the coated particles was done with the imaging technique like Field Emission Scanning Electron Microscope (Leo 1530VP) and particles size distribution was obtained using laser scattering instrument (Coulter LS 230). A small

amount of powder was placed on an adhesive tape and then sputter coated with carbon in a Baltec MED 020 unit. The coated particles were then analyzed under SEM instrument at various magnifications. Coulter LS 230 employs light scattering to measure the mean diameter of micron and submicron sized particles. A sample was prepared by sonicating a small amount of powder in deionized water with a Fisher Scientific FS30 bath sonicator. Several samples were analyzed with LS 230.

3.2.2 Results and Discussion

Silica particles (2μm) were used as a host material. Polyvinyl fluoride (PVDF) polymer was used as a coating material. The ratio of PMMA to silica was varied from 9.1 to 23 wt/wt% for various experiments.

3.2.2.1 Effects of Pressure on Coatings

Coating experiments were done at three different pressures 2300 psi, 1500 psi and 0 psi respectively. However, once the pressure was chosen for a particular experiment, it was kept constant inside the vessel throughout an experiment. Higher the pressure, PVDF dissolves in CO_2 in higher amount. Hence, better coating was obtained when higher pressure was used. Also, higher pressure drop during spraying the suspension resulted in lesser agglomeration in coated particles. Hence better coating on silica particles was observed when 2300 psi was used as compared with when 1500 psi was used. Also, higher pressure difference helps in deagglomeration of coated particles. Hence, less agglomeration in the coated silica particles were found with increase in pressure. Figure 3.3 shows the effects of pressure on the coating.

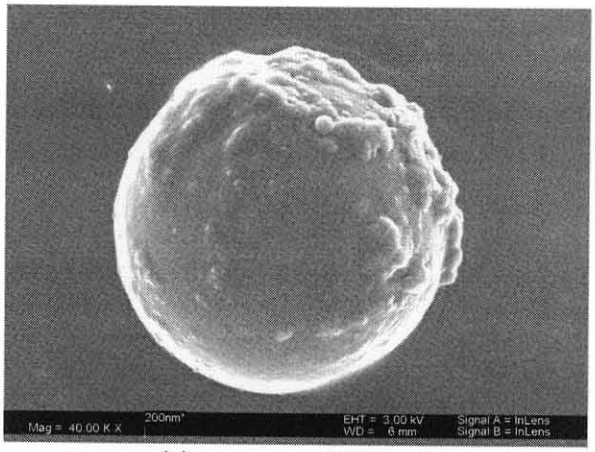

(a): pressure 2300 psi

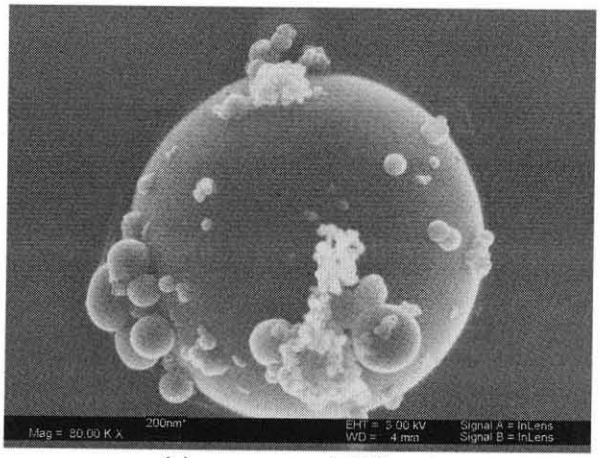

(c): pressure 1500 psi

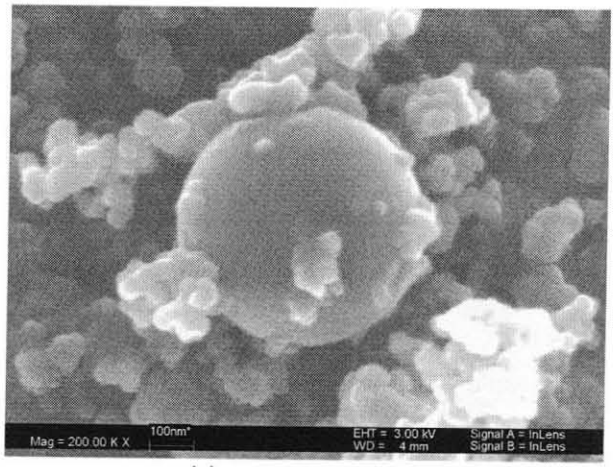

(c): pressure: 0 psi

Figure 3.10 PVDF coating on 2μm sized silica particles at different pressures and nozzle sizes.

3.2.2.2 Effects of Nozzle on Coatings

Two different nozzles (254μm and 508μm) were used to spray the supercritical solution in the coating experiments. Using Bernoulli's Equation it can be seen that the smaller nozzle produces larger velocity, which results in reduction in agglomeration of the coated particles. Figure 3.4 shows the mean size of agglomerate when two sprayed through two different nozzles at various pressures. PVDF 9.1 wt/wt% to silica was used as a coating material in all of the experiments. Various pressure ranging from 2300 psi to 0 psi were used to prepare the supercritical solution and the pressure and temperature (65°C) of the vessel containing supercritical solution was kept constant throughout the experiment. As the supercritical solution was sprayed through a capillary nozzle to achieve the coating, fresh CO_2 was continuous fed to the supercritical vessel to maintain the pressure.

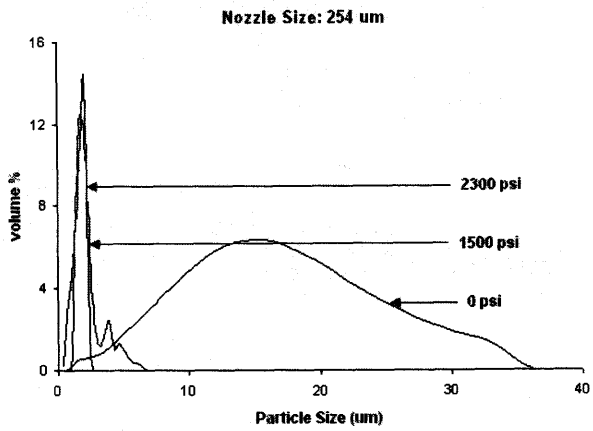

(a): PVDF 9.1 wt %

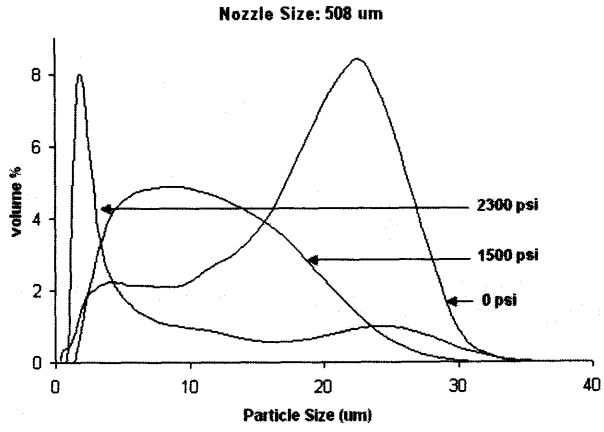

(b): PVDF 9.1 wt %

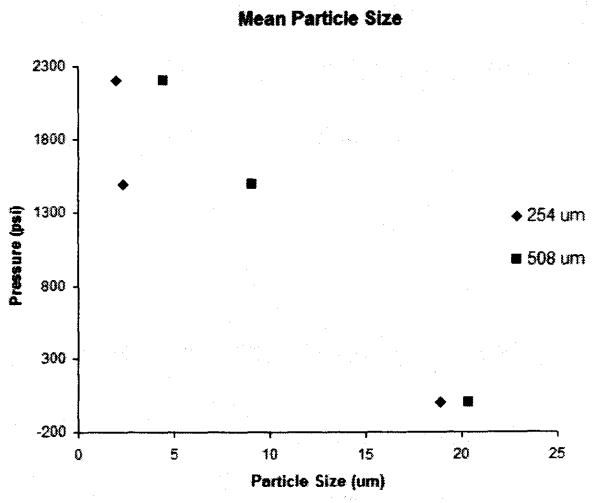

(c)

Figure 3.11 Particle size distribution of coated silica.

3.3 Particle Coatings using PGSS Technique

The PGSS method for the production of polymer particles is very useful because the diffusivity of SC CO_2 in most of the biopolymers and similar compounds is very high. PGSS has big advantages for highly viscous, waxy, and low glass transition temperature polymers [173]. In PGSS, a molten polymer is saturated with supercritical fluid (e.g. SC CO_2) and then the gas-saturated solution is expanded through a nozzle from a supercritical to sub-critical pressure. The gas-saturated solution has low viscosity due to an increase in the free volume. During depressurization, supersaturation of the gas leads to a rapid expansion of the polymer melt and gas so that fine particles are formed. The particles are solidified by the cooling effect of the expanded gas. Moreover, the gas is also easily separated. A dense gas can be solubilized in large quantities in a liquid.

In PGSS, it is possible to obtain different morphologies and particle sizes by changing processing conditions. These properties mainly control the degradation rate or solubility of biodegradable polymer particles and hence, the release rate of an encapsulated drug can be controlled. Encapsulation of drugs in biodegradable materials is very attractive field of pharmaceutical industry [174]. F. Mandel et al. [175] patented the method of impregnating a polymer (disc or particles) with a drug from solution; CO_2 plasticizes the polymer, the allowing the diffusion rate of the drug to be controlled. It can be applied in batch mode, where a single phase solution is formed using a mechanical stirrer, and, in continuous mode, where a static mixer is used to saturate molten polymer with a gas. Particles with different morphologies, foam and dense, were obtained by tuning the processing conditions that determine the amount of CO_2 dissolved. With this

process, controlling the physical properties, such as particle size, particle size distribution and morphology is easy.

E. Weidner et al. [173] investigated micronization of polyethylene glycols (PEG) in pilot plant PGSS apparatus. The PEG was melted in a stirred vessel by increasing temperature and pressure of CO_2 to supercritical state. The gas partly dissolved in the polymer phase. The mixture of gas and liquid was then expanded through a nozzle. Volume increase of the gas causes the liquid to disintegrate into tiny droplets. As the gas cooled down, the droplets solidified into fine particles. In a cyclone, particles were separated from the gas. Very uniform sized particles from 15μm to 50μm were formed depending upon the operating conditions and molecular weight of polyethylene glycols. He also produced the micron size particles of acrylic coatings, polyester - epoxy systems and low-melting polyester coatings using PGSS process [176]. Similarly, the synthesis of polyethylene glycol, polyethylene oxide and poly(DL-lactic acid) of various molecular weights were produced by this method [174, 177, 178]. It was even possible to produce particles below the melting temperature of the polymer, which is always an important concern in processing polymers with heat-sensitive drugs.

The general advantages of PGSS process are the reduction of melting temperatures allowing users to mix and dissolve sensitive, reactive and/or immiscible substances in the liquid state. Fast dissolution rates allow users to reduce the solubility of crystallizing substances in classical solvents rapidly. Reduced viscosities and surface tensions allowing users to mix/dissolve liquid compounds even with high viscosities e.g. by static mixers, generate sprays from gas containing liquids with a broad range of viscosities. Large volume increase during expansion allows users to generate small

droplets in sprays, and mix and agglomerate additives at high turbulence in expanding sprays. Rapid and large temperature reduction by expansion and direct heat transfer allowing users to very quickly solidify droplets, establish a high degree of supersaturation, that help to make the powders, that are difficult to crystallize, rapidly immobilize and ''freeze'' immiscible liquid compounds and to reduce losses of compounds with high volatility.

3.3.1 Experimental Setup

PGSS method eliminates some of the drawbacks associated with RESS method. This is also a 'solvent free' process like RESS. PGSS takes advantage of the unique property of a polymer that in the SC CO_2, the glass transition temperature of the polymer decreases by 10 to 50°C [179-182]. Hence, for coating, the temperature of the reaction vessel is kept near melting temperature of a polymer ensuring the melting of a polymer inside the vessel. The host material is stirred in the molten polymer ensuring the liquid polymer film on the host particles. The mixture is then expanded through a capillary nozzle. This results in a temperature drop solidifying a polymer film on the host particles. Hence, the PGSS can be worked at lower pressures and temperatures by choosing coating polymers with low Tm.

Polyethylene glycol (PEG) was purchased from Sigma Aldrich. 5 grams of silica particles were placed in a high pressure chamber. PEG powder was then placed at pr-calculated quantity (9.1 to 23 wt/wt % to silica). The temperature and pressure of the chamber was then increased to 60C and 1500 psi or 2300 psi (depending upon the experiment). The mixture of the host particles and molten polymer was then stirred

continuously for two hours to obtain the homogeneous mixture. Because of stirring, the host particles were coated with the liquid film of the molten polymer. The solution was then sprayed in another vessel maintained at the atmospheric pressure through a capillary nozzle (508 μm). The pressure and temperature of the supercritical solution was maintained constant throughout the experiment. Because of sudden expansion, the temperature of the polymer reduces solidifying the polymer film on the host material. An experimental setup for particles coating using PGSS is shows in Figure 3.12.

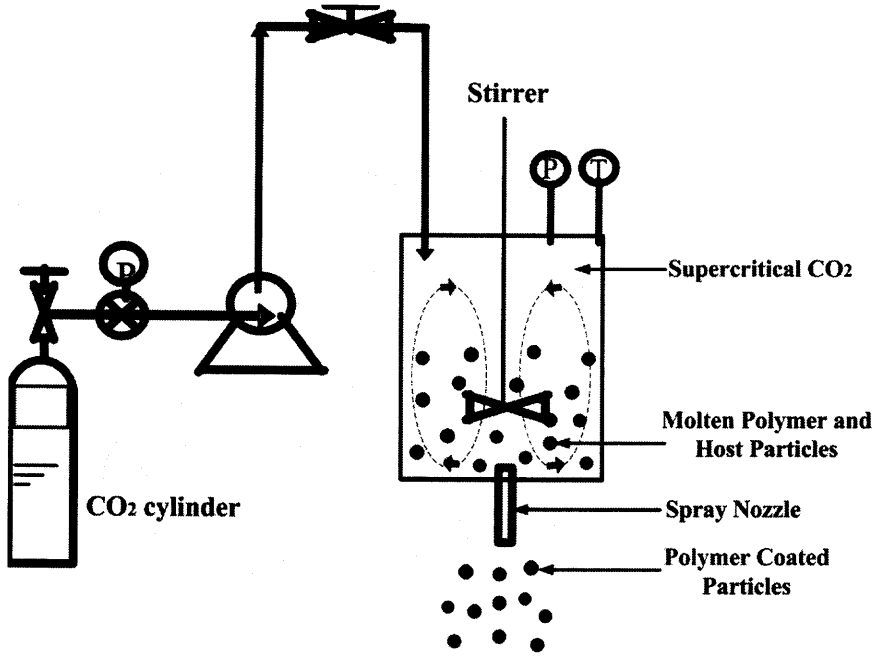

Figure 3.12 Schematic diagram of an experimental setup used for particle coating using PGSS method.

Characterization of the coated particles was done with the imaging technique like Field Emission Scanning Electron Microscope (Leo 1530VP) and particles size distribution was obtained using Coulter LS230. A small amount of powder was placed on an adhesive tape and then sputter coated with carbon in a Baltec MED 020 unit. The

coated particles were then analyzed under SEM instrument at various magnifications. Coulter LS230 employs light scattering to measure the mean diameter of micron and submicron sized particles. A sample was prepared by sonicating a small amount of powder in deionized water with a Fisher Scientific FS30 bath sonicator. Several samples were analyzed with LS 230. Thermo gravimetric analyzer (TGA) was used to analyze thickness of the coating.

3.3.2 Results and Discussions

Coating experiments were done at various pressures ranging from 2300 psi to 0 psi and coating polymer to host particle ratio ranging from 9.1 wt/wt% to 23 wt/wt%.

3.3.1.1 Effects of Pressure on Coatings

The supercritical solution containing silica particles and molten polymer was sprayed through a 508 μm capillary to the atmospheric pressure. Higher the pressure difference, less agglomeration in coated silica particles was observed. PEG 9.1 wt/wt % was used to coat the 180 nm sized silica particles. Figure 3.13 shows the effects of pressure on coating of silica particles. The operating pressure and temperature of supercritical solution was kept constant throughout the experiment. As the supercritical solution was sprayed through a capillary nozzle to achieve the coating, fresh CO_2 was continuous fed to the supercritical vessel to maintain the pressure.

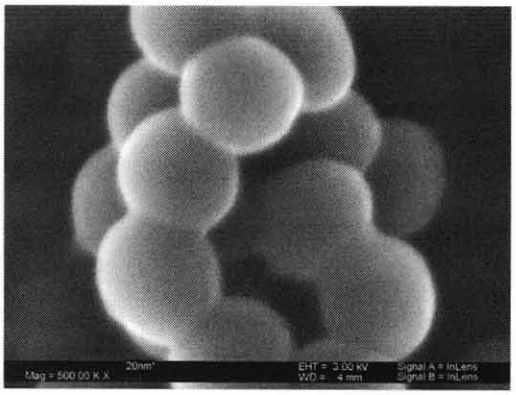

(a): pressure 2300 psi

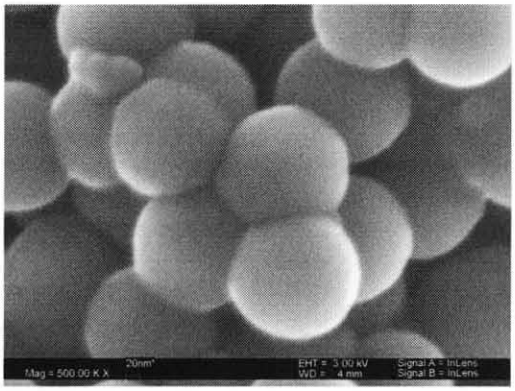

(b): pressure 1500 psi

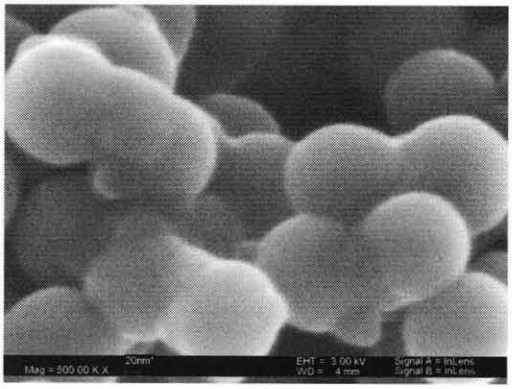

(c): pressure 0 psi

Figure 3.13 Silica particle coatings using PGSS process. PEG 9.1 wt% was used to coat silica particles.

3.3.1.2 Effects of Polymer Ratio on Coatings

The polymer (PEG) to host particle (Silica 180nm) ratio was varied from 9.1 wt/wt% to 23 wt/wt% to silica particles. The particles size distribution is shown in Figure 3.14. The operating pressure varied from 0 psi to 2300 psi for different experiments. As the supercritical solution was sprayed through a capillary nozzle to achieve the coating, fresh CO_2 was continuous fed to the supercritical vessel to maintain the pressure.

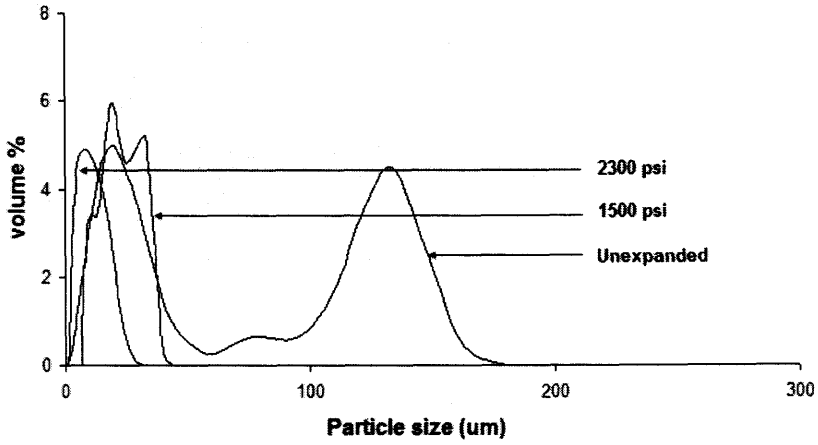

(a): PEG 9.1 wt%

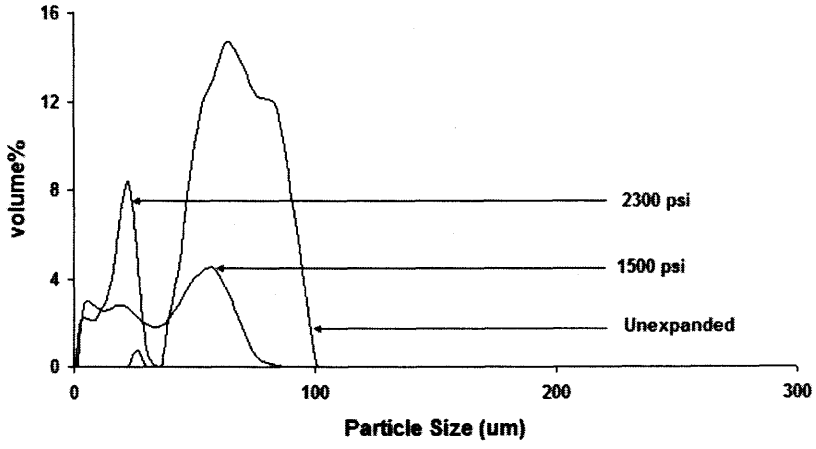

(b): PEG 16.7 wt%

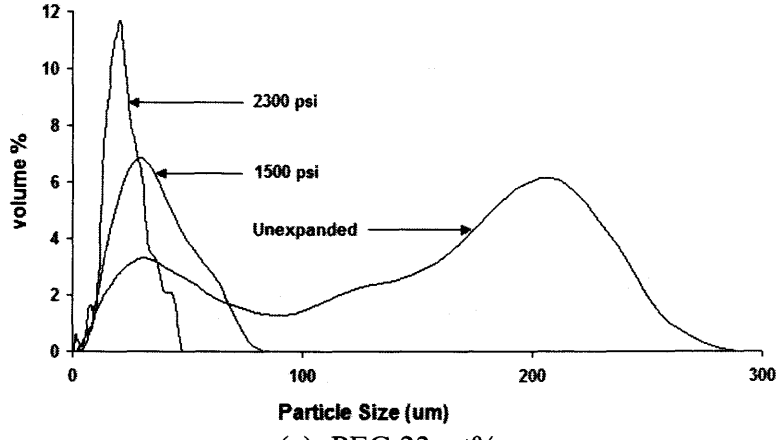

(c): PEG 23 wt%

Figure 3.14 Particles size distribution for different polymer to host particles ratio for PGSS process.

3.4 Conclusion

In SAS method, the deagglomerated particles with high coating efficiency were achieved. With increase in polymer ratio, the agglomeration increased. Larger the host particles size, lower was the degree of agglomeration. Ultrasonic nozzle helped in reduction in agglomeration and increase in production without affecting the coating quality. With poor solvent agglomeration was reduced when DCM was used as a solvent.

RESS is a solvent free process and hence it is desirable for pharmaceutical applications where the residue solvent is undesirable. Few polymers are soluble in SC CO_2 and hence it is limited with the choice of the coating material. As the solubility of several polymers into SC CO_2 is very limited, a coating efficiency is low and scaling up of the process is difficult. But as a general rule, if the coating material has a significant solubility in the SCF, the RESS process will be the first choice for the coating because of its simplicity. The operating parameters like temperature and pressure are higher than SAS process which is undesirable for several active pharmaceutical ingredients.

As PGSS is solvent free process like RESS, it is generating a wide interest in pharmaceutical industry. By choosing biopolymers with lower melting temperatures (Tm), the operating parameters of the process (like temp, pressure) can be kept low. Hence, it eliminates the disadvantages of RESS process. As a coating material (e.g. Polymers, lipids) does not need to be soluble in the SC CO_2, it can be used for a wide range of coating materials. Deagglomerated particles like RESS method can be produced because of sudden expansion. The disadvantage of this process is it is limited to low Tm polymers (or lipids etc.), if the host material is active pharmaceutical ingredient.

CHAPTER 4

SYNERESIS OF SILICA GEL

4.1 Scientific and Technical Objectives

Gelled propellants eliminate disadvantages associated with the liquid, solid or hybrid propellants. Hence, they are favored in advanced missiles and similar products. Study of syneresis of gelled propellants is very important to identify and quantify of the main material properties affecting the gel syneresis to form a stable propellant gel. Silica gels are used as simulants of propellants in this investigation. Three different silica gels were provided by CFD Research Corp. (CFDRC) namely, SILICA50, SILICA8.50 and SILICA8.25. Effect of gravity on syneresis was studied by exposing the silica gels to higher gravities from 500G to 30000G from 1 min to 90 min. Supercritical Fluids extraction was used to extract water from the gel and the dried silica structure was investigated using SEM analysis. Oxygen-17 NMR relaxation was employed for the quantification of gel structures and the particle-water interactions. Based on results of experimental studies, a multi-scale computational strategy for modeling gel formation and syneresis was proposed.

4.2 Review of Syneresis Studies

The propellants used in missiles or rockets are in liquid, solid or hybrid forms. All three forms have several advantages and disadvantages. Gelled propellants are expected to combine the advantages of solid, liquid and hybrid forms and eliminate the disadvantages associated with them. The general properties of propellants in various forms are summarized below:

4.2.1 Liquid Propellants [183, 184]

In case of liquid propellants, the fuel and oxidizer are stored in separate tanks and are fed through a system of pipes, valves, and turbo pumps to a combustion chamber where they are combined and burned to produce a thrust. Liquid propellants are classified into three types: petroleum, cryogenics, and hypergolics. The advantages of liquid propellants are highest energy per unit of fuel mass, variable thrust, and a restart capability. Raw materials, such as oxygen and hydrogen are in abundant supply and a relatively easy to manufacture. The disadvantages are requirements for complex storage containers, complex plumbing, precise fuel and oxidizer injection metering, high speed/high capacity pumps, and difficulty in storing fueled rockets.

4.2.2 Solid Propellants [183, 184]

Solid propellant rockets are combustion chamber tubes packed with a propellant that contains both fuel and oxidizer blended together uniformly. The principal advantage of a solid propellant is relatively stable therefore it can be manufactured and stored for future use. Solid propellants have a high density and can burn very fast. They are relatively

insensitive to shock, vibration and acceleration. No propellant pumps are required thus the rocket engines are less complicated. Disadvantages are that, once ignited, solid propellants cannot be throttled, turned off and then restarted because they burn until all of the propellant is used. The surface area of the burning propellant is critical in determining the amount of thrust being generated. Cracks in the solid propellant increase the exposed surface area, thus the propellant burns faster than planned. If too many cracks develop, pressure inside the engine rises significantly and the rocket engine may explode. Solid propellant manufacturing is an expensive, precision operation.

4.2.3 Hybrid Propellants [183, 184]

Hybrid propellant engines represent an intermediate group between solid and liquid propellant engines. One of the substances is solid, usually the fuel, while the other, usually the oxidizer, is liquid. The liquid oxidizer is injected into the solid fuel, whose reservoir serves as the combustion chamber. The main advantage of such engines is that they have high performance, similar to that of solid propellants, but the combustion can be moderated, stopped, or even restarted. It is difficult to make use of this concept for vary large thrusts, and thus, hybrid propellant engines are rarely built.

4.2.4 Gelled Propellants

The gelled propellants are researched in present time hoping to eliminate the disadvantages associated with both solid and liquid propellants. A gel holds its shape initially under stress and does not flow until pushed beyond its yield stress [183, 184]. However, once its yield stress is passed, the gel flows freely as a liquid. This allows

gelled propellant flows to be turned on and off sharply without leakage, giving gels more accurate firing control compared to traditional liquid fuels. Gels also have safety advantages over liquid fuels, such as reduced flammability, detonability, spill susceptibility and fuel tank sloshing. Gels can also hold energetic particles in suspension to act as a loading agent to improve the combustion performance. The other advantages of gelled propellants include extended range, greater mission flexibility, and lower operational costs. Gel propellants provide rocket propulsion systems of high specific impulse, low sensitivity, and low vulnerability in combination with the capability to control the thrust, that is, variation of thrust and thrust cutoff [183, 184].

The syneresis of silica gels was intensively studied by Dr. D. G. R. Bonnell [185-189]. He devised a special synerometer to investigate effects of various parameters like pH of the gel, silica concentration, coagulants and hydrogen ion concentration etc. on syneresis of silica gels. The investigation of gelation and syneresis was then followed by many researchers [190-194]. The rheological and small angle neutron scattering measurements were conducted to observe the gelation process and final structure of the gels [195]. Teipel [196, 197] investigated the mechanical properties and rheological behavior of gelled propellants. The nitromethane / silica gels exhibited pronounced shear thinning behavior with a yield stress when subjected to stationary shear flow. This behavior is attributable to the inner structure of the gel, which leads it to exhibit solid-like properties. At high shear rates, the hydrodynamic forces exceed the interparticle interaction forces, producing flow-induced structuring of the nanometer-sized silica particles and pronounced nonlinear flow behavior. The oscillatory shear experiments

showed that the storage and loss moduli were independent of frequency in the range examined, meaning that the gel exhibits elastic behavior at low frequencies.

Investigation of arrangements of silica particles in the gel is an important factor to understand the mechanism of gel formation and syneresis. Imaging techniques help in better understanding about the silica structure formation in the gels. The silica networks in silica gels were investigated under Scanning Electron Microscope (SEM). To see the network under SEM, it is important to remove the water from the gel without affecting gel structure. Supercritical Fluids method (SCF) was used to extract water from silica gels without affecting the silica structure in the gel [198]. For example, G. Ruben [199] studied the morphology of ultra-low density silica gels. The structure of the silica particles in the gel was characterized by High Resolution Transmission Electron Microscopy (HRTEM). The gels were first dried with Supercritical CO_2 and then images were taken with HRTEM instrument. The structure of the gel was studied for size and shape of voids within the silica network.

Nuclear Magnetic Resonance (NMR) spectroscopy was used as a probe of the interaction of water molecules with silica particles [200, 201]. Water strongly interacts with particle surfaces in the suspension resulting in a fraction of water bound on the surface which has a lower mobility compared with free water. Water mobility is an appropriate parameter to study the rheological properties of aqueous suspensions, and ^{17}O NMR relaxation was employed to determine the mobility of water in aqueous suspensions. The NMR investigation with alumina particles was done by M. Akinc [202]. This study showed that bound water is associated with lower molecular mobility. The overall mobility of the bound water decreased with the solid volume fraction. Calculated

correlation time tc increased from 15.8 to 29.0 ns as the solids volume fraction increased from 25 to 40 vol%. Addition of 18 wt% fructose to 40 vol% alumina suspension reduced the correlation time, tc, to 21.2 ns. NMR relaxation time study showed that the reduction in viscosity by the addition of fructose to particle suspension was because of displacement of water from the solid surface by the fructose molecules.

4.3 Dynamics of Syneresis

Syneresis of silica gels (SILICA 50, SILICA 8.25 and SILICA 8.50 provided by CFDRC) was studied by exposing them to higher gravities from 500G to 30000G. A DuPont Sorvall RC 28S SUPRAspeed Centrifuge was used to accelerate silica gels at 20^0C. The weight of centrifuging vial was noted with and without silica gel before centrifuging experiment. The weight of exuded water after centrifuging was noted and syneresis was expressed in terms of the mass of the exudated water as the fraction of the initial sample mass. Figure 4.1 represents a typical example of centrifuging vials before and after centrifuging. The circle indicates the location of water exudated from the gel.

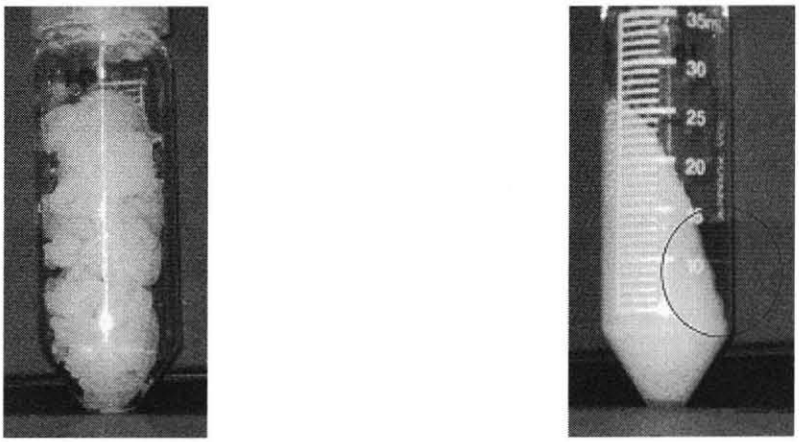

Figure 4.1 Photos of a SILICA 50 sample before (*left*) and after (*right*) the 30-min exposure to 5,500 G at 20°C.

Effect of Gravity on Syneresis

The effect of gravity on syneresis of gels was studied by exposing the gels to wide range of gravities for 30min at 20. Plots in Figure 4.2 show the syneresis of various silica gels when exposed to wide range of gravities for 30 min at 20^0C. Equations in Table 4.1

correspond to syneresis curves in Figure 4.2. In these equations, x corresponds to the magnitude of the acceleration in G whereas y corresponds to the mass of exudated water as the fraction of the initial sample mass.

Table 4.1 The Equations of Syneresis for Different Silica Gels When Exposed to Higher Gravities.

Silica Gel	Equation for Syneresis curve	Regression (R^2)	Gravity corresponding start of syneresis
SILICA 50	y = 11.648 Ln(x) – 89.782	0.966	2226 G
SILICA 8.25	y = 13.887 Ln(x) – 88.593	0.974	590 G
SILICA 8.50	y = 12.854 Ln(x) – 80.516	0.987	526 G

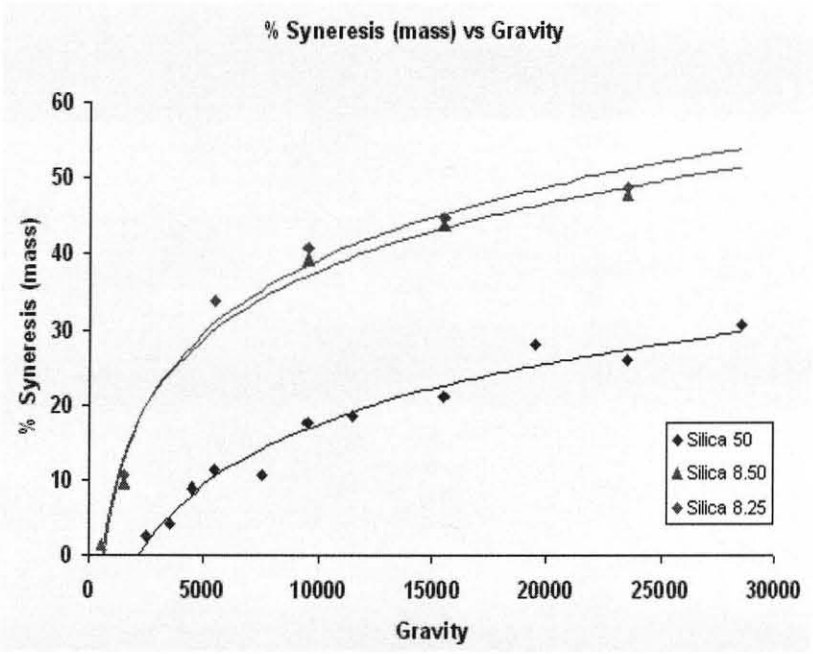

Figure 4.2 Syneresis of silica gels SILICA 50, SILICA 8.25 and SILICA 8.50 for 20^{0}C following the 30-min exposure to acceleration (in G).

(Originally published in "Computational Design Tool for the Synthesis and Optimization of Gel Formulations (SOGeF), Phase I STTR Final Report," Roberto Di Salvo, Boris Khusid, Morton M. Denn, Jeff F. Morris, and Stanley I. Sandler, CFD Research Corporation Report No. 8730/6, Contract No. W911NF-05-C-0101, 2006, Copyright © 2006 by CFD Research Corporation. Reprinted with permission.)

Effect of Centrifuging Time on Syneresis

The effect of centrifuging time on the dynamics of syneresis was studied by exposing silica gels to centrifuging for different time scales. To study the dynamics of syneresis of SILICA 50, the period of centrifuging varied from 1 min to 90 min for several magnitudes of the applied acceleration. For comparison, the time dependence of syneresis of SILICA 8.25 and SILICA 8.50 for the acceleration of 5500G was also measured by varying the exposure time from 1 min to 30 min. The mass fraction of water exudated from SILICA 50 during the 90-min exposure to 1500 G was found to be about 0.28%. Plots in Figures 4.3 show the syneresis of SILICA 50 as a function of the exposure time for the accelerations 5500 G, 15500 G, and 23500 G. Plots in Figure 4.4 present data on syneresis of SILICA 50, SILICA 8.25 and SILICA 8.50 for the acceleration of 5500G. The amount of exudated water is given as the fraction of the mass of the initial sample.

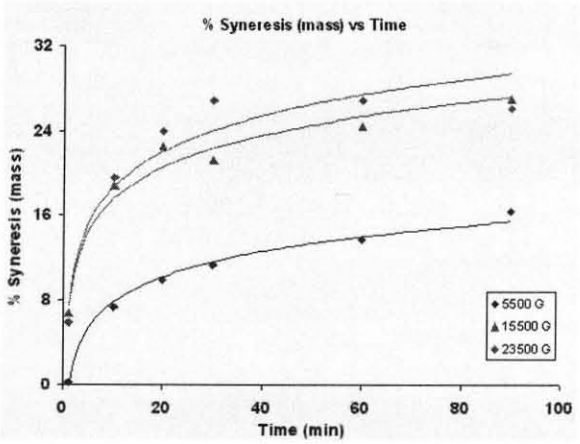

Figure 4.3 Time dependence of syneresis of SILICA 50 following the exposure to acceleration for 20°C.

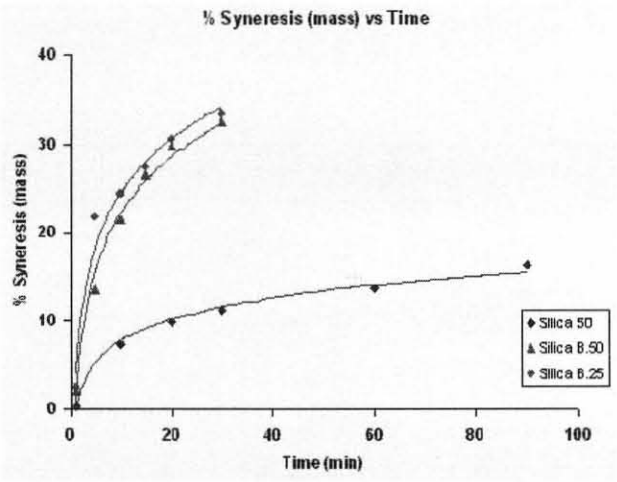

Figure 4.4 Time dependence of syneresis of SILICA 50, SILICA 8.25 and SILICA 8.50 following the exposure to acceleration of 5,500G for 20°C.

(Originally published in "Computational Design Tool for the Synthesis and Optimization of Gel Formulations (SOGeF), Phase I STTR Final Report," Roberto Di Salvo, Boris Khusid, Morton M. Denn, Jeff F. Morris, and Stanley I. Sandler, CFD Research Corporation Report No. 8730/6, Contract No. W911NF-05-C-0101, 2006, Copyright © 2006 by CFD Research Corporation. Reprinted with permission.)

The time dependence of the amount of exudated water as the fraction of the mass of the initial sample is summarized in Table 4.2.

Table 4.2 The Equations of Syneresis for Different Silica Gels When Exposed to Higher Gravities for Wide Range of Time Scale.

Silica Gel	Equation for Syneresis curve	Regression (R^2)	Gravity (G)	Time corresponding start of syneresis (sec)
SILICA 50	y = 3.4634 Ln(x) - 1711	0.99	5500	63.6
SILICA 50	y = 4.3385 Ln(x) + 7.5831	0.96	15500	18.2
SILICA 50	y = 6.3966 Ln(x) + 7.6496	0.92	23500	10.5
SILICA 8.25	y = 8.8452 Ln(x) + 4.142	0.97	5500	38
SILICA 8.50	y = 9.2587 Ln(x) + 0.8768	0.98	5500	55

where, x is the exposure time in minutes. The extrapolation of these expressions to y = 0 indicates the starting time for syneresis and are listed in the Table 4.2.

The reproducibility of measurements was studied by repeating experiments with randomly chosen operating conditions. Tables 4.3 and 4.4 summarize the data.

Table 4.3 The Reproducibility Study by Choosing The Silica Gels and Operating Conditions Arbitrary and Repeating the Syneresis Experiments.

No	Silica Gel	Operating Conditions			% Syneresis		% Variation
		Acceleration (G)	Temp (°C)	Time (min)	Run 1	Run 2	
1	SILICA 50	5500	20	60	13.67	12.90	-5.87
2	SILICA 50	15500	20	20	22.50	20.33	-9.66
3	SILICA 50	23500	20	10	24.00	23.73	-1.13
4	SILICA 8.25	5500	20	30	33.40	33.95	1.65

4.4 Characterization of gel

4.4.1 Supercritical Extraction of Water for Characterization of Network Formed by Silica Particles

The temperature and pressure of the supercritical carbon dioxide was set above critical point of water-CO_2 mixture. Above critical point, water and CO_2 are fully miscible with each other and hence the water-CO_2 surface tension is zero. Thus capillary forces that would collapse the pores and rearrange the particles during the water extraction are avoided. The supercritical extraction process was carried out in a high pressure extraction vessel. The sample was first placed in an inline cylindrical filter with 0.5 μm pores for 12 hours for forming the equilibrium gel structure. The filter was then transferred into a high pressure extraction vessel. The pressure inside the vessel was increased to 140 bars at room temperature and once the steady state condition was achieved, the temperature is increased to 60°C. The back-pressure regulator was adjusted in a way that an increase in pressure inside the vessel is compensated by continuous CO_2 flow to avoid the saturation of CO_2 with water. The SCF extractions were carried out for an hour. Maintaining the CO_2 flow, the chamber was then depressurized and the filter was retrieved. The structure formed by silica particles was coated with carbon in a sputtering coater, Baltec MED 020, for the analysis on a Field Emission Scanning Electron Microscope (SEM), Leo 1530VP. The SigmaScan Pro (version 5) software was used to quantify the SEM images. The developed technique for the supercritical extraction of solvent in liquid carbon dioxide can also be used for the quantification of the structure of a gelled propellant system. A typical example of the filter filled with silica gel before and after SCF extraction is shown in Figure 4.5.

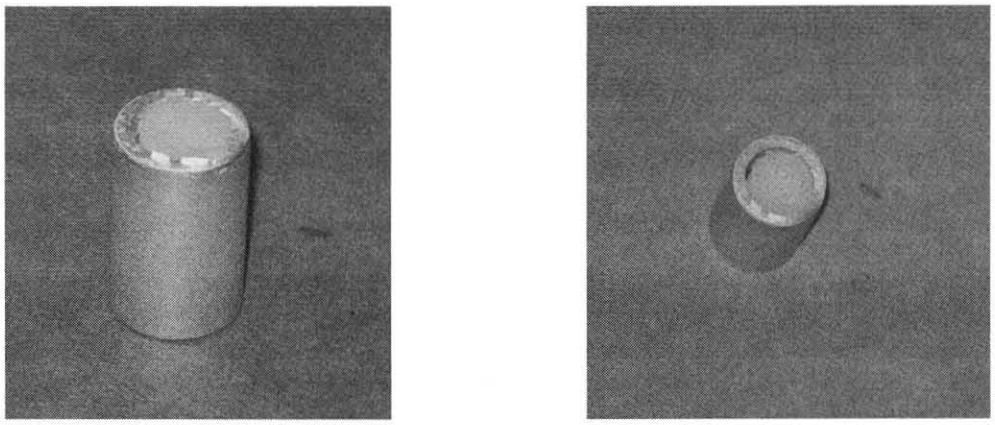

Figure 4.5 A sample of SILICA 50 in a 0.5-μm filter (*left*) before and (*right*) after the supercritical extraction of water.

(Originally published in "Computational Design Tool for the Synthesis and Optimization of Gel Formulations (SOGeF), Phase I STTR Final Report," Roberto Di Salvo, Boris Khusid, Morton M. Denn, Jeff F. Morris, and Stanley I. Sandler, CFD Research Corporation Report No. 8730/6, Contract No. W911NF-05-C-0101, 2006, Copyright © 2006 by CFD Research Corporation. Reprinted with permission.)

SCF extraction of silica gels before and after centrifuging was done and silica structures were investigated under SEM. To extract the water from centrifuged silica gels, the vials were cut without affecting the gel and then the vials were exposed to SC CO_2. The typical example is shown in Figure 4.6.

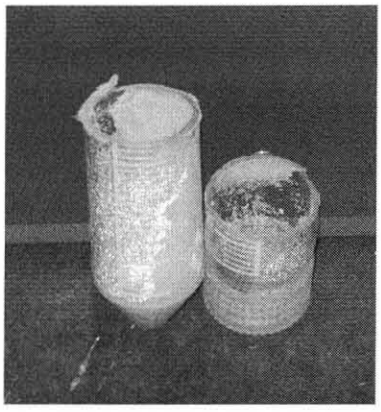

Figure 4.6 Lower (*left*) and upper (*right*) parts of the vial in Figure 4.6 (*right*) cut to size of SILICA 50 sample.

(Originally published in "Computational Design Tool for the Synthesis and Optimization of Gel Formulations (SOGeF), Phase I STTR Final Report," Roberto Di Salvo, Boris Khusid, Morton M. Denn, Jeff F. Morris, and Stanley I. Sandler, CFD Research Corporation Report No. 8730/6, Contract No. W911NF-05-C-0101, 2006, Copyright © 2006 by CFD Research Corporation. Reprinted with permission.)

Several SEM images of the silica gels as received and after syneresis were taken by drying the gels with supercritical extraction. The imaging software (sigma scan version 5) was used to investigate SEM images of gel structures for the pore size analysis. The reproducibility of the experiments was studied by repeating the extraction experiments. Figure 4.6 shows the SEM images of as received gels and gels after syneresis. SCF extraction was used to extract water from silica gels. (a) shows the SEM images of the structure in gel SILCA 50; (b) The SEM image of the structure in SILICA 8.25; (c) The SEM image of the structure in SILICA 8.50; (d) The SEM image of structure in SILICA 50 following the 30-min exposure to 11,500 G at 20^0C, syneresis 33.12 (v/v) %.

The Table 4.4 shows the surface fraction of pores, shape factor of pores and the mean diameter obtained from image analysis of SEM images. The reproducibility was studied by repeating several experiments. For SILICA 50, the image analysis shows the ratio of the surface fraction of pores, shape factor of pores and the mean diameter are 0.66, 86.29 nm and 0.434 respectively. For SILICA 8.25, the ratio of the surface fraction of pores, shape factor of pores and the mean diameter are 0.67, 95.63 nm and 0.60 respectively. For SILICA 8.50, the ratio of the surface fraction of pores, shape factor of pores and the mean diameter are 0.52, 158.5nm and 0.61 respectively. For SILICA 50 with 30-min exposed to 11,500 G at 20^0C (syneresis 33.12v/v %), the ratio of the surface fraction of pores, shape factor of pores and the mean diameter are 0.67, 73nm and 0.153 respectively.

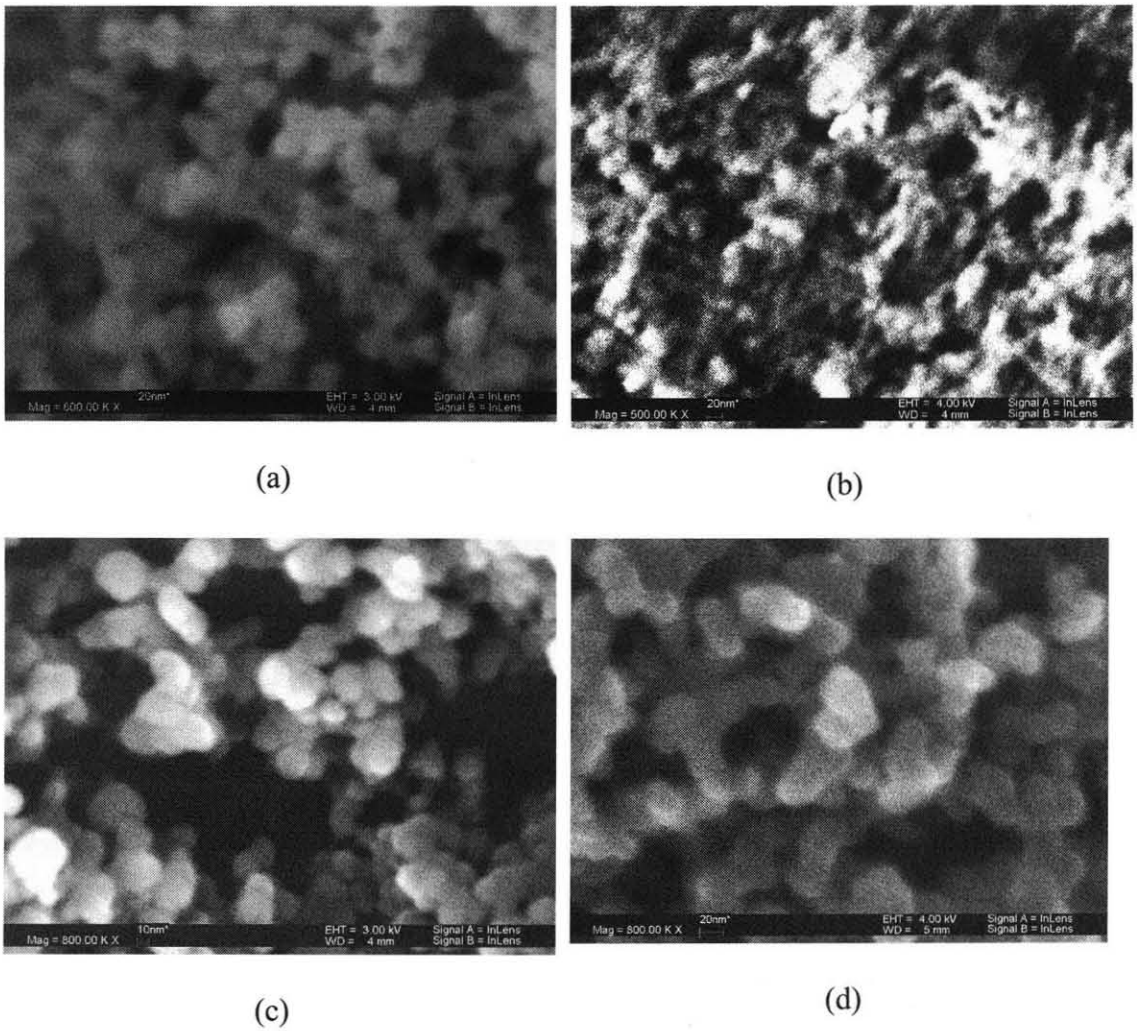

Figure 4.7 SEM images of the structures formed by the silica particles in gels.

(Originally published in "Computational Design Tool for the Synthesis and Optimization of Gel Formulations (SOGeF), Phase I STTR Final Report," Roberto Di Salvo, Boris Khusid, Morton M. Denn, Jeff F. Morris, and Stanley I. Sandler, CFD Research Corporation Report No. 8730/6, Contract No. W911NF-05-C-0101, 2006, Copyright © 2006 by CFD Research Corporation. Reprinted with permission.)

Table 4.4 Characteristics of Structures Formed by Silica Particles.

Gel	Sample No	Void shape factor	Mean void diameter, nm	Area fraction of voids
SILICA 50	*Run 1*	0.66	86.29	0.434
	Run 1	0.71	98.72	0.592
SILICA 8.25		0.64	92.86	0.625
	Run 2	0.68	95.32	0.601
	Run 1	0.54	171.22	0.617
SILICA 8.50		0.62	154.22	0.585
	Run 2	0.41	150.10	0.641
SILICA 50 *30-min exposed to 11,500 G at 20^{0}C; syneresis 33.12(v/v)%*	*Run 1*	0.68	74.25	0.144
		0.69	80.88	0.176
	Run 2	0.64	63.46	0.132
		0.68	73.80	0.159

The bulk density of the silica particles and silica structures in gels were measured and compared. To evaluate the bulk density, the water from silica gels was extracted with supercritical CO_2 in a similar way used for image analysis. The bulk density of the structure formed by silica particles after the supercritical extraction of water from the inline filter loaded with a SILICA50 gel (Figure 4.8a) was found to be $527.76\,kg/m^3$ (Figure 4.8b). For comparison, the same filter was filled with a dry Degussa A200 fumed silica powder. The properties of the silica powder provided by the manufacturer are as follows: the apparent powder density $30\,kg/m^3$, the particle mean

size 16 nm, the specific surface area $200\,m^2/g$. The apparent density of the powder filled the filter without compacting was found to be $31.44\,kg/m^3$ (Figure 4.8c). The compact density of this silica powder was found to be $214.22\,kg/m^3$ (Figure 4.8d). Taking the specific gravity of fumed silica as $2200\,kg/m^3$ the volume concentration of the silica particles was found to be 1.4% in dry Degussa A200 powder without compacting (Figure 4.8c) and 9.7% following the compacting of dry Degussa A200 powder (Figure 4.8d), whereas 24% in the structure formed in SILICA 50 (Figure 4.8b), i.e., the particle content of the gel network is 2.5 times larger than that of a compacted dry powder. In Figure 4.8, the filters with: (a) as-received SILICA 50; (b) structure of SILICA 50 after supercritical extraction of water; structure density $527.76\,kg/m^3$, 24(v/v) % particles; (c) dry Degussa A200 fumed silica powder, apparent density $31.44\,kg/m^3$, 1.4(v/v) % particles; (d) compacted dry Degussa A200 fumed silica powder, apparent density $214.22\,kg/m^3$, 9.7(v/v) % particles.

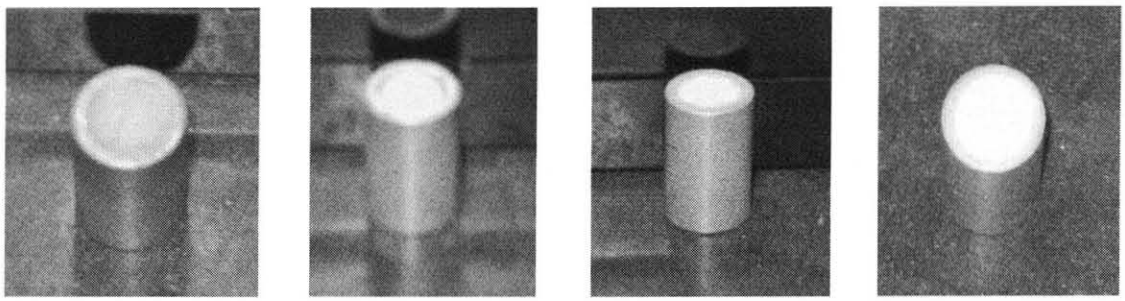

a **b** **c** **d**

Figure 4.8 The silica loaded filter for the density experiments.

4.4.2 NMR for Characterization of Interaction of Water with Silica Particles

Water molecules are dynamically exchanged between an environment in which they relax slowly (free water) and one in which they relax rapidly (bound water). Under conditions of rapid exchange between free water and bound water on the NMR time scale, a single relaxation rate was observed, which represents the weighted average of the individual rate for each environment. Compared with proton and deuterium magnetic relaxation, the major advantage of using ^{17}O relaxation is its exchange processes are generally slower. In addition, ^{17}O nuclear magnetic relaxation is unaffected by either cross-relaxation or chemical exchange and provides a more direct means for probing hydration. Therefore, ^{17}O nuclear magnetic relaxation is used to probe the mobility of water molecules in silica gels. Room-temperature Oxygen-17 relaxation rates were recorded in 10-mm O.D. tubes on Bruker ARX300 NMR spectrometer (Bruker Instruments Inc., Billerica, MA) equipped with 10 mm Bruker VSP probehead. Samples were prepared using D_2O with ^{17}O natural abundance. For comparison, Oxygen-17 NMR measurements were carried out for an empty glass tube, a tube filled with D_2O up to 2 inches of height, a tube loaded with D_2O and 8 wt/wt % Degussa A200 silica powder and a tube loaded with D_2O mixed with SILICA 50. For the latter, the tube was first filled with D_2O and then a silica gel was added. The tube was stirred with a glass rod for half an hour to obtain a homogeneous sample. A single peak was observed for each sample (Figure 4.9), which implies that ''free water'' and ''bound water'' exchange rapidly on the NMR time scale so that the observed single relaxation rate represents the weighted average of the individual relaxation rates. The chemical shift of the ^{17}O resonance peak appears to be about 3.5 ppm for D_2O, 3.7 ppm for D_2O with Degussa A200 silica powder,

and 4.7 ppm for D_2O with SILICA 50. The difference between the chemical shifts of the peaks for D_2O and D_2O with Degussa A200 silica powder falls within the experimental uncertainty. On the other hand, the difference between the peaks for D_2O and D_2O mixed with SILICA 50 exceeds the experimental uncertainty. These results indicate that the ^{17}O NMR relaxation can be employed to characterize the interactions of water molecules with particles in water-based silica gels.

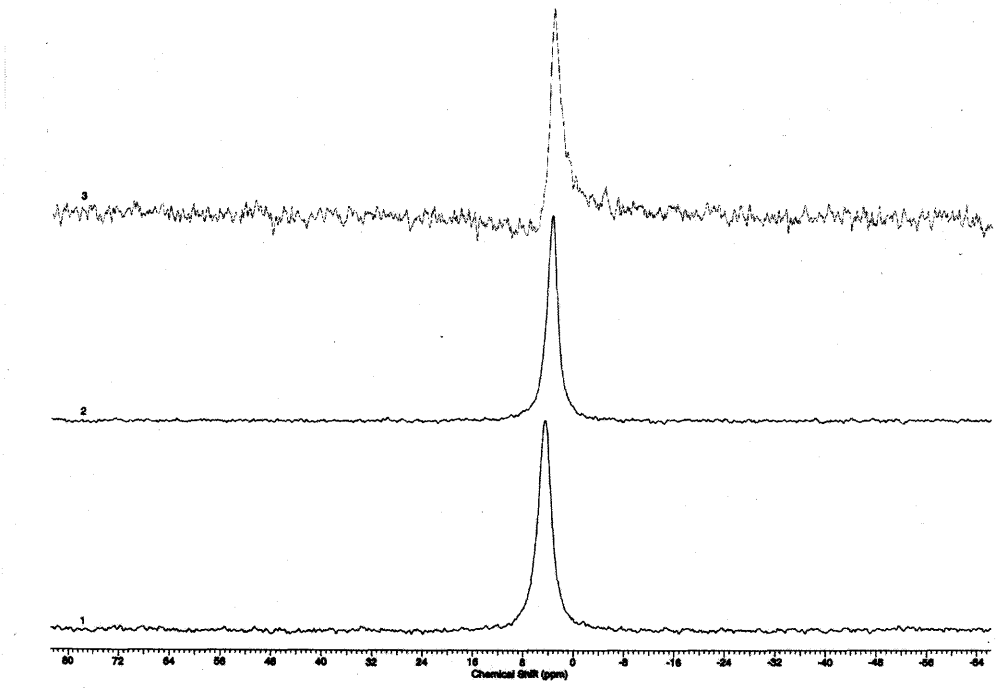

Figure 4.9 Oxygen-17 NMR resonance peaks for (1) D_2O, (2) D_2O with Degussa A200 silica powder, and (3) D_2O with SILICA 50.

(Originally published in "Computational Design Tool for the Synthesis and Optimization of Gel Formulations (SOGeF), Phase I STTR Final Report," Roberto Di Salvo, Boris Khusid, Morton M. Denn, Jeff F. Morris, and Stanley I. Sandler, CFD Research Corporation Report No. 8730/6, Contract No. W911NF-05-C-0101, 2006, Copyright © 2006 by CFD Research Corporation. Reprinted with permission.)

4.5 Strategy for Modeling of Gel Formation and Syneresis

4.5.1 Basic Principles of Proposed Computational Strategy

Based on the results obtained in experiments, a strategy is developed for the development of a computational model capable of simulating and predicting the formation and syneresis of nanoparticle gel materials. The system would use the silica particles of 10-30 nm in diameter. The volume fraction of the particles would be about 10% of the total volume. The process of gel formation takes place at the molecular level, hence, a molecular model that tracks the motion and interaction of individual particles is suitable for simulating this process. The detail information obtained from molecular simulations will help in understanding the mechanisms of the gel formation. On the other hand, syneresis (the expulsion of solvent due to gel structure shrinkage) is a macroscopic phenomenon. Its length scale is on the order of a few mm or above and the time scale ranges from minutes to hours. Hence, a multi-scale approach would be adopted to simulate the gel formation and syneresis.

At the molecular level, a coarse-grained meso-scale model would be used to simulate the formation of the gel network. The motion of the nanoparticles would be simulated and treat the solvent as a continuum medium. Recent simulations of this type typically handled on the order of 1,000 particles [200]. Assuming the diameter of a particle is 15 nm and the volume fraction of the particles is 10%, the size of a sample that can be simulated is on the order of 800 nm. To investigate syneresis, the continuum mechanics would be used. However, the continuum model would require certain material parameters as input. The material parameters needed by the continuum model would be extracted from molecular simulations of the gel networks. Through this procedure, the

starting point would be with molecular properties of the constituent particles and end point would be in predicting the gel properties at the macroscopic level.

4.5.2 Modeling of Gel Formation

Brownian dynamics (BD) would be used to simulate the process of gel formation using. In this approach, the nanoparticles are assumed to be much larger and more massive than the small solvent molecules. The solvent is treated as a continuum and the motion of individual solvent molecules are not tracked. Only the motion of the particles would be simulated. The particles would move under the influence of the intermolecular forces acting between them as well as the drag forces exerted on them by the solvent when they move through. At the same time, the small solvent molecules would kick the particles continuously and randomly due to thermal motion, giving rise to the Brownian motion of the particles. The effect of these random kicks is described by a stochastic force in the equation of motion of the nanoparticles. This approach is justified by the fact that the size of a typical solvent molecule (about 0.4 nm) is much smaller than the size of the nano-particles being considered. Moreover, based on the densities of silica (2.2 g/cc) and solvent (1 g/cc), a nanoparticle could be estimated at least about 40,000 times more massive than a solvent molecule in our case, therefore, the use of BD is appropriate.

The computational model for the gel formation includes N spherical particles of mass m located in a cubic box of size L. Each one represents a nanoparticle. The migration of particle i, $\mathbf{r}_i(t)$ (i = 1 to N), is given by the Langevin equation [201]:

$$\frac{d\mathbf{r}_i}{dt} = \sum_j \mathbf{H}_{ij} \cdot \left(-\frac{\partial U}{\partial \mathbf{r}_j} + \boldsymbol{\eta}_j(t) \right) \tag{1}$$

Here **H** is the Oseen tensor that incorporates the effects of the hydrodynamic interaction mediated by the solvent and $\boldsymbol{\eta}_j(t)$ is a random force having zero mean and satisfying the relation $\langle \eta_{i\alpha}(t)\eta_{j\beta}(t')\rangle = 2\zeta k_B T\delta_{ij}\delta_{\alpha\beta}\delta(t-t')$. The friction coefficient ζ is given by the expression $\zeta = 6\pi\eta_s R$, where η_s the solvent viscosity and R is is the particle radius. The long-ranged hydrodynamic interactions would be handled using a technique based on Ewald summation, which has recently been successfully applied to simulate polyelectrolyte solutions [203]. The potential energy U is a pair wise summation of the interaction energy between two particles, and the interaction energy of a particle pair is modeled by a center-shifted Lennard-Jones potential:

$$V(r) = 4\varepsilon\left[\left(\frac{\sigma}{r-s}\right)^{12} - \left(\frac{\sigma}{r-s}\right)^{6}\right] \tag{2}$$

This approximates the particle-particle interactions by the van der Waals interactions between atoms on their surfaces. Here r is the separation between the two particles. The range (σ) of the interaction would be short compared to the diameter (s) of the particle. The depth (ε) and the range of the potential would be chosen to mimic the actual intermolecular forces between gel particles.

Recent simulations utilizing a short-ranged attractive potential have shown the ability to model the formation of network-type structures in colloidal systems [200]. The final structures obtained depend on parameters such as the potential depth of the interparticle interaction, the temperature, and the particle volume fraction. This approach would be used to simulate the formation of gel network and identify the conditions that would lead to network structures similar to those observed in gelled systems using the supercritical solvent extraction. In addition to the van der Waals forces, the gel particles

may be charged. The effects of electrical interactions could be taken care of by adding a Debye-Huckel-type potential, i.e., a term of the form $e^{-r/\lambda_D}/r$ to the above interaction potential. The Debye length λ_D is inversely proportional to the square root of the ionic strength of the solution. Particles may also form bonds upon contact, which could be modeled by adding Morse-type potentials.

4.5.3 Modeling of Syneresis

The phenomenon of syneresis is macroscopic both in length and time scales so that the continuum approach would be suitable for simulations. Recently, a continuum model has been proposed and applied to the analysis of the swelling dynamics of gels [204]. In a nutshell, this model consists of the following three equations:

$$\zeta(\mathbf{v}_s - \partial_t \mathbf{u}) = -(1-\phi)\nabla p \tag{3}$$

$$\nabla \cdot (\boldsymbol{\sigma} - p\mathbf{I}) = 0 \tag{4}$$

$$\nabla \cdot [\phi \partial_t \mathbf{u} + (1-\phi)\mathbf{v}_s] = 0 \tag{5}$$

Here $\mathbf{v}_s = \mathbf{v}_s(\mathbf{r},t)$ and $\mathbf{u} = \mathbf{u}(\mathbf{r},t)$ are the solvent velocity and the displacement of the gel relative to the reference state, respectively; ζ is the friction coefficient, p is the pressure, and ϕ is the volume fraction of the gel particles. These three equations respectively represent Darcy's law for the permeation of solvent through the gel network, force balance of the network, and the incompressibility condition. The stress tensor σ of the gel network is assumed to have the following linear form

$$\sigma_{\alpha\beta} = (K - 2G/3)\sum_{\gamma}(\partial_\gamma u_\gamma)\delta_{\alpha\beta} + G(\partial_\alpha u_\beta + \partial_\beta u_\alpha) \tag{6}$$

where K and G are the bulk and shear moduli of the gel, respectively.

The dynamics of syneresis is similar to the dynamics of the gel swelling/shrinking in the sense that the gel network collapses and shrinks under gravity and solvent permeates outward through the gel structure. The only modification would be to add the term $\rho\mathbf{g}$, with ρ being the difference between densities of the gelling particles (silica in this case) and fluid, to the left-hand side of the force balance equation to account for the action of gravity. With suitable boundary and initial conditions, the three equations above can be solved and the solvent velocity at the surface will define a flux, from which the amount of solvent expelled can be calculated.

4.5.4 Bridging Molecular and Macroscopic Scales

The information required in the solution of the continuum equations is K and G. This information would be obtained through molecular simulations. The dependence of the gel structure and permeability on the volume fraction ϕ would be found from direct examination of the gel networks obtained from the BD simulations. To find the bulk modulus K and the shear modulus G, we shall perform molecular dynamics simulations of the behavior of the gel structures subject to compression and shear. Specifically, external forces would be applied at different surfaces and allow the gel networks to relax. Then the displacement of the network components would be measured. Data on the dependence of the network displacement on the magnitudes of the external forces and the particle volume fractions would enable the accurate calculation of the bulk and shear moduli of the gels.

4.6 Conclusions

Experiments were conducted on samples of water-based silica gels provided by CFDRC. Centrifuging of gels over a broad range of applied accelerations from 500G to 30,000G was used to measure the dynamics of syneresis. The supercritical water extraction in liquid carbon dioxide and the Oxygen-17 NMR relaxation are demonstrated to be well suited for the quantification of structures formed by silica particles and the characterization of the silica particle-water interactions. These methods can also be used for the characterization of gelled propellant systems. The proposed multiscale computational strategy for simulating gelled propellant systems combines Brownian dynamics modeling of the gel formation and a continuum approach for the syneresis dynamics.

Acknowledgement
This work was sponsored partly by the New Jersey Institute of Technology and partly by CFD Research Corporation Small Business Technology Transfer Program (STTR) under US Army RDECOM contract # W911NF-05-C-0101, Principal Investigator Dr. Roberto Di Salvo.

APPENDIX A

IMAGES OF SOLVENT JET BREAKUP INTO SUPERCRITICAL CARBON DIOXIDE

The jet breakup of acetone, DCM, mixtures of solvents and PVP solution into supercritical CO_2 were investigated by varying the velocity of solvent injection. PVP with Mw: 1,300,000 was used to prepare the solution for jet breakup study. This appendix presents the graphs of jet breakup of solvents and solution at fixed temperature (35^0C) and pressure (82 bar) injected into supercritical CO_2 using $20-\mu m$ and $40-\mu m$ capillary nozzles.

1. Acetone jet breakup into supercritical CO_2. The operating conditions are 82 bar and 35^0C. 20 um and 40 um nozzles were used to inject acetone.

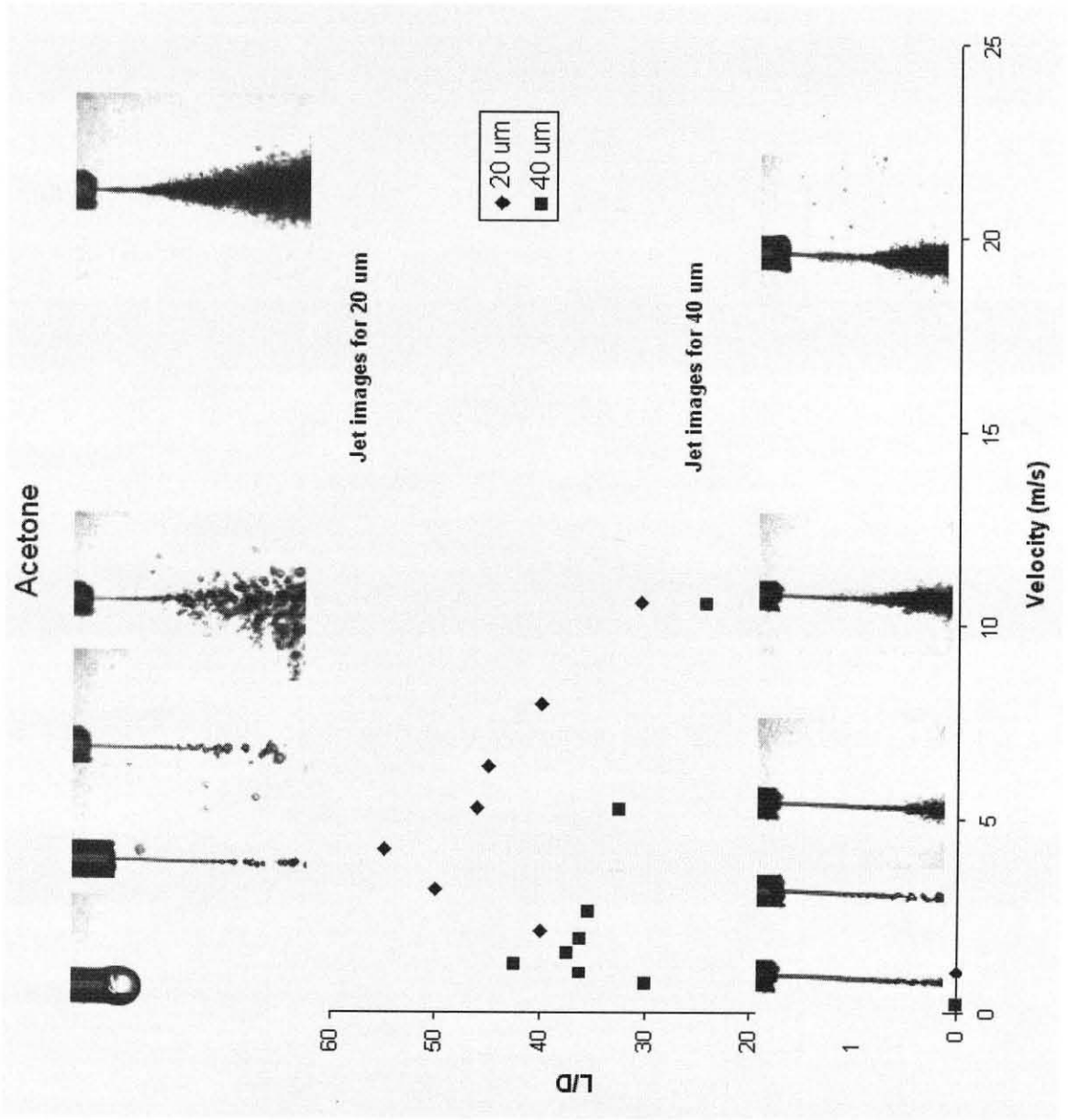

Figure A.1 Acetone jets into supercritical CO_2.

2. Jet breakup of solvent mixture (acetone 60 vol % in DCM). The operating conditions are 82 bar and 35^0C. 20 um and 40 um nozzles were used to inject solvent mixture.

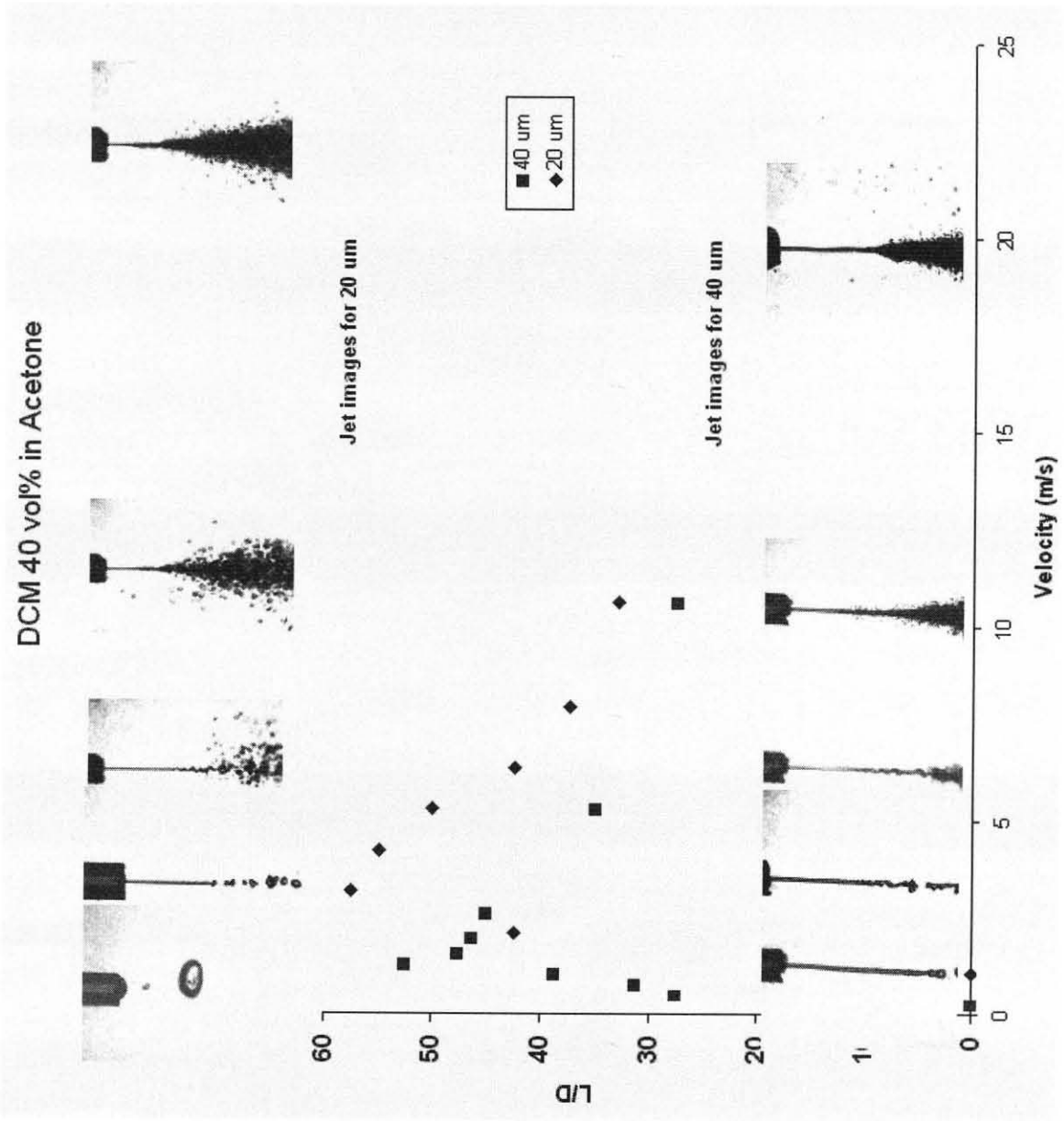

Figure A.2 Jets of solvent mixture (DCM 40 vol% in acetone) into supercritical CO_2.

3. Jet breakup of solution (PVP 2wt/vol% in the mixture of DCM 40vol% in acetone) into supercritical CO_2. The operating conditions are 82 bar and 35^0C. 20 um and 40 um nozzles were used to inject the solution.

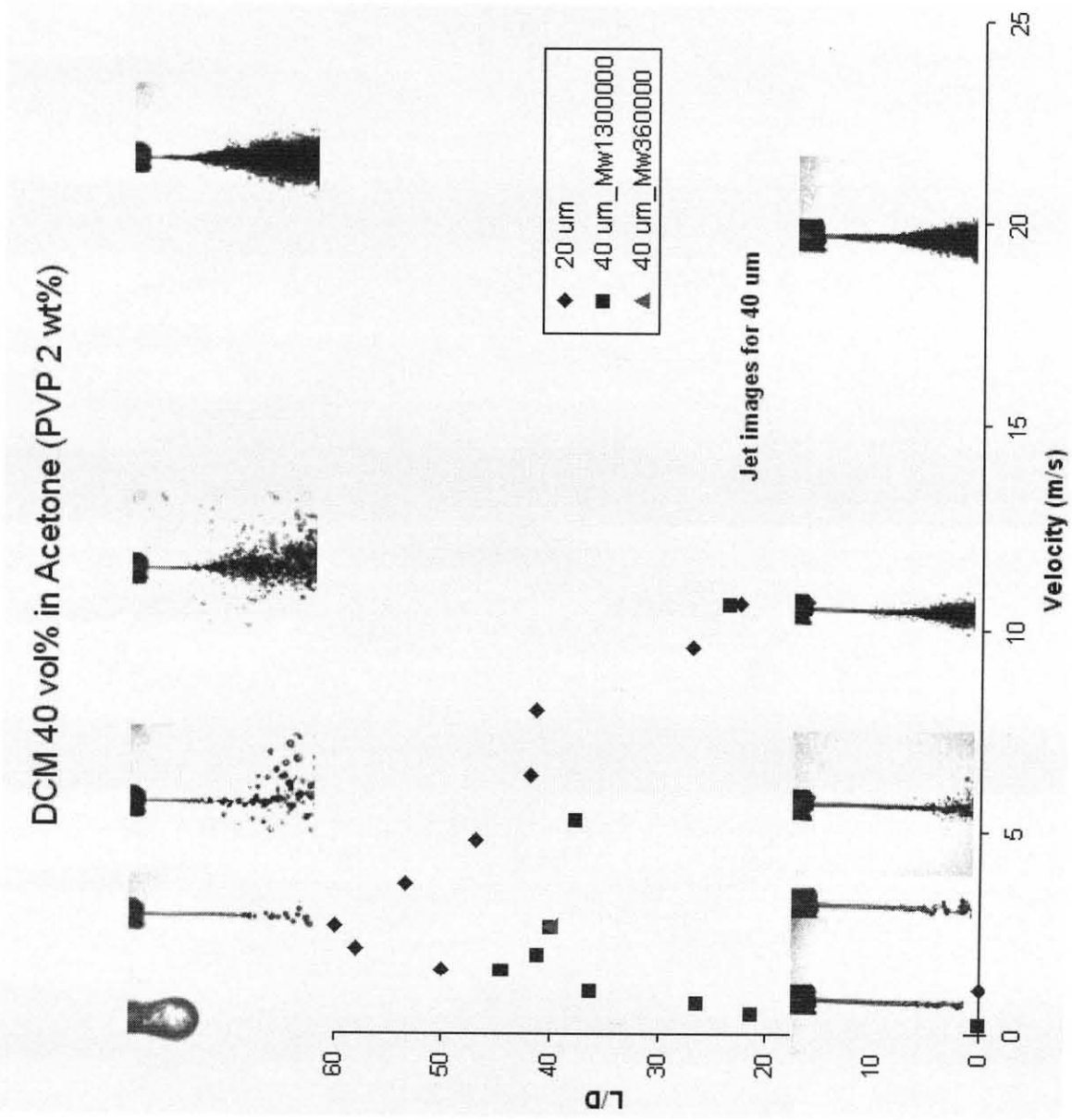

Figure A.3 Jets of solution (PVP 2 wt% into mixture of solvent DCM 40 vol% in acetone) into supercritical CO_2.

Table A.1 L/D for Acetone Jets into Supercritical CO_2

No	20μm Nozzle		40μm Nozzle	
	Velocity	*L/D*	*Velocity*	*L/D*
1	1.06	0	0.2652	0
2	2.122	40	0.5304	15
3	3.183	50	0.7956	30
4	4.244	55	1.0608	36.25
5	5.305	46	1.326	42.5
6	6.366	45	1.5912	37.5
7	7.958	40	1.989	36.25
8	10.61	30.5	2.653	35.5
9			5.304	32.5
10			10.608	24.25

Table A.2 L/D for DCM Jets into Supercritical CO_2

No	20μm Nozzle		40μm Nozzle	
	Velocity	*L/D*	*Velocity*	*L/D*
1	1.06	0	0.2652	0
2	2.122	30	0.5304	23.75
3	3.183	42.5	0.7956	31.25
4	4.244	50	1.0608	37.5
5	5.3	45	1.326	43.75
6	6.366	40	1.5912	41.25
7	7.958	27.5	1.989	38.75
8	9.5496	22.5	2.653	32.5
9	10.6	20	5.304	27.5
10			10.608	20
11			15.912	8.75

Table A.3 L/D for Solvent Mixture of Acetone 60 vol% in DCM Jets into Supercritical CO_2

No	20μm Nozzle		40μm Nozzle	
	Velocity	*L/D*	*Velocity*	*L/D*
1	1.061	0	0.2652	0
2	2.122	42.5	0.5304	27.5
3	3.183	57.5	0.7956	31.25
4	4.244	55	1.0608	38.75
5	5.305	50	1.326	52.5
6	6.366	42.5	1.5912	47.5
7	7.958	37.5	1.989	46.25
8	10.61	33	2.653	45
9			5.304	35
10			10.608	27.5
11			15.912	25
12			19.89	21.25

Table A.4 L/D for Solution Jets (PVP 2 wt/vol% into Solvent Mixture of DCM 40vol% into acetone) Jets into Supercritical CO_2

No	20μm Nozzle		40μm Nozzle	
	Velocity	*L/D*	*Velocity*	*L/D*
1	1.061	0	0.2653	0
2	1.5915	50	0.5306	21.25
3	2.122	58	0.7959	26.25
4	2.6525	60	1.0612	36.25
5	3.183	60.5	1.5918	44.5
6	3.7135	53.5	1.9898	41.25
7	4.7745	47	2.653	40
8	6.366	42	5.304	37.75
9	7.9575	41.5	10.608	23.5
10	9.549	27		
11	10.61	22.5		

APPENDIX B

PARTICLE COATING IMAGES

Silica particles were coated with various methods using supercritical fluids. Different methodologies were used to coat the particles. In SAS-EM method of coating, PMMA was used to coat the 180 nm and 2 μm particles. The operating conditions pressure: 82 bar, temperature: 35C, solution flow rate: 4 mL/min and ultrasonic nozzle frequency: 4W were used for all of the SAS experiments. In case of RESS method, PVDF 9.1 wt/wt % was used to coat the 2 μm particles. For PGSS method, PEG with Mw: 8000 and melting temperature (Tm) 68^0C was used as a coating material. PEG 9.1 wt/wt % was used to coat the silica (180nm) particles.

1. SEM images of PVDF coated silica particles using RESS method. The operating pressures were (a) 2300psi; (b) 1500psi and (c) 0 psi.

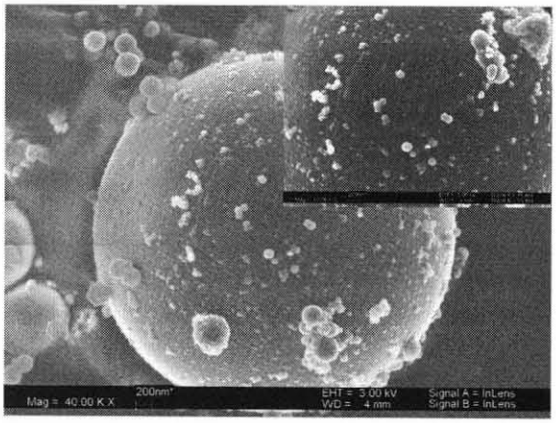

(a)

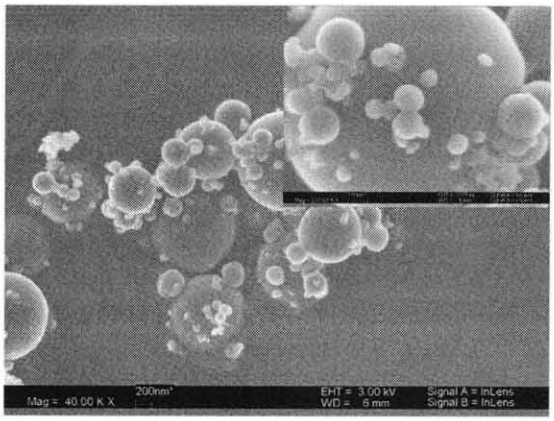

(b)

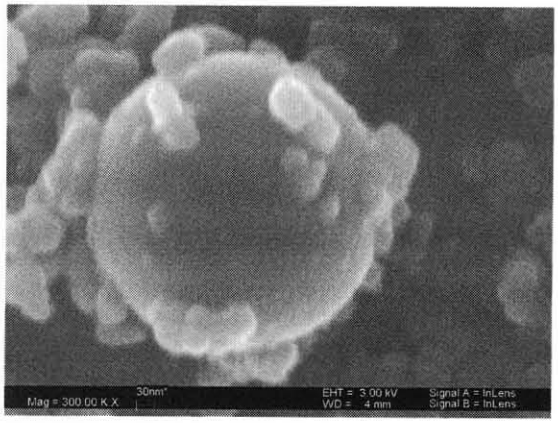

(c)

Figure B.1 PVDF coated silica particles using RESS method. PVDF 9.1 wt/wt% was used to coat the 2um sized silica particles.

2. SEM images of PEG coated silica particles using PGSS method. The operating pressures were (a) 2300psi; (b) 1500psi and (c) 0 psi.

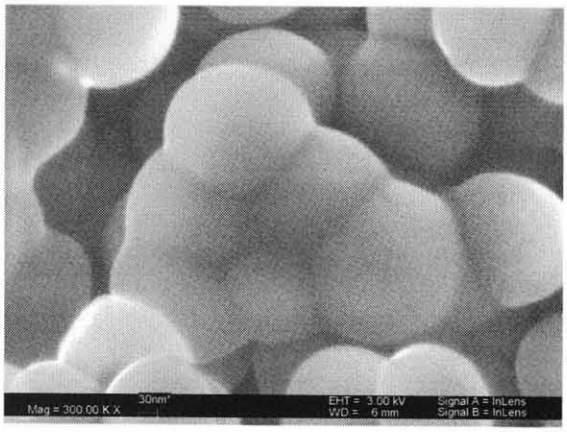

(a)

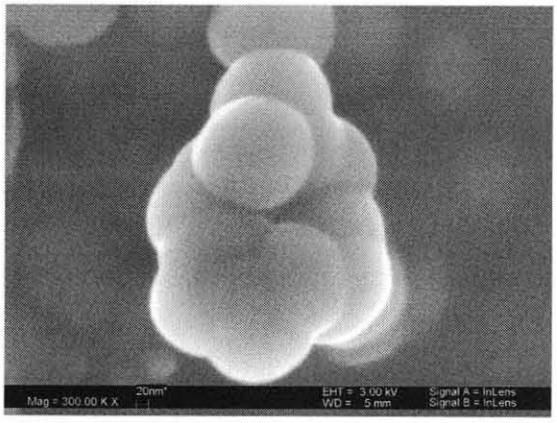

(b)

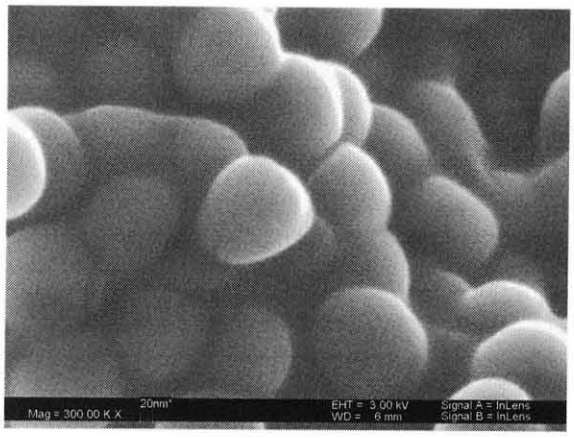

(c)

Figure B.2 PEG coated silica particles using PGSS method. PEG 16.7 wt/wt% was used to coat the 180 nm sized silica particles.

3. SEM images of PEG coated silica particles using PGSS method. The operating pressures were (a) 2300psi; (b) 1500psi and (c) 0 psi.

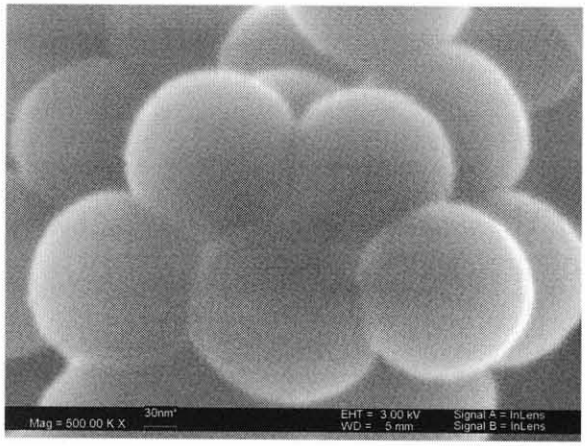

(a)

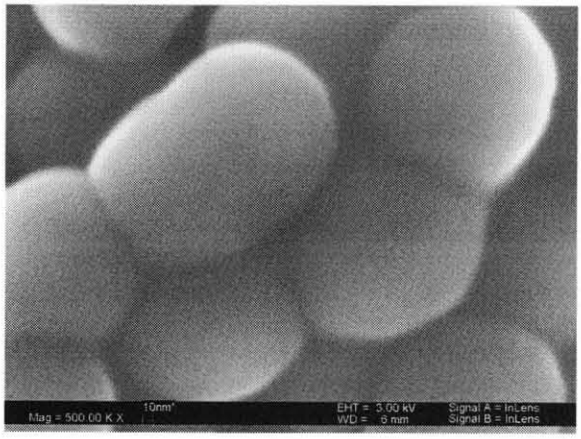

(b)

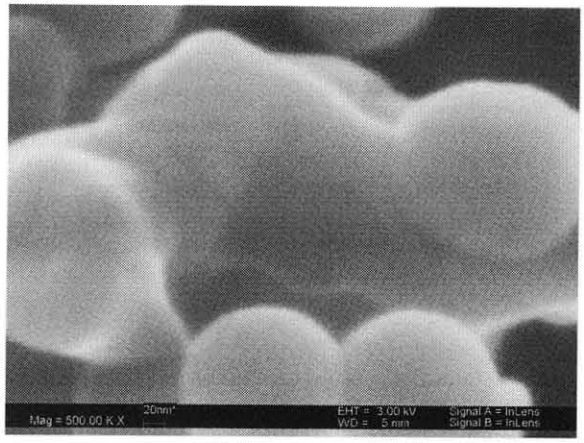

(c)

Figure B.3 PEG coated silica particles using PGSS method. PEG 23 wt/wt% was used to coat the 180 nm sized silica particles.

REFERENCES

1. Hans ML, Lowman AM, Biodegradable nanoparticles for drug delivery and targeting. 2002. Current Opinion in Solid State and Materials Science 6 (2): 319–327.

2. Kastin A, Akerstrom V, Pan W. 2003. Interleukin-10 as a CNS therapeutic: the obstacle of the blood–brain /blood–spinal cord barrier; Molecular Brain Research 114 (1): 168–171.

3. Salata OV, Applications of nanoparticles in biology and medicine. 2003. Journal of Nanobiotechnology. 2: 1-6.

4. Angelica V, Pegaz B, Debefve E, Konan-Kouakou Y, Lange N, Ballini J, Van den Bergh H, Gurny R, Delie F. 2004. Improved photodynamic activity of porphyrin loaded into nanoparticles: an in vivo evaluation using chick embryos; International Journal of Pharmaceutics. 286 (1): 131-145.

5. Debuigne F, Cuisenaire J, Jeunieau L, Masereel B, Nagy JB. 2001. Synthesis of Nimesulide Nanoparticles in the Microemulsion Epikuron/Isopropyl Myristate/Water/ n-Butanol (or Isopropanol); Journal of Colloid and Interface Science 243: 90–101.

6. Alonso M. 2004. Nanomedicines for overcoming biological barriers; Biomedicine & Pharmacotherapy 58 (1): 168–172.

7. Tartaj P, Morales MP, Gonzalez-Carreno T, Veintemillas-Verdaguer S, Serna CJ. 2001. Advances in magnetic nanoparticles for biotechnology applications; Journal of Magnetism and Magnetic Materials 15: 85-91.

8. Raula J, Hannele E, Kauppinen. 2004. Influence of the solvent composition on the aerosol synthesis of pharmaceutical polymer nanoparticles; International Journal of Pharmaceutics 284 (1): 13-21.

9. Barratt G. 2000. Therapeutic applications of colloidal drug carriers. PSTT. 3 (5): 95-105.

10. Kim I, Kim S. 2002. Development of a polymeric nanoparticulate drug delivery system In vitro characterization of nanoparticles based on sugarcontaining conjugates. International Journal of Pharmaceutics 245 (1): 67 - 73.

11. Chen J, Min Y, Shao L, Wang Y, Yun J, Nora Y.K. 2004. Feasibility of preparing nanodrugs by high-gravity reactive precipitation; International Journal of Pharmaceutics 269 (2): 267–274.

12. Shekunov B, York P. 2000. Crystallization processes in pharmaceutical technology and drug delivery design; Journal of Crystal Growth 2 (11): 122-136.

13. Sahoo S, Labhasetwar V. 2003. Nanotech approaches to drug delivery and imaging. DDT. 8 (4) 41-63.

14. Labhasetwar V, Song C, Humphrey W, Shebuski R, Levy R. 1998. Arterial Uptake of Biodegradable Nanoparticles: Effect of Surface Modifications; Journal of Pharmaceutical Sciences. 87 (10) 829-839.

15. Schiavone H, Palakodaty S, Clark A, York P, Tzannis S. 2004. Evaluation of SCF-engineered particle-based lactose blends in passive dry powder inhalers. International Journal of pharmaceutics 281: 55–66.

16. Larhrib H, Martin G, Marriott C, Prime D. 2003. The influence of carrier and drug morphology on drug delivery from dry powder formulations; International Journal of Pharmaceutics 257 (2): 283–296.

17. Zeng X, Martin G, Marriott G, Pritchard J. 2000. The influence of carrier morphology on drug delivery by dry powder inhalers; International Journal of Pharmaceutics 200: 93–106.

18. Rocket and Space technology presents the detailed analysis on different types of propellants and their advantages and disadvantages, Retrieved on 15 July 2006 from World Wide Web: http://www.braeunig.us.

19. US Army Training and Doctrine Command presents the comparison between different types of propellant and Future Missiles Technologies. Retrived on 15 July 2006 from World Wide Web: http://www.tradoc.army.mil.

20. Subra P. 1999. Powders elaboration in supercritical media: comparison with conventional routes. Powder Technology 103: 2-9.

21. Kiran E, Debenedetti P. 2000. Supercritical Fluids–fundamentals and application. Kluwer Academic Publishers.

22. Midoux N, Hoek P, Pailleres L, Authelin J. 1999. Micronization of pharmaceutical substances in a spiral jet mill. Powder Technology. 104 (2) 113-120.

23. Takano K, Nishii K, Horio M. 2003. Binderless granulation of pharmaceutical fine powders with coarse lactose for dry powder inhalation. Powder Technology. 131 (2-3) 129-138.

24. Alfano G, Saba P, Surracco M. 1996. Development of a new jet mill for very fine mineral grinding. International Journal of Mineral Processing, 44-45: 327-336

25. Gonçalves M, Amorim D. 2001. Microparticles for delivering therapeutic peptides and proteins to the lumen of the small intestine. European Journal of Pharmaceutics and Biopharmaceutics, 52 (1): 39-44.

26. Garti N. 1997. Double emulsions - scope, limitations and new achievements. Colloids and Surfaces A: Physicochemical and Engineering Aspects, 123(4): 233-246.

27. Rodriguez L, Passerini N, Cavallari C. 1999. Description and preliminary evaluation of a new ultrasonic atomizer for spray-congealing processes. International Journal of Pharmaceutics, 1839 (2): 133-143.

28. Dewettinck K, Huyghebaert A. 1999. Fluidized bed coating in food technology. Trends in Food Science & Technology. 10 (4-5): 163-168.

29. Debuigne F, Cuisenaire J, Jeunieau L, Masereel B, Nagy J. 2001. Synthesis of Nimesulide Nanoparticles in the Microemulsion Epikuron/Isopropyl Myristate/Water/ n-Butanol (or Isopropanol). Journal of Colloid and Interface Science. 243: 90–101.

30. Tom J, Debenedetti P. 1991. Particle formation with supercritical fluids-a review, J. Aerosol Sci., 22: 555-567.

31. Debenedetti P, Tom J, Yeo S, Lim G. 1993. Application of supercritical fluids for the production of sustained delivery devices. J. Controlled Release. 24: 27-39.

32. Benedetti L, Bertucco A, Pallado P. 1997. Production of micronic particles of biocompatible polymer using supercritical carbon dioxide, Biotechnol. Bioeng., 53: 232 -243.

33. Mishima K, Matsuyama K, Taruta Y, Ezawa M. 1998. Production of polyethylene glycol and polyoxyalkylenealkylphenyl ether microspheres using supercritical carbon dioxide. Stud. Surf. Sci. Catal. 114: 661-675.

34. Lele AK, Shine AD. 1992. Morphology of polymers precipitated from a supercritical solvent, AIChE J. 38 (2): 742-748.

35. Hay JN, Khan A. 2002. Review: environmentally friendly coatings using carbon dioxide as the carrier medium. J. Mater. Sci. 37 (6): 4743-4758.

36. Tepper G, Levit N. 2000. Polymer deposition from supercritical solutions for sensing applications. Ind. Eng. Chem. Res. 39 (12): 4445-4449.

37. Fulton JL, Deverman GS, Yonker CR, Grate JW, Young J, McLain JB. 2003. Thin fluoropolymer films and nanoparticles coating from rapid expansion of

supercritical carbon dioxide solutions with electrostatic collection. Polymer, 44 (8): 3627-3639.

38. Chernyak Y, Henon F, Harris RB, Gould RD, Franklin RK, Edwards JR, DeSimone JM. 2001. Formation of perfluoropolyether coatings by the rapid expansion of supercritical solutions (RESS) process. Part 1. Experimental results, Ind. Eng. Chem. Res., 40: 6118-6125.

39. Glebov EM, Yuan L, Krishtopa LG, Usov OM, Krasnoperov LN. 2001. Coating of metal powders with polymers in supercritical carbon dioxide. Ind. Eng. Chem. Res., 40: 4058-4068.

40. Matsuyama K, Mishima K, Umemoto H, Yamaguchi S. 2001. Environmentally benign formation of polymeric microspheres by rapid expansion of supercritical carbon dioxide solution with nonsolvent. Environ. Sci. Technol.. 35 (11): 4149-4162.

41. Wang YL, Wei DG, Dave R, Pfeffer R, Sauceau M, Letourneau JJ, Fages J. 2002. Extraction and precipitation particle coating using supercritical CO_2. Powder Technology 127: 32-42.

42. Shim JJ, Johnston KP. 2002. Aqueous latexes formed from polymer/CO_2 suspensions. 2. Hydrophilic surfactants in water. Ind. Eng. Chem. Res. 41 (14): 4750-4757.

43. Han SJ, Lohse DJ, Radosz M, Sperling LH. 2000. Morphologies of blends of isotactic polypropylene and ethylene copolymer by rapid expansion of supercritical solution and isobaric crystallization from supercritical solution. J. Appl. Polym. Sci. 77: 1478-1487.

44. Subra P. 1999. Powders elaboration in supercritical media: comparison with conventional routes, Powder Technology. 103 (1): 2-9.

45. Perrut M. 2001. Particle design using supercritical fluids: Literature and patent survey. Journal of Supercritical Fluids. 20 (2): 179-219.

46. Kiran E, Debenedetti P. Supercritical Fluids–fundamentals and application, Kluwer Academic Publishers.

47. Erdogan Kiran, Joan Brennecke. 1993. Supercritical Fluid Engineering Science-Fundamentals and Application, Washington D.C.: American Chemical Society.

48. Kerc J, Srcic S, Knez Z. 1999. Micronization of drugs using supercritical carbon dioxide. Int. J. Pharm. 182: 33-39.

49. Knez Z. 2000. Micronization of pharmaceuticals using supercritical fluids, in: M. Perrut, E. Reverchon (Eds.). Proceedings of the Seventh Meeting on Supercritical Fluids, 1: 1–26.

50. Morley J, Rummelt A, Matin L. 1998. Cyclosporine form for pulmonary administration. United States Patent No. 5,719,123.

51. McHugh MA, Yogan TJ. 1984. Three-phase solid–liquid–gas equilibria for three carbon dioxide–hydrocarbon solid systems, two ethane–hydrocarbon solid systems, and two ethylene–hydrocarbon solid systems. J. Chem. Eng. Data. 29: 112–115.

52. Tandya A, Dehghani F, Foster N. 2006. Micronization of cyclosporine using dense gas techniques. J. of Supercritical Fluids. 37 (6): 272–278.

53. Shekunov B. 2001. Analysis of the supersaturation and precipitation process with supercritical CO_2. Journal of Supercritical Fluids 21(2): 257-271.

54. Gupta R. 2001. Production of griseofulvin nanoparticles using supercritical CO_2 antisolvent with enhanced mass transfer. International Journal of Pharmaceutics 228: 19-31.

55. Reverchon E, Della G. 2000. Supercritical antisolvent micronization of some biopolymers, J. Supercrit. Fluids, 18: 239-253.

56. Sarkari M, Darrat I, Knutson BL. 2000. Generation of microparticles using CO_2 and CO2-philic antisolvents, AIChE J. 46: 1850-1860.

57. Breitenbach A, Mohr D, Kissel T. 2000. Biodegradable semi-crystalline comb polyesters influence the microsphere production by means of a supercritical extraction technique. J. Controlled Release. 63 (1): 53-63.

58. Shekunov BY, Edwards AD, Forbes R. 2003. Crystallization and plasticization of poly(l-lactide) (PLLA) with supercritical CO_2, in: Proceedings of the Sixth International Symposium on Supercritical Fluids, Versailles, France, 28–30. pp. 1801–1806.

59. Werling J, Debenedetti P. 1999. Numerical modeling of mass transfer in the supercritical antisolvent process. Journal of Supercritical Fluids. 16 (2): 167–181.

60. Werling J, Debenedetti P. 2000. Numerical modeling of mass transfer in the supercritical antisolvent process: miscible conditions, Journal of Supercritical Fluids 18 (1): 11–24.

61. Carretier E, Badens E, Guichardon P, Boutin O, Charbit G. 2003. Hydrodynamics of supercritical antisolvent precipitation: characterization and influence on particle morphology, Ind. Eng. Chem. Res. 42: 331-341.

62. Lengsfeld CS, Delplanque JP, Barocas VH, Randolph TW. 2000. Mechanism Governing Microparticle Morphology during Precipitation by a Compressed Antisolvent: Atomization vs Nucleation and Growth. J. Phys. Chem. B. 104 (6): 2725-2735.

63. Roberts CJ, Debenedetti PG. 2002. Engineering pharmaceutical stability with amorphous solids. AIChE J. 48 (12): 1140– 1144.

64. Lang Q, Wai C. 2001. Supercritical fluid extraction in herbal and natural product studies - a practical review. Talanta 53 (5): 771-782.

65. Cohen Z, Vonshak A. 1991. Fatty acid composition of Spirulina and Spirulina-like cyanobacteria in relation to their chemotaxonomy. Phytochemistry. 30: 205-206.

66. Mahajan G, Kamat M. 1995. c-Linoleic acid production from Spirulina platensis. Applied Microbiology and Biotechnology. 43 (5): 466–469.

67. Bhat VB, Madyastha KM. 2000. C-Phycocyanin: a potent peroxyl radical scavenger in vivo and in vitro. Biochemical and Biophysical Research Communications, 275: 20–25.

68. Madhava C, Bhat VB, Kiranmai G, Reddy MN, Reddanna P, Madyastha KM. 2000. Selective inhibition of cyclooxygenase-2 by C-phycocyanin, a biliprotein from spirulina platensis. Biochemical and Biophysical Research Communications. 277 (20): 599–603.

69. Estrada JE, Bascos P, FresnoAM. 2001. Antioxidant activity of different fractions of Spirulina platensis protean extract. Il Farmaco, 56 (2): 497–500.

70. Borowitzka MA, Borowitzka LJ. 1988. Micro-algal biotechnology (pp. 96–100). Cambridge, UK: Cambridge University Press.

71. King JW, Favati F, Taylor SL. 1996. Production of tocopherol concentrates by supercritical fluid extraction and chromatography. Separation Science and Technology, 31: 1843–1857.

72. Senorans FJ, Ibanez E, Cavero S, Tabera J, Reglero G. 2000. Liquid chromatographic-mass spectrometric analysis of supercritical fluid extracts of rosemary plants. Journal of Chromatography A. 870 (20): 491-499.

73. Shen W, Vela N, Sheppard B, Caruso J. 1991. Evaluation of inductively coupled plasma mass spectrometry as an elemental detector for supercritical-fluid chromatography. Anal Chem. 63: 1491–1496.

74. Vela N, Caruso J. 1992. Determination of tri- and tetra-organotin compounds by supercritical-fluid chromatography with inductively coupled plasma mass spectrometric detection. J Anal Atom Spectrom. 7: 971–977.

75. Zeng X, Martin G, Marriott G, Pritchard J. 2000. The influence of carrier morphology on drug delivery by dry powder inhalers; International Journal of Pharmaceutics 200: 93–106

76. J. Jung, M. Perrut. 2001. Particle design using supercritical fluids: Literature and patent survey. Journal of Supercritical Fluids 20: 179–219

77. A. Shariati, C. Peters. 2003. Recent developments in particle design using supercritical fluids. Current Opinion in Solid State and Materials Science 7: 371–383

78. Liu H. 1999. Science and engineering of droplets: Fundamental and Applications. Yoyes Publications.

79. Rayleigh FRS. 1879. On the instability of jets. Proc. London Math. Soc. 29: 71-97

80. A.H. Lefebvre, Atomization and sprays, Hemisphere Publishing Co., 1989.

81. Chavez FC, Debenedetti PG, Luo JJ, Dave RN, Pfeffer R. 2003. Estimation of the characteristic time scales in the supercritical antisolvent process. Ind. Eng. Chem. Res. 42: 3156-3162.

82. Liu H. Science and engineering of droplets: fundamentals and applications. 1999. William Andrew Publishing, LLC. NY.

83. Dukhin SS, Zhu C, Dave R, Pfeffer R, Luo, JJ, Chavez F, Shen Y. 2003. Dynamic interfacial tension near critical point of solventantisolvent mixture and laminar jet stabilization, Colloids Surf. A: Physicochem. Eng. Aspects 229: 199-210.

84. Carretier E, Badens E, Guichardon P, Boutin O, Charbit G. 2003. Hydrodynamics of supercritical antisolvent precipitation: characterization and influence on particle morphology, Ind. Eng. Chem. Res. 42: 331-338.

85. Kerst AW, Judat B, Schlunder EU. 2000. Flow regimes of free jets and falling films at high ambient pressure, Chem. Eng. Sci. 55: 4189-4200.

86. Czerwonatis N, Eggers R. 2001. Disintegration of liquid jets and drop drag coefficients in pressurized nitrogen and carbon dioxide, Chem. Eng. Technol. 24: 6-12.

87. Lengsfeld CS, Delplanque JP, Barocas VH, Randolph TW. 2000. Mechanism governing microparticle morphology during precipitation by a compressed antisolvent: atomization versus nucleation and growth, J. Phys. Chem. B. 104 (2): 2725-2735.

88. Tamba J, Ohara T, Alhara T. 1997. MD study on interfacelike phenomena in supercritical fluid. Microscale Thermophys Eng 1(1):19-30.

89. Tamba J, Takahashi T, Ohara T, Aihara T. 1998. Transition from boiling to free convection in supercritical fluid. Exp Therm Fluid Sci 17(3):248-255.

90. Van Oss CJ, Giese RF, Good RJ. 2002. The zero time dynamic interfacial tension. J Dispersion Sci Technol 23(4):455-464.

91. Cahn JW, Hillard JE. 1958. Free energy of a nonuniform system. I. interfacial free energy. J Chem Phys 28(2):258-267.

92. Lengsfeld CS, Delplanque JP, Barocas VH, Randolph TW. 2000. Mechanism governing microparticle morphology during precipitation by a compressed antisolvent: atomization versus nucleation and growth, J. Phys. Chem. B. 104: 2725-2735.

93. Dukhin SS, Zhu C, Dave R, Pfeffer R, Luo JJ, Chavez F, Shen Y. 2003. Dynamic interfacial tension near critical point of solvent-antisolvent mixture and laminar jet stabilization. Colloids Surf. A: Physicochem. Eng. Aspects 229 (1): 199-206.

94. Badens E, Boutin O, Charbit G. 2005. Laminar jet dispersion and jet atomization in pressurized carbon dioxide, J. Supercrit. Fluids. 36 (1): 81–90.

95. Chavez FC, Debenedetti PG, Luo JJ, Dave RN, Pfeffer R. 2003. Estimation of the characteristic time scales in the supercritical antisolvent process. Ind. Eng. Chem. Res. 42 (6): 3156-3162

96. Tyn MT, Calus WF. 1975. Diffusion coefficients in dilute binary liquid mixtures. J. Chem. Eng. Data 20: 106-109

97. Quayle OR. 1953. The parachors of organic compounds. An interpretation and catalogue. Chem. Rev. 1439-1589

98. H.-L. Zhang. 2003. Viscosity and Density for Binary Mixtures of Carbon Tetrachloride+ Chloroform, Carbon Tetrachloride + Dichloromethane, and Chloroform + Dichloromethane and One Ternary Mixture of Chloroform + 1:1

(Carbon Tetrachloride + Dichloromethane) at 303.15 K, J. Chem. Eng. Data. 48, 52-55

99. T.M. Aminabhavi and K. Banerjee. 1998. Density, Viscosity, Refractive Index, and Speed of Sound in Binary Mixtures of Dimethyl Carbonate with Methanol, Chloroform, Carbon Tetrachloride, Cyclohexane, and Dichloromethane in the Temperature Interval (298.15-308.15) K, J. Chem. Eng. Data. 43, 1096-1101

100. B. Gonzalez, A. Domınguez, and J. Tojo. 2005. Dynamic Viscosities of the Binary Systems Cyclohexane and Cyclopentane with Acetone, Butanone, or 2-Pentanone at Three Temperatures T = (293.15, 298.15, and 303.15) K, J. Chem. Eng. Data. 50, 1462- 1469

101. National Institute of Standards and Technology presents the viscosity data for various organic solvents and gases on their website. Retrieved on 01 February 2006 from World Wide Web: http://www.nist.gov

102. D.R. Lide. 1995. Handbook of Organic Solvents, CRC Press, Boca Raton.

103. T. Funazukuri, C. Y. Kong, and S. Kagei. 2000. Binary diffusion coefficients of acetone in carbon dioxide at 308.2 and 313.2 K in the pressure range from 7.9 to 40 MPa; International Journal of Thermophysics. 21: 651-669

104. Kojima M, Hinch EJ, Acrivos A. 1984. The formation and expansion of a toroidal drop moving in a quiescent fluid. Phys. Fluids. 1: 1309-1313

105. Baumann N, Joseph DDJ, Mohr P, Renardy Y. 1992. Vortex rings of one fluid in another in free fall, Phys. Fluids A. 4 (2): 567-580

106. Arecchi FT, Buah-Bassuah PK, Francini F, Residori S. 1996. Fragmentation of a drop as it falls in a lighter miscible fluid. Physical Review E. 54 (4): 424-429

107. Residoria S, Pampalonib E, Buah-Bassuahc PK, Arecchid FT. 2000. Surface tension effects in the zero gravity inflow of a drop into a fluid, Eur. Phys. J. B 15: 331-334

108. Flory P. J., 1953. Principles of Polymer Chemistry. Cornell University Press. New York.

109. M. Doi, H. See. 1996. Introduction to Polymer Physics, Oxford University Press, New York.

110. A. William. 2001. Handbook of solvent. ChemTec. Toronto.

111. Salata OV. 2003. Applications of nanoparticles in biology and medicine. Journal of Nanobiotechnology. 2: 1 - 6.

112. Vargas A, Debefve B, Kouakou Y, Lange N, Ballini J, Bergh H, Gurny R. 2004. Improved photodynamic activity of porphyrin loaded into nanoparticles: an in vivo evaluation using chick embryos. International Journal of Pharmaceutics 286: 131-145.

113. Hans ML, Lowman AM. 2002. Biodegradable nanoparticles for drug delivery and targeting. Current Opinion in Solid State and Materials Science 6: 319-327.

114. Debuigne F, Cuisenaire J, Jeunieau L, Masereel B. 2001. Synthesis of Nimesulide Nanoparticles in the Microemulsion Epikuron/Isopropyl Myristate/Water/ n-Butanol (or Isopropanol); Journal of Colloid and Interface Science 243 (10): 90–101.

115. Alonso M. 2004. Nanomedicines for overcoming biological barriers; Biomedicine & Pharmacotherapy. 58: 168-172.

116. Tartaj P, Morales MP, Gonzalez-Carreno T, Verdaguer S, Serna CJ. 2005. Advances in magnetic nanoparticles for biotechnology applications. Journal of Magnetism and Magnetic Materials. 290 (1): 28-34.

117. Raula J, Ainena H, Kauppinen E. 2004. Influence of the solvent composition on the aerosol synthesis of pharmaceutical polymer nanoparticles. International Journal of Pharmaceutics 284: 13-21.

118. Barratt G. 2000 Therapeutic applications of colloidal drug carriers. PSTT 3 (5) 163-171

119. Kim I, Kim S. 2002. Development of a polymeric nanoparticulate drug delivery system In vitro characterization of nanoparticles based on sugarcontaining Conjugates. International Journal of Pharmaceutics 245 (4): 67-73.

120. Chen J, Zhou M, Shao L, Wang Y, Yun J, Nora YK, Chew H. 2004. Feasibility of preparing nanodrugs by high-gravity reactive precipitation; International Journal of Pharmaceutics 269 (3): 267-274.

121. Shekunov B, York P. 2000. Crystallization processes in pharmaceutical technology and drug delivery design. Journal of Crystal Growth 211: 122-136

122. Sahoo S, Labhasetwar V. 2003. Nanotech approaches to drug delivery and imaging. 8 (24): 1112-1120.

123. Hans ML, Lowman AM. 2002. Biodegradable nanoparticles for drug delivery and targeting; Current Opinion in Solid State and Materials Science 6 (2): 319-327.

124. Kastin A, Akerstrom V, Pan W. 2003. I nterleukin-10 as a CNS therapeutic: the obstacle of the blood–brain /blood–spinal cord barrier; Molecular Brain Research 114: 168–171.

125. Labhasetwar V, Song C. 1998. Arterial Uptake of Biodegradable Nanoparticles: Effect of Surface Modifications. Journal of Pharmaceutical Sciences. 87 (10): 1229-1234.

126. Schiavone H, Palakodaty S, Clark A, York P, Tzannis S. 2004. Evaluation of SCF-engineered particle-based lactose blends in passive dry powder inhalers; International Journal of pharmaceutics 281: 55-66.

127. Larhrib H, Martin G, Marriott C, Prime D. 2003. The influence of carrier and drug morphology on drug delivery from dry powder formulations; International Journal of Pharmaceutics 257 (1): 283–296

128. E. Reverchon, G. Della Porta, A. Di Trolio, S. Pace, Supercritical antisolvent precipitation of nanoparticles of superconductor precursors, Ind. Eng. Chem. Res. 37 (1998) 952.

129. Reverchon E, Marco I, Porta D. 2002. Tailoring of nano- and micro-particles of some superconductor precursors by supercritical antisolvent precipitation. J. Supercritical Fluids 23: 81-92.

130. Reverchon E, Della Porta G, Sannino D, Ciambelli P. 1999. Supercritical antisolvent precipitation of nanoparticles of a zinc oxide precursor, Powder Technol. 102 (1): 127-139

131. Wu H, Lee W, Lin H. 2005. Nano-particles formation for pigment red 177 via a continuous supercritical anti-solvent process. J. Supercrit. Fluids 33: 173-183.

132. Reverchon E, Adami R, Marco I. 2005. Disperse red 60 micronization using supercritical fluid based techniques. J. Supercrit. Fluids 35 (2): 76-86.

133. Chattopadhyay P, Gupta RB. 2000. Supercritical CO_2-Based Production of Fullerene Nanoparticles, Ind. Eng. Chem. Res. 39 (10): 2281-2290.

134. Reverchon E, Della Porta G. 1999. Production of antibiotic micro- and nanoparticles by supercritical antisolvent precipitation. Powder Technol. 106 (1): 23-39.

135. Chattopadhyay P, Gupta RB. 2001. Production of griseofulvin nanoparticles using supercritical CO2 antisolvent with enhanced mass transfer, Int. J. Pharm. 228 (1): 19-28.

136. Chattopadhyay P, Gupta RB. 2002. Protein nanoparticles formation by supercritical antisolvent with enhanced mass transfer, AIChE J. 48: 235-245.

137. Reverchon E, Della Porta G, Rosa L, Subra P, Letourneur D. 2000. Supercritical antisolvent micronization of some biopolymers. J. Supercrit. Fluids 18 (2): 239-243.

138. Yoshihisa K, Yasuo T, Yasuo Y, Haruhiko K, Yoko Y, Hiroshi K, Tsunoda S, Takayuki O, Yohei M, Hiroko S, Shinsaku N, Tadanori M. 2004. The use of PVP as a polymeric carrier to improve the plasma half-life of drugs. Biomaterials 25 (14) 3259-3266.

139. Lukyanov A, Torchilin V. 2004. Micelles from lipid derivatives of water-soluble polymers as delivery systems for poorly soluble drugs. Advanced Drug Delivery Reviews 56 (12): 1273– 1289

140. Mukherjee B, Mahapatra S, Gupta R, Patra B, Tiwari A, Arora P. 2005. A comparison between povidone-ethylcellulose and povidone-eudragit transdermal dexamethasone matrix patches based on in vitro skin permeation. European Journal of Pharmaceutics and Biopharmaceutics 59 (3): 475-483

141. Grassi I. Colombo R, Lapasin R. 2000. Drug release from an ensemble of swellable crosslinked polymer particles; Journal of Controlled Release 68 (1): 97–113

142. Labhasetwar V, Song C, Humphrey W, Shebuski R, Levy R. 1998. Arterial Uptake of Biodegradable Nanoparticles: Effect of Surface Modifications. Journal of Pharmaceutical Sciences. 87 (10): 1229-1234

143. Schiavone H, Palakodaty S, Clark A, York P. 2004. Evaluation of SCF-engineered particle-based lactose blends in passive dry powder inhalers. International Journal of pharmaceutics 281 (1): 55-66.

144. Hassan L, Martin G, Marriott C, Prime D. 2003. The influence of carrier and drug morphology on drug delivery from dry powder formulations; International Journal of Pharmaceutics 257 (2): 283-296.

145. Zeng X, Martin G, Marriott C, Pritchard J. 2000. The influence of carrier morphology on drug delivery by dry powder inhalers; International Journal of Pharmaceutics 200 (1): 93-106.

146. Reverchon E. 2002. Rifampicin microparticles production by supercritical antisolvent precipitation. 2002. International Journal of Pharmaceutics. 243: 83-91.

147. Krober H. 2002. Materials processing with supercritical Antisolvent precipitation: process parameters and morphology of tartaric acid. Journal of Supercritical Fluids 22(2): 229-235.

148. Dixon D, Johnston P. 1993. Formation of microporous polymer fibers and oriented fibrils by precipitation with a compressed fluid antisolvent J Appl Polym Sci 50 (11): 1929-1942.

149. Dixon D, Johnston K, Bodmeier R. 1993. Polymeric materials formed by precipitation with a compressed fluid antisolvent. AIChE Journal. 39 (1): 127-139

150. Ghaderi R. 2000. A new method for preparing biodegradable microparticles and entrapment of hydrocortisone in DL-PLG microparticles using supercritical fluids. European Journal of Pharma Sciences 10 (1): 1-9.

151. Yeo S. 2003. Recrystallization of sulfathiazole and chloropropamide using the supercritical fluid antisolvent process, J. of Supercritical Fluids 25 (1): 143-154.

152. Krober H, Teipei U. 2002. Materials processing with supercritical Antisolvent precipitation: process parameters and morphology of tartaric acid, Journal of Supercritical Fluids 22 (2): 229-235.

153. Magnan, C., Badens, E., Commenges, N., Charbit, G. 2000. Soy lecithin micronization by precipitation with a compressed fluid antisolvent - influence of process parameters. Journal of Supercritical Fluids 19 (1): 69-77.

154. Rantakyla R, Jäntti M, Aaltonen O, Hurme, M. 2002. The effect of initial drop size on particle size in the supercritical antisolvent precipitation (SAS) technique, Journal of Supercritical Fluids 24 (3) 251-263.

155. Werling J, Debenedetti P. 1999. Numerical modeling of mass transfer in the supercritical antisolvent process. Journal of Supercritical Fluids 16 (1) 167-181.

156. Wang Y, Wei D, Dave R, Pfeffer R, Sauceau M, Letourneau J, Fages J. 2002. Extraction and precipitation particle coating using supercritical CO_2. Powder Technology. 127 (1): 32-44.

157. Wang Y, Dave R, Pfeffer R. 2004. Polymer coating/encapsulation of nanoparticles using a supercritical anti-solvent process. J. of Supercritical Fluids 28 (1) 85-99.

158. Leroux JC, Allemann E, Jaeghere FE, Doelker E, Gurny R. 1996. Biodegradable nanoparticles - from sustained release formulations to improved site specific drug delivery. J. Control. Rel. 39 (2) 339-350.

159. Boutin O, Badens E, Carretier E, Charbit G. 2004. Co-precipitation of a herbicide and biodegradable materials by the supercritical anti-solvent technique. J. of Supercritical Fluids. 31 (1): 89-99

160. Dos Santos IR, Richard J, Pech B, Thies C, Benoit JP. 2002. Microencapsulation of protein particles within lipids using a novel supercritical fluid process. International Journal of Pharmaceutics. 242 (1): 69-78.

161. Schreiber R, Carsten V, Werther J, Brunner G. 2002. Fluidized bed coating at supercritical fluid conditions. Journal of Supercritical Fluids. 24 (1) 137-151.

162. Schreiber R, Reinke B, Carsten V, JWerther J, Brunner G. 2003. High-pressure fluidized bed coating utilizing supercritical carbon dioxide. Powder Technology. 138 (1) 31-38.

163. Krober H, Teipel U. 2005. Microencapsulation of particles using supercritical carbon dioxide. Chemical Engineering and Processing. 44 (2): 215-219.

164. Wang Y, Pfeffer R, Dave R, Enick R. 2005. Polymer Encapsulation of Fine Particles by a Supercritical Antisolvent Process. AIChE Journal 51 (5) 440-455.

165. Shen Y. Dissertation on supercritical antisolvent process for particle formation and polymer coating, New Jersey Institute of Technology, December 2005

166. Day CY, Chang CJ. 1996. Phase Equilibrium of Ethanol + CO_2 and Acetone + CO_2 at Elevated Pressures. J. Chem. Eng. Data. 41 (6) 839-843.

167. Tsivintzelis I, Missopolinou D, Kalogiannis K, Panayiotou C. 2004. Phase compositions and saturated densities for the binary systems of carbon dioxide with ethanol and dichloromethane, Fluid Phase Equilibria, 224 (1): 89–96

168. Stievano M, Elvassore N. 2005. High-pressure density and vapor–liquid equilibrium for the binary systems carbon dioxide-ethanol, carbon dioxide-acetone and carbon dioxide-dichloromethane, J. of Supercritical Fluids, 33 (1) 7–14.

169. Wang Y., 2005. Development of supercritical fluid processes for particle coating / encapsulation with polymers. PhD Thesis (chapter 5).

170. Debenedetti, P. G. 1990. Homogeneous nucleation in supercritical fluids. AIChE J. 36 (12): 1289-1298.

171. Kim JH, Paxton TE, Tomasko DL. 1996. Microencapsulation of naproxen using rapid expansion of supercritical solutions. Biotechnol Prog, 12(5):650-661.

172. Mishima K, Matsuyama K, Tanabe D, Yamauchi S, Young TJ, Johnston KP. 2000. Microencapsulation of proteins by rapid expansion of supercritical solution with a nonsolvent. AIChE Journal, 46(4):857-865.

173. Weidner E, Petermann M, Knez Z. 2003. Multifunctional composites by high-pressure spray processes. Curr Opin Solid Mater Sci.7 (2): 385–390.

174. Mishima K, Matsuyama K, Tanabe D, Yamauchi S, Young TJ, Johnston KP. 2000. Microencapsulation of proteins by rapid expansion of supercritical solution with a nonsolvent. AIChE Journal, 46(4):857-865.

175. Mandel FS, Green CD, Scheibelhoffer AS. Method of preparing coating materials. (Ferro Corporation, Cleveland, USA). US:5548004, 1996.

176. Weidner E, Petermann M, Blatter K, Rekowski V. 2001. Manufacture of powder coatings by spraying of gas-enriched melts. Chem Eng Tech. 24(3) 529-533.

177. Weidner E, Knez Z, Steiner R. 1996. Powder generation from polyethyleneglycols with compressible fluids. High Pressure Chem Eng Proc Process Tech. 223-228.

178. Hao J, Whitaker MJ, Serhatkulu G, Shakesheff KM, Howdle SM. 2005. Supercritical fluid assisted melting of poly(ethylene glycol): a new solvent-free route to micro particles. J Mater Chem. 15 (14): 1148-1153.

179. Petra S, Stane S, Zeljko K, Janez K. 1997. Improvement of nifedipine dissolution characteristics using supercritical CO_2, International Journal of Pharmaceutics. 148 (2) 123 -130.

180. Ker J, Srcic S, enar-B. 1999. Micronization of drugs using supercritical carbon dioxide. International Journal of Pharmaceutics. 182 (1) 33-39.

181. Rodrigues M. Peiriço N, Matos H, Gomes E, Lobato M, Almeida A. 2004. Microcomposites theophylline/hydrogenated palm oil from a PGSS process for controlled drug delivery systems. J. of Supercritical Fluids. 29 (2) 175–184.

182. Kerc J., Srcic S., Knez Z., Sencar P. 1999. Micronization of drugs using supercritical carbon dioxide. International Journal of Pharmaceutics. 182 (1) 33-39

183. Rocket and Space technology presents the detailed analysis on different types of propellants and their advantages and disadvantages, Retrieved on 15 July 2006 from World Wide Web: http://www.braeunig.us.

184. US Army Training and Doctrine Command presents the comparison between different types of propellant and Future Missiles Technologies. Retrived on 15 July 2006 from World Wide Web: http://www.tradoc.army.mil.

185. Bonnell DGR. 1932. Studies in gel I: Syneresis of silica gel. Transactions of the Faraday Society. 28 (1) 1-11.

186. Bonnell DGR. 1932. Studies in gels II: Effect of hydrogen-ion concentration on the syneresis of silica gel. Transactions of the Faraday Society. 28 (1) 12-19.

187. Bonnell DGR. 1932. Studies in gels III: Vapor pressure of silica gels. Transactions of the Faraday Society, 28 (2) 463-471.

188. Bonnell DGR. 1933. Studies in gels IV: Swelling of silica gel. Transactions of the Faraday Society. 29 (6) 1217-1220.

189. Bonnell DGR. 1933. Studies in gels V: Effect of neutral electrolytes on the syneresis of silica gels. Transactions of the Faraday Society. 29 (6) 1221-1226.

190. Acker EG. 1970. The characterization of acid-set silica hydrosols, hydrogels and dried gel. Journal of Colloid and Interface Science. 32 (1) 41-54.

191. H. Hoffmann. 2002. Novel Ringing Silica Gels That Do Not Shrink. J. Phys. Chem. B 106 (11) 1528-1533.

192. Vollet DR. 2001. From sol to aerogel: a study of the nanostructural characteristics of TEOS derived sonogels. Journal of Non-Crystalline solids. 292 (1) 44-49.

193. Birch DJS. 2000. Nanometer resolution of silica hydrogel formation using time-resolved fluorescence anisotropy. Journal of Non-Crystalline Solids 270 (2) 191-204.

194. Scherer GW. 1997. Interaction of Formic Acid with the Silica Gel Network. Journal of Sol-Gel Science and Technology. 8 (1) 165-171.

195. Scherer GW. 1996. Influence of Viscoelasticity and Permeability on the Stress Response of Silica Gel. Langmuir. 12 (10) 1109-1116.

196. Teipel U, Foerter B. 2004. Mechanical Properties of Gel Propellants with Nanoparticles. Energetic Materials. 22 (1) 69-82.

197. Teipel U, Forter B. 2005. Rheological Behavior of Nitromethane Gelled with Nanoparticles. Journal of Propulsion and Power. 21 (1) 40 - 44.

198. L.T. Taylor, Supercritical Fluid Extraction, John Wiley & Sons, New York, 1996.

199. Ruben GC, Hrubesh LW, Tillotson TM. 1995. High resolution transmission electron microscopy nanostructure of condensed-silica aerogels. Journal of Non-Crystalline Solids. 186 (2): 209-218.

200. J. Clifford and B.A. Pethica, Hydrogen-Bonded Solvent Systems, Taylor and Francis, London, 1968.

201. Zimmerman JR, Brittin W. 1957. Nuclear-Magnetic-Resonance studies in multiple-phase systems: Lifetime of a water molecule in an adsorbing phase on silica gel, J. Phys. Chem. 61 (10) 1328–1333.

202. Li C, Akinc M. 2005. Relationship between water mobility and viscosity of nanometric alumina suspensions. J. Am. Ceram. Soc. 88 (20) 2762–2768.

203. Fotti G, Michele C, Sciortino F, Taraglia P. 2005. Arrested phase separation in a short-ranged attractive colloidal system: A numerical study. J. Chem. Phys. 122 (1) 1-14.

204. Yamaue T, Doi M. 1996 Theory of one-dimensional swelling dynamics of polymer gels under mechanical constraint. Phys. Rev. E. 69 (1) 1-5.